Quasi-Optical Discrete Lens Arrays for Synthetic Aperture Radar

by

GARY LOUIS RAIT
B.S.E.E., Ohio Northern University, 1978
M.S.E.E., University of Southern California, 1980
M.B.A, Claremont Graduate School, 1988

A thesis submitted to the
Faculty of the Graduate School of the
University of Colorado in partial fulfillment
of the requirement for the degree of
Doctor of Philosophy
Department of Electrical and Computer Engineering
2002

This thesis entitled:
Quasi-Optical Discrete Lens Arrays for Synthetic Aperture Radar
written by Gary Louis Rait
has been approved for the Department of Electrical and Computer Engineering

____
Prof. Zoya B. Popović

____
Prof. William J. Emery

Date ______________________________

The final copy of this thesis has been examined by the signatories, and we find that both the content and the form meet acceptable presentation standards of scholarly work in the above mentioned discipline.

Rait, Gary Louis (Ph.D., Electrical Engineering)
Quasi-Optical Discrete Lens Arrays for Synthetic Aperture Radar
Thesis directed by Professor Zoya B. Popović

Over the last twenty years, electronically-scanned arrays (ESAs) have benefited from significant research and development to become the state-of-the-art in both spaceborne and airborne synthetic aperture radar (SAR) remote sensing systems, but the resources required to provide the necessary RF performance are often substantial. While some alternative antenna technologies have been investigated, the use of Quasi-Optical (QO) antennas in SAR applications has not received much attention.

This thesis focuses on the ability of QO antenna technology to provide the RF performance likely to be required by future SAR remote sensing systems, both spaceborne and airborne. Based on the types of SAR missions thus far conducted and the evolution of the corresponding mission-level requirements, the requirements for future SAR missions are extrapolated. SAR performance equations for curved-earth geometry are derived from the standard relationships described in the literature and are used to allocate mission-level requirements to the antenna level.

This thesis concludes that QO antenna technology is applicable to spaceborne and airborne SAR systems and offers advantages over traditional ESA technology in certain cases. Antenna subsystem design work is done using both antenna technologies for each of three future SAR missions to determine the prime power, mass, and cost resources required to achieve the necessary performance. The fundamental efficiency with which the QO beamforming network performs and is implemented provides the potential for mass and cost savings. The ability of the QO beamforming network to easily accommodate multiple, simultaneous beams enables a new SAR operational mode that can provide either prime power reduction or wider-swath/finer-resolution coverage not achievable with any single-beam SAR antenna.

DEDICATION

I dedicate this to my wife Maureen who has always supported me and encouraged me to do better. She is the reason this is complete. I owe her everything.

ACKNOWLEDGMENTS

First and foremost, I wish to thank my thesis advisor, Professor Zoya Popović, for giving me this chance. She did not have the time to take on another student, let alone a non-traditional student without the sense to take a leave of absence from work to complete his research. She could have justifiably declined, but instead she took me into her student group and provided wise technical guidance and support. I would also like to thank the members of my committee, Professor William Emery, Professor Susan Avery, Professor K.C. Gupta, and Professor Penina Axelrad, for their review of this work. The classes I took from these professors were years ago, yet they did not hesitate to be on my committee. I am indebted to a few generations of Professor Popović's students for the development of Quasi-Optical antenna technology as well as bearing with me over the years. Stein Hollung's and Darko Popović's work is especially applicable and is referenced herein.

Ball Corporation financially enabled this effort and continues to provide me with challenging work opportunities in the antenna and SAR fields. In my 14 years with Ball I have had the privilege of working with the Jet Propulsion Laboratory on two spaceborne SAR missions and have learned much as a result. Continuing to work at Ball while completing this research was usually stressful and at times seemed hopeless. I wish to thank Janeil Walter for covering for me at work and bailing me out of conflicts on many occasions. Lastly, a friend for 14 years who worked with us as a subcontractor on the SIR-C mission, Ron Petersen, proofread all of the text and provided valuable feedback and moral support.

I would not be here were it not for my family. My mother and father always emphasized higher-level education and gave me the opportunity to pursue it, an opportunity that they were not fortunate enough to have. Along with my brother, they also gave me the confidence necessary to pursue it. It was my wife's daily indulgence and positive support, though, that pulled me through the last few laps of the race.

CONTENTS

FIGURES

FIGURE

TABLES

TABLE

CHAPTER 1

INTRODUCTION

1.1 Synthetic Aperture Radar Missions

Since synthetic aperture radar (SAR) operation requires a moving platform, both airborne and spaceborne sensors are in use today. The movement of the platform allows the "synthesis" of a larger aperture over time via coherent data processing [92]. A valuable artifact of this processing is that the resolution cell size achievable in the direction of platform movement is roughly equal to one-half the "real" aperture length and is independent of the range to the target [7]. This enables the viability of spaceborne SAR sensors to perform moderate-resolution military and scientific mapping and unlikely data extraction (measurement of sea state and ocean wave conditions, geological and mineral explorations, soil moisture, types of vegetation, etc.) that can be used for environmental monitoring of the Earth [93][94]. This also enables the consideration of future SARs designed to detect moving targets on the ground or in the air from space.

While spaceborne sensors have the advantage of a much-wider field of regard, airborne sensors are much less expensive and are more operationally flexible. Airborne SAR missions have generally been more tactical in nature and have provided higher-resolution performance for both commercial two-dimensional imaging and military terrain matching for navigation [51][45]. Airborne SARs have also traditionally been testbeds for technology development, capability demonstration, or processing development [36][39][40][37][38]. Spaceborne SAR missions have been scientific in nature while gradually demonstrating more significant performance and hardware sophistication. In particular, the series of SAR systems flown on the Space Shuttle over the last 20 years has shown that the SAR antenna drives not only the performance of the SAR but the prime power, mass, and cost requirements as well [96]. Even for cases where the SAR antenna is not physically large, so much of the SAR system performance is directly tied to the antenna characteristics that the antenna is the dominant feature of the SAR system. As higher and higher levels of performance are required by future SAR missions, the efficiency of resources will become as important as the ability to provide a given level of performance. It will do no good to be capable of providing a significant performance enhancement if one cannot afford the SAR hardware necessary to do so.

1.2 Traditional SAR Antenna Technologies

Antenna technologies used in the SAR systems fielded to date include simple horns and reflectors along with planar arrays that implement either low-loss passive beamforming networks or beamforming networks with transmit and receive amplifiers and electronic beam steering capabilities. Since the individual antenna aperture dimensions determine the SAR performance achievable (resolution, swath) and the aperture area helps to determine the range within which such performance can be provided (sensitivity), antenna technology is often constrained by the mission requirements imposed [91]. The attractiveness of horns and reflectors is their relative simplicity, but the performance flexibility is limited. Airborne missions in particular have utilized horns and reflectors to provide the performance required [39][40][49][50]. As mission requirements escalate, however, the performance potential provided by planar array technology becomes important.

Planar array or phased array technology has a tremendous performance upside, but it is essentially a brute-force approach. The phased array can be implemented in virtually any aspect ratio, can be stowed and deployed with relative ease, and can provide relatively independent performance in antenna gain, radiated power, and noise temperature. Its flexibility and performance potential are its most alluring qualities. A problem with phased array technology is that the prime power, mass, and cost resources required to produce the performance desired are often too great to afford [97]. While the desired performance may indeed be possible, it may not be practically implementable. Spaceborne SAR applications are perfect examples. Although many planar arrays have been flown, few are active phased arrays and fewer yet implement the level of performance possible with the technology. The development of Space-Based Radar (SBR) has been stymied by the power, mass, and cost resources necessary although the required RF performance is certainly possible [98]. The technology development that has been sponsored as a result has focused on reducing the resource requirements of phased array components (lightweight/low-cost/low-power T/R modules, exotic structural materials, low-loss phase shifters, optical control signal distribution, etc.). While this has certainly improved the situation, in the end it can only go so far. There is definitely room for a different antenna approach that may not necessarily be limited by the same resource requirements. The question is whether the trade-offs necessary to get there are worth the trouble.

1.3 Quasi-Optical Antenna Technology

Quasi-optical (QO) antenna technology was developed as an efficient way of transmitting RF energy. It is distinguished by the low-loss, wideband, spatial or optical combining of energy that reduces the necessary prime power, mass, and cost resources. Taken to the extreme for radar applications, QO antenna technology not only uses spatial combining of the transmitted signal but implements a spatial beamforming network as well. This requires a precisely-positioned feed antenna but eliminates the constrained-transmission-line beamforming networks normally associated with phased arrays. High-power amplifiers (HPAs) and low-noise amplifiers (LNAs) can be distributed at the aperture-element level just like a phased array, but beam steering can be implemented without active phase shifter devices. This can be done, given that the planar radiating aperture is a lens, by switching between different antenna feeds positioned along the focal arc of the lens. One can therefore consider QO antenna technology to be a combination of some of the defining characteristics of phased array and reflector antenna technology.

1.4 Objective of Work

The overall objective of this work is to present several new SAR antenna approaches, using QO antenna technology, that will either deliver RF performance more efficiently and affordably or provide RF performance heretofore unachievable. In support of this objective, the following tasks are completed:

- Create a comprehensive comparison of basic mission parameters for previous and future SAR systems, both spaceborne and airborne
- Conduct an in-depth analysis of the performance available from the specific legacy antenna approaches used in order to determine the types of antennas most efficiently used with the various classes of SAR missions
- Derive the SAR system performance relationships for the non-ideal, curved-earth geometry and appropriately sequence these relationships in a model that can be used to allocate mission requirements down to the antenna level or predict SAR performance given antenna performance
- Extrapolate the performance requirements appropriate for representative future SAR missions from the evolution of performance demonstrated thus far
- Predict the power, mass, and cost resource requirements for both traditional and new QO antenna approaches that provide the performance required by the set of representative future SAR missions and assess the origin and significance of any resulting QO advantages
- Propose a new SAR operational mode, enabled by the use of QO antenna technology, that provides either additional prime power economy or a performance capability not practical with traditional antennas
- Analyze the driving components of the power, mass, and cost resources required by the QO antenna approaches generated to recommend areas for future study that could make QO antenna technology more attractive for SAR applications

1.5 Organization of Work

This work is organized according to the objectives described in the previous section. Chapter 2 identifies many of the airborne and spaceborne SAR systems fielded to date and notes their mission requirements and hardware characteristics. Future SAR missions are also described with the focus being the evolution of the SAR antenna requirements. Chapter 2 categorizes the space spanned by future SAR antenna requirements and evaluates the ability of traditional antenna technologies to provide practical solutions to the various classes of requirements.

Chapter 3 summarizes the work done in Appendix A on SAR mission requirement allocation. Appendix A collects the approximate radar relationships from the literature that address the allocation of SAR mission requirements down to the antenna and then derives the exact equations that take into account the Earth's curvature as well as specific antenna features such as beamwidth and various losses. Appendix A also describes an Excel model developed as a vehicle to determine antenna solutions to SAR mission requirement problems by exercising the developed relationships.

Chapter 4 describes quasi-optical antenna technology by tracing its evolution to date. The characteristic aspects of the technology are disclosed, relative to those of traditional antenna technology, and calculations of antenna performance unique to QO antennas are described. Chapter 4 concludes with an evaluation of the likely advantages and disadvantages of QO antenna technology as it applies to SAR.

Chapter 5 determines a set of representative SAR missions for which QO antenna technology would presumably apply. The relationships developed in Appendix A are used to determine combinations of mission requirements that are both practical and achievable. The model described in Appendix A is used to generate the necessary antenna performance required to satisfy the set of mission requirements.

Chapter 6 contains the system-level antenna design work done for the representative airborne SAR mission. The antenna design activities are taken only as far as necessary to be in a position to estimate the prime power, mass, and cost required to achieve the antenna performance needed. Chapter 6 presents functional block diagrams, RF performance predictions, and power, mass, and cost calculations.

Chapter 7 contains the system-level antenna design work done for the representative wide-swath spaceborne SAR mission and summarizes the comparable design work done for the representative high-resolution spaceborne SAR mission in Appendix C. Chapter 7 presents functional block diagrams, RF performance predictions, and power, mass, and cost estimates.

Chapter 8 describes a new multiple-beam SAR operational mode, facilitated by the use of QO antenna technology, that can either significantly reduce prime power requirements or provide SAR performance significantly in excess of that available with any single-beam antenna.

Chapter 9 concludes by comparing the power, mass, and cost resources required by the single-beam QO antenna approaches relative to those required by the traditional antenna approach to attempt to uncover any fundamental QO advantage for SAR applications. Chapter 9 also assesses the potential value of the multiple-beam operational mode proposed in Chapter 8.

Appendix B contains the Excel model generated to provide a tool to exercise the complex SAR relationships developed in Appendix A to either allocate mission requirements down to the antenna or to predict mission performance given antenna performance. Appendix D defines the acronyms used throughout the text.

CHAPTER 2

SAR MISSIONS AND ANTENNA TECHNOLOGY

Many SAR missions using either airborne or spaceborne platforms have been fielded, and many more are being considered for the future. This chapter traces the evolution of SAR missions and requirements to date and projects that evolution into the future. Missions representative of this evolution are documented for later use in comparative antenna evaluations. Not surprisingly, certain types of antennas are better suited to certain missions. This chapter notionally identifies this mapping relative to the evolving requirements to determine the antenna improvements necessary to support future missions.

2.1 SAR Mission Legacy

SAR originated from an idea by Carl Wiley in the early 1950s to use the doppler frequency information inherent in target return echoes over time to improve resolution in the direction of movement of the radar platform [32]. Prior to this invention the ability of a moving real aperture radar (RAR) to resolve distinct targets or features was driven by the beam footprint (range x beamwidth) in the along-track dimension. The only way to improve along-track resolution at a given range was to increase the along-track antenna dimension, thereby reducing the beamwidth. Wiley suggested synthesizing the larger along-track antenna dimension over time, using the motion of the platform, as an alternative to implementing a large single antenna. The counter-intuitive implications of this idea, namely that the resulting along-track resolution improves with smaller apertures and is independent of range, have enabled even the modest-resolution imaging demonstrated in the last 50 years from both airborne and spaceborne platforms.

Given that moving imaging radars can provide range-independent resolution in the along-track dimension (via the synthetic aperture technique) as well as the cross-track dimension (via pulse compression), what purposes can they serve? In addition to the obvious military applications of high-resolution ground mapping for battlefield intelligence, surveillance, and reconnaissance (ISR), autonomous navigation via terrain matching, ground-target classification [33], weapons guidance [34], and concealed target detection, the following commercial/civilian applications can be addressed [34] [35]:

- Topographic imaging of land surface
- Assessing the condition of crops
- Underground resources (e.g., oil) exploration
- Autonomous aircraft landing
- Air traffic control
- Mine detection
- Land surface change detection
- Land-use monitoring
- Man-made and natural hazard monitoring

The moving platforms carrying these imaging radars can be grouped into the airborne and spaceborne categories. Airborne implementations have been more numerous due to their relative ease of implementation and cost advantage. Spaceborne platforms provide greater fields of view and less-restricted access but are much more expensive and risky.

The implementation of imaging radars using the SAR technique has included both airborne and spaceborne vehicles to date. Many airborne platforms have been used as technology testbeds in the interests of risk reduction prior to space implementation. Accordingly, the airborne radar systems have generally been more complicated and flexible while spaceborne radar systems have been more special-purpose.

2.1.1 Airborne SAR Legacy

Some of the airborne SAR systems fielded to date are summarized in rough chronological order in Table 2-1. This collection is intended to be representative rather than exhaustive.

System	Yr	FB **	Pol	Slant Range Res (m)	Swath (km)	Alt (km)	Speed (m/s)	Antenna Size (m) (el x az)	BW (MHz)	Antenna Type*	Elect Beam Steering ***
AirSAR	87	P L C	quad quad quad	3.8-7.5 3.8-7.5 3.8-7.5	10-15 10-15 10-15	7.9	230	0.9 x 1.8 0.5 x 1.6 0.2 x 1.4	20-40 20-40 20-40	PA PA PA	N N N
C/X-SAR	88	C X	quad dual	5 5	18-63 18-63	6.5			30 30	H H	N N
Lincoln Lab ADTS	92	Ka	quad	0.25	0.375		100		600	R	N
PHARUS	95	C	quad	1.5-3.8	10-20	12	150	0.1 x 1.0	40-100	AESA	AZ+EL
Open Skies	96	X		3	18	13.1			50	PA	N
EMISAR	96	L C	quad quad	2-8 2-8	12-48 12-48	12.5			19-75 19-75		N N
E-SAR	96	P L S C X	dual dual dual dual dual	2.5 1.5 1.2 1.2 1.2	3-15 3-15 3-15 3-15 3-15	3.7	100	0.5 x 1.3	60 100 120 120 120	PA PA PA PA H	N N N N N
Pi-SAR	96	L X	quad quad	3-20 1.5-3	20-42 4-42	12	250	0.6 x 1.6 0.2 x 1.0	25-50 50-100	PA PA	N N
JSTARS	96	X	HH	~0.5		12.8	275	0.6 x 7.3	~300	ESA	AZ
TESAR	96	Ku		0.25	0.8	7.6	35		600	AESA	AZ
IFSARE/ STAR-3i	97	X		2.5	10	12.2			60	PA	N

***H = horn**
R = reflector
PA = planar array (no distributed amplifiers, no beam steering)
ESA = electronically-scanned array (no distributed amplifiers, beam steering)
AESA = active electronically-scanned array (distributed amplifiers, beam steering)

****FB = frequency band**

*****N = no electronic beam steering**
AZ = electronic beam steering in azimuth
EL = electronic beam steering in elevation

Table 2-1 Representative airborne SAR systems to date.

In the polarization column the following definitions apply. HH polarization denotes transmit on horizontal polarization and then receive on horizontal polarization. VV polarization denotes transmit on vertical polarization and then receive on vertical polarization. Dual polarization implies the ability to select between HH and VV. Quad polarization denotes the ability to transmit on both polarizations, either simultaneously or sequentially, and then receive on both polarizations simultaneously.

AirSAR. AirSAR was developed by the Jet Propulsion Laboratory (JPL) in the 1980s as a testbed for SAR technologies. It is a multi-frequency, polarimetric radar system that is installed on a DC-8 aircraft (see Figure 2-1). It implements P-Band, L-Band, and C-Band dual-polarized, planar array antennas to provide polarimetric, along-track interferometric, and cross-track interferometric SAR performance [36].

Figure 2-1 The NASA multi-frequency, polarimetric AirSAR imaging system resides on the NASA DC-8 aircraft.

C/X-SAR. The C/X-SAR was developed by the Canadian Centre for Remote Sensing (CCRS) in the 1980s to support the initial marketing of the eventual Radarsat program and as an optimization testbed for future satellite systems. It is a C-Band and X-Band radar system, polarimetric and cross-track interferometric at C-Band, that is installed on a Convair 580 aircraft (see Figure 2-2). The main antennas are horns mounted on a three-axis stabilized pedestal in a pod below the fuselage. The C-Band interferometric antenna is mounted above the main antennas on the side of the fuselage [39][40].

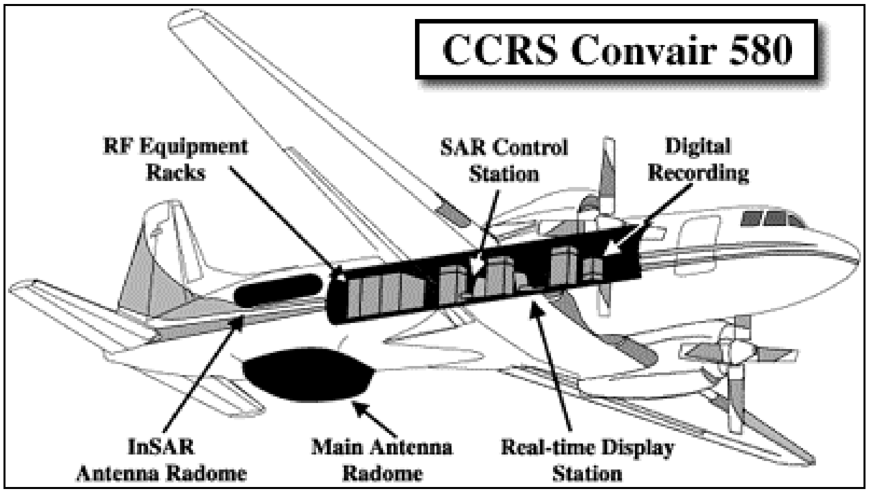

Figure 2-2 The CCRS C/X-SAR imaging system resides on the Convair 580 aircraft.

Lincoln Laboratory MMW SAR. Lincoln Laboratory developed a millimeter-wave SAR to investigate the detection and classification of stationary targets. It is a polarimetric Ka-Band (33 GHz) radar system that is installed on a Gulfstream G1 aircraft. This Advanced Detection Technology Sensor (ADTS) reflector antenna is mounted on a gimbal inside a pod hanging below the fuselage of the aircraft [49][50].

PHARUS. PHARUS (Phased Array Universal SAR) was developed by the Netherlands Ministry of Defence in the 1990s for environmental monitoring and military applications and to facilitate technology demonstrations leading to the European Space Agency's Advanced Synthetic Aperture Radar (ASAR). It is a polarimetric C-Band radar system that is installed on a Cessna Citation II aircraft (see Figure 2-3). The antenna is a modular active electronically-scanned array with two-dimensional beam steering [37] [38].

Figure 2-3 The PHARUS imaging system resides on the Cessna Citation II aircraft.

Open Skies. The SAR for Open Skies (SAROS) was integrated by Sandia National Laboratory in the 1996 timeframe in support of the bilateral surveillance negotiated as part of the Open Skies treaty. It is an X-Band sidelooking SAR that is limited to no better than 3 m resolution by the treaty. It utilizes a slotted-waveguide array mounted on a modified OC-135B aircraft [41].

EMISAR. EMISAR (Electromagnetics Institute SAR) was developed by the Danish Center for Remote Sensing (DCRS) in the 1990s to provide SAR data for DCRS research. It is an L-Band and C-Band radar system that is installed on a Gulfstream G3 aircraft (see Figure 2-4). Polarimetric, gimballed, L-Band or C-Band antennas are mounted in a pod below the fuselage. Two C-Band antennas, flush-mounted to the fuselage, are used for interferometry [42].

Figure 2-4 The DCRS EMISAR imaging system resides on a Gulfstream G3 aircraft.

E-SAR. E-SAR (Experimental SAR) was developed by the German Aerospace Research Establishment (DLR) in the 1990s as a vehicle for testing new technologies and signal processing algorithms. It is a polarimetric, multiple-frequency (P-Band, L-Band, S-Band, C-Band, and X-Band) radar system that is installed on a Dornier DO 228 aircraft. Separate antennas, fixed to the aircraft, are used for each frequency band [43].

Pi-SAR. Pi-SAR was developed by the Communications Research Laboratory (CRL) and the National Space Development Agency of Japan (NASDA) in the mid-1990s as a scientific instrument. It is an L-Band and X-Band polarimetric radar system that is installed on a Gulfstream II aircraft. The antennas (one L-Band and two X-Bands for cross-track interferometry) are mounted in pods below the aircraft [44].

Joint STARS. The Joint Surveillance and Target Attack Radar System (Joint STARS) was jointly developed by the U.S. Army and U.S. Air Force and became operational in 1996.

It is a ground-target surveillance and command/control radar system, utilizing Moving Target Indicator (MTI) and SAR modes, that is installed on a Boeing 707-300 series aircraft (see Figure 2-5). The 24-foot-long X-Band antenna features electronic beam steering in azimuth [45].

Figure 2-5 Joint STARS is an operational military ground-target surveillance and command/control sensor resident on a Boeing 707-300 aircraft.

TESAR. Northrop Grumman developed the Tactical Endurance SAR (TESAR) to provide high-resolution tactical aerial imagery in real time. It is an operational Ku-Band radar system that is installed on the Predator Unmanned Aerial Vehicle (UAV). The TESAR antenna offers electronic beam steering in the azimuth dimension and is mounted on a gimbal inside a pod hanging below the fuselage of the aircraft (see Figure 2-6) [51].

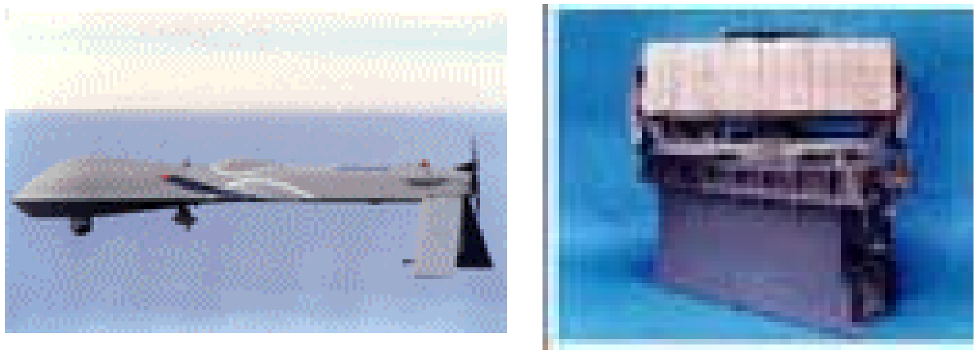

Figure 2-6 The TESAR high-resolution SAR utilizes the Predator UAV platform and features a gimbaled Ku-Band active phased array.

IFSARE. IFSARE (Interferometric SAR for Elevation) was developed by the Environmental Research Institute of Michigan (ERIM) in the 1990s for high-precision topographic mapping applications. It was transitioned to Intermap in 1997 for commercial mapping usage and renamed STAR-3i. It is an X-Band radar system that is installed on a Learjet 36A aircraft. Its two antennas, separated in the cross-track dimension, are fixed to a gimballed platform in the pod below the fuselage [46][47][48].

2.1.2 Spaceborne SAR Legacy

The spaceborne SAR systems fielded to date are summarized in Table 2-2. Due to the smaller numbers of spaceborne systems put in service, this collection is much more complete.

System	Yr	FB **	Pol	Slant Range Res (m)	Swath (km)	Alt (km)	Speed (m/s)	Antenna Size (m) (el x az)	BW (MHz)	Antenna Type*	Elect Beam Steering ***
Seasat	78	L	HH	7.5	100	800	7450	2.2 x 10.7	19	PA	N
SIR-A	81	L	HH	25	50	250	7750	2.2 x 9.4	6	PA	N
Venera	83	S		1500	120			1.4 x 6		R	N
SIR-B	84	L	HH	12.5	18-63	250	7750	2.2 x 10.7	12	PA	N
Magellan	89	S	HH	65	25	290-2000		3.7 dia	2.3	R	N
Almaz-1	91	S	HH	12	45	320	7720	1.5 x 15	12.5	PA (2)	N
ERS-1 ERS-2	91 95	C C	VV VV	10 10	100 100	780 780	7465 7465	1 x 10 1 x 10	15.5 15.5	PA PA	N N
JERS	92	L	HH	10	75	570	7575	2.8 x 12	15	PA	N
SIR-C/X-SAR	94	L C X	quad quad VV	3.8-15 3.8-15 3.8-15	10-90 10-90 40	235	7770	2.9 x 12 0.8 x 12 0.4 x 12	10-40 10-40 10-40	AESA AESA PA	EL EL N
Radarsat	95	C	HH	5-12.5	50-500	800	7450	1.5 x 15	12-30	ESA	EL
Cassini	97	Ku		175-350				4 dia	0.42-0.85	R	N
SRTM	00	C X	quad VV	3.8-15 3.8-15	225 50	235	7770	0.8 x 8 0.4 x 6	10-40 10-40	AESA PA	EL N

***H = horn**
R = reflector
PA = planar array (no distributed amplifiers, no beam steering)
ESA = electronically-scanned array (no distributed amplifiers, beam steering)
AESA = active electronically-scanned array (distributed amplifiers, beam steering)

****FB = frequency band**

*****N = no electronic beam steering**
AZ = electronic beam steering in azimuth
EL = electronic beam steering in elevation

Table 2-2 Spaceborne SAR systems fielded to date.

In the polarization column the following definitions apply. HH polarization denotes transmit on horizontal polarization and then receive on horizontal polarization. VV polarization denotes transmit on vertical polarization and then receive on vertical polarization. Dual polarization implies the ability to select between HH and VV. Quad polarization denotes the ability to transmit on both polarizations, either simultaneously or sequentially, and then receive on both polarizations simultaneously.

Seasat. The National Aeronautics and Space Administration's (NASA) Seasat in 1978 was the first spaceborne SAR for scientific applications. It was an L-Band, single-polarization radar system designed for ocean-wave imaging. Its antenna was a lightweight, fixed-beam planar array whose deployment structure has become the baseline design for subsequent systems (see Figure 2-7). The operational lifetime of the Seasat satellite ended after 90 days due to a power system failure [52][53].

Figure 2-7 NASA's Seasat was the first spaceborne SAR for scientific remote sensing.

SIR-A. The Shuttle Imaging Radar A (SIR-A) flew in 1981 as the first operational Space Shuttle payload. It was an L-Band, single-polarization radar system designed for higher-incidence-angle imaging of geological features (see Figure 2-8). The antenna was a passive planar array on a fixed mount in the Shuttle cargo bay [53].

Figure 2-8 The SIR-A imaging system was the first Shuttle operational payload.

Venera. Venera 15 and 16 in 1983 were the last in a long line of Soviet missions to the planet Venus.   Both spacecraft orbiters were equipped with S-Band SARs used to study the planet's surface properties. The SAR antenna was an elliptical parabolic reflector (see Figure 2-9) [54].

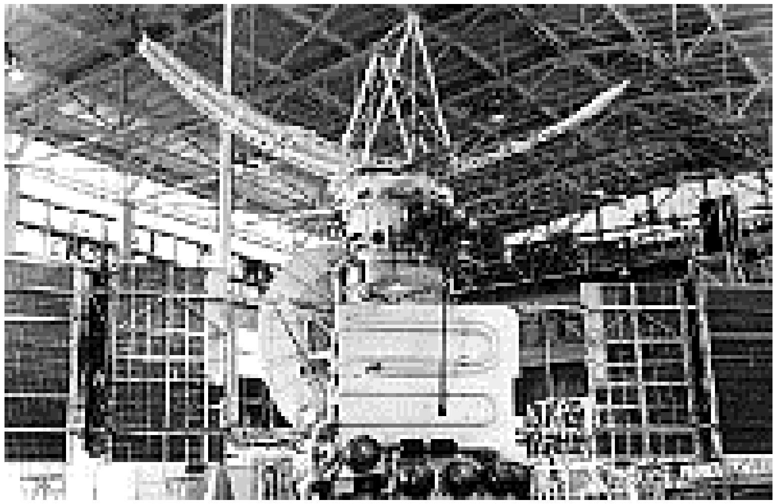

Figure 2-9 The Venera spacecraft was one of two launched by the Soviet Union in 1983 to study the planet Venus.

SIR-B. The NASA Shuttle Imaging Radar B (SIR-B) mission in 1984 was the first spaceborne SAR to intentionally produce multi-incidence-angle image data. It was an L-Band, single-polarization, fixed-beam system that incorporated elevation beam steering via mechanical tilt mechanisms. The planar array also mechanically folded into thirds to accommodate other Shuttle payloads [53].

Magellan. The Magellan spacecraft was launched in 1989 with a mission to study Earth's sister planet Venus. During its four years in orbit of Venus, it used its S-Band SAR to map 98% of the planet's surface, most at resolution ten times better than the previous Venera mission. The antenna is a 3.7 m reflector that was used both for SAR and for telecommunications back to Earth (see Figure 2-10) [55][56]:

Figure 2-10 The Magellan system utilized a large reflector for SAR imaging of Venus as well as mission telecommunications.

Almaz-1. Almaz-1 was developed and operated by the Russian missile/space company NPO Mashinostroyenia for exploration and monitoring of the Earth's natural resources. It was an S-Band, single-polarization SAR launched in 1991 that featured two large, fixed, planar arrays mounted on either side of the spacecraft (see Figure 2-11). Its mission was terminated in 1992 [57].

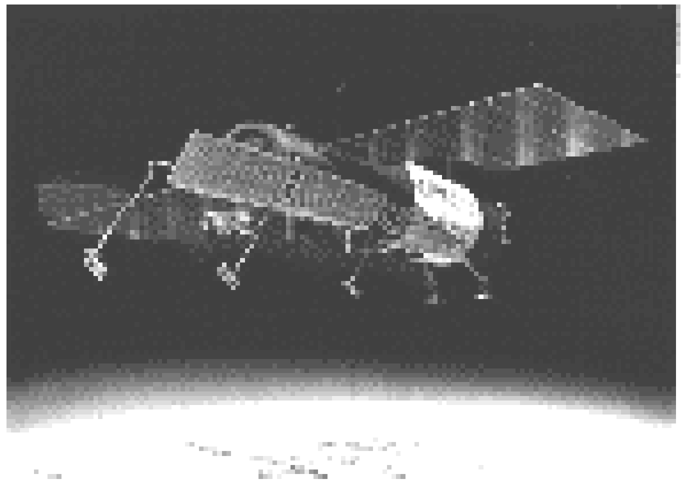

Figure 2-11 The Almaz-1 satellite was distinguished by two large SAR antennas on either side of the spacecraft.

ERS-1/2. The European Space Agency's Earth Resources Satellite 1 (ERS-1) was launched in 1991 as the first satellite designed to provide commercially-available microwave remote sensing data. It is a C-Band, single-polarization radar system with a deployable slotted-waveguide array whose primary mission is the imaging of oceans, ice caps, and coastal regions (see Figure 2-12). A second satellite (ERS-2), identical to the first, was launched in 1995 [58][59][60].

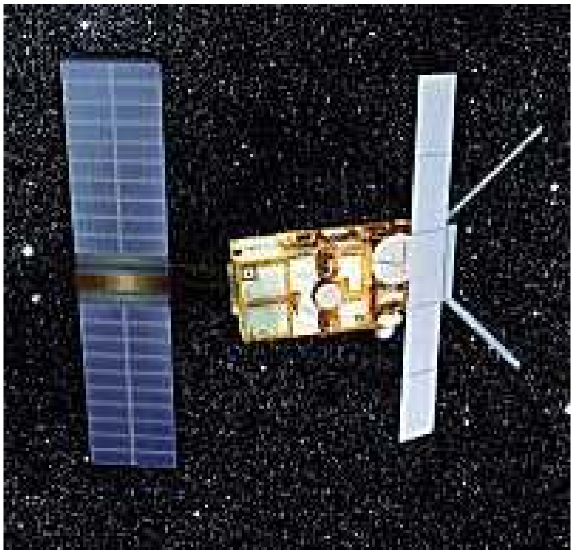

Figure 2-12 The ERS-1 imaging system was the first spaceborne SAR to generate commercially-available remote sensing data.

JERS. The Japan Earth Resources (JERS) satellite was developed by NASDA for launch in 1992 as a scientific instrument. It was a single-polarization, L-Band radar system that produced Earth remote sensing data until mission termination in 1998. Its antenna was a deployable, passive, planar array similar to Seasat [61][62].

SIR-C/X-SAR. The Shuttle Imaging Radar C/X-Band Synthetic Aperture Radar (SIR-C/X-SAR) experiment was a collaboration between the space agencies of the United States, Germany, and Italy. It was a multi-frequency, multi-polarization, multi-incidence-angle radar system that demonstrated the value of multi-parameter imaging in two 1994 Shuttle flights (see Figure 2-13). The L-Band and C-Band antennas were quad-polarized, active electronically-scanned arrays with beam steering in elevation. The X-Band antenna was a single-polarized, slotted-waveguide array that was mechanically steered [63][64].

Figure 2-13 The SIR-C/X-SAR imaging system demonstrated the value of multi-parameter imagery.

Radarsat-1. Radarsat-1 was developed by the Canadian Space Agency (CSA) in the early 1990s to be the first commercial remote sensing satellite with the primary mission of monitoring sea ice. It is a C-Band radar system that has the flexibility to operate in various modes that trade off resolution performance versus swath performance. Its antenna is a large, slotted-waveguide array with electronic beam steering in elevation (see Figure 2-14) [53][63].

Figure 2-14 CSA's Radarsat-1 system provides multi-mode commercial remote sensing data today.

Cassini. The Cassini spacecraft was developed jointly by the space agencies of the United States and Europe to study the planet Saturn. It is one of the largest interplanetary spacecrafts ever built and includes a Ku-Band radar system designed to study Saturn's moon Titan via SAR imaging, altimetry, and radiometry. It was launched in 1997 and will be inserted into Saturn orbit in 2004. The multi-purpose high-gain antenna is a 4 m reflector with multiple feeds [65][66][67].

SRTM. The Shuttle Radar Topography Mission (SRTM) was a joint project between NASA and the National Imaging and Mapping Agency (NIMA) to generate a contiguous topographic map of the Earth's surface between roughly ±60° latitudes. The radar hardware included the C-Band radar from SIR-C and added a receive-only C-Band antenna at the end of a 60 m deployable mast (see Figure 2-15). Topographic imaging was enabled by the combination of cross-track interferometry and SAR processing.   Both C-Band antennas were polarimetric, electronically-scanned arrays that used multiple-beam capability and beam steering to achieve the swath width necessary to cover the Earth in one eleven-day Shuttle mission [68].

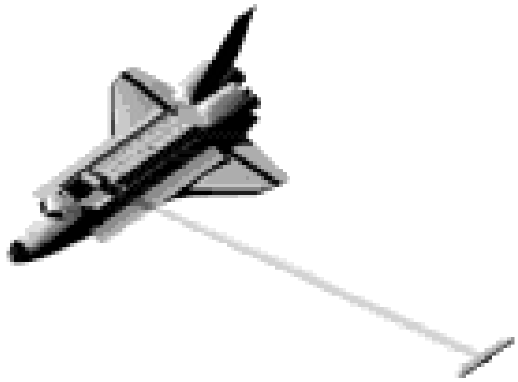

Figure 2-15 SRTM used interferometric SAR processing to generate data from which the first contiguous topographic map of the Earth's surface will be generated. The righthand photograph shows the 60m mast in the deployed configuration during the 2000 Shuttle flight.

2.2 SAR Mission Future

"Although one cannot reliably predict what will be in the future, one can wish for desired improvements in radar so long as they don't violate the laws of physics and they would make a difference." – Merrill Skolnik [75]

Future SAR missions will attempt to build on the successes of past missions in order to achieve better performance. Better performance can mean enhanced RF performance (e.g., wider bandwidth, lower noise figure, higher transmit power, lower sidelobes), the addition of new capabilities (e.g., electronic beam steering, interferometry, polarimetry), or enhanced efficiency in terms of mass, power, and cost. As implied above, design engineers have the tendency to focus on enhanced RF performance or the addition of new capabilities. The key to the future, however, is the last phrase of the quotation. In order for a technical improvement to make a difference, its implementation must also be affordable in the context of the particular application.

2.2.1 Airborne SAR Future

While affordability is especially important in the spaceborne environment, it is also key in future airborne systems. For commercial applications it is indeed true that the benefit of an improvement needs to exceed its cost. Although conflicting objectives often make this less clear for government applications, it is no less important. Airborne SARs have already demonstrated most if not all of the SAR functionality currently envisioned: strip mapping, spotlight mapping, high-resolution mapping, wide-swath mapping, low-frequency (UHF), high-frequency (Ka-Band), multiple-frequency, polarimetry, and interferometry. While better resolution, wider field of view, and higher sensitivity remain desirable improvements, they appear to be less desirable than the ability to implement existing performance less expensively.

The U. S. government has successfully sponsored the development of airborne surveillance over the last 45 years, starting with the U-2 (photographic and SAR mapping) and continuing with AWACS (Airborne Warning and Control System – airborne target tracking) and Joint STARS (ground target tracking and SAR). The cost and value of these assets, however, are sufficiently high to foster consideration of the development of smaller aircraft and smaller sensors for the future [75]. The U-2 is still in service but will likely be replaced by the more affordable Global Hawk UAV [77]. The Radar Technology Insertion Program (RTIP), originally conceived to upgrade the Joint STARS radar, has produced smaller but more capable radar electronics that, together with active electronically-scanned antenna technology, can enable the joint implementation of AMTI and GMTI/SAR on the same airborne platform (AMTI = airborne moving target indication, GMTI = ground moving target indication). Furthermore, this platform can be a smaller, more modern, and more capable aircraft that is more affordably operated and maintained [76].

The North Atlantic Treaty Organization (NATO) established the Airborne Ground Surveillance (AGS) program in 2000 to provide ground surveillance similar to that provided by Joint STARS. In fact the Natar (NATO Transatlantic Advanced Radar) solution is based on Joint STARS/RTIP radar technology. Of the other two likely AGS solutions, Sostar (Stand-Off Surveillance and Target Acquisition Radar) and ASTOR (Airborne Stand-Off Radar), the United Kingdom's ASTOR seeks to provide Joint STARS radar performance without the battlefield command functionality to be more affordable and to enable the use of a more capable aircraft [77].

2.2.2 Spaceborne SAR Future

Due to the cost and associated risk of putting a sophisticated sensor into space, extensive effort is usually undertaken to mitigate risk. Of particular interest here, demonstrations from airborne platforms are effective risk-reduction measures. Several of the airborne legacy systems described in Section 2.1.1 were indeed conceived as testbeds for technologies planned for space applications. Examples include the demonstration of polarimetry, interferometry, multiple frequencies, electronic beam steering, high-resolution imaging, and multi-function operation. NASA took this concept a step further in 1994 by sponsoring the SIR-C/X-SAR program as a Space-Shuttle demonstration of some of these advanced capabilities prior to implementation on long-term operational platforms (satellites). Therefore, while cost-efficiency is even more important for spaceborne systems, the implementation of additional capabilities is also planned.

The future directions of civilian/scientific and military space-based radars share some common aspects while having different goals. Given that high-resolution imaging from space was made possible by the invention of the synthetic aperture technique, finer (smaller resolution cells) resolution is desirable in both camps. Both camps also want the enhanced instantaneous field of view made possible by electronic beam steering. While multifunctional capability in the form of SAR polarimetry and SAR interferometry is a goal of civilian/scientific applications [78], the military hopes to combine the functions of SAR imaging with ground and air target surveillance. The addition of new capabilities runs counter to the conclusion that operational focus is necessary to reduce cost to an acceptable level [78]. This makes the concept of cost efficiency or cost effectiveness that much more important. Reducing the cost of implementing a particular capability, where cost also reflects size, mass, and power requirements, will be as important as improving the radar performance of that capability.

Future spaceborne SAR systems either being built or planned to satisfy future needs are summarized in Table 2-3. Note that this listing is characterized by enhanced performance in polarization diversity, resolution via wider bandwidth, and angular field of view via electronic beam steering.

System	Yr	FB **	Pol	Slant Range Res (m)	Swath (km)	Alt (km)	Speed (m/s)	Antenna Size (m) (el x az)	BW (MHz)	Antenna Type*	Elect Beam Steering ***
Envisat	01	C	quad	>9	5-400	800	7450	1.3 x 10	<16	AESA	EL
Radarsat 2	03	C	quad	1.5-12.5	20-500	798	7450	1.5 x 15	12-100	AESA	EL
ALOS	03	L	quad	5.4-10.8	20-350	700	7500	3.1 x 9	14-28	AESA	EL
TerraSAR	05	L X	quad dual	>15 >1	60 10	600	7560	? x 12.5 ? x 6.5	>10 <150	AESA AESA	EL EL
Discoverer II	?	X	single	>0.25	15-70	770	7470	5 x 8	<600	AESA	EL

***H = horn**
R = reflector
PA = planar array (no distributed amplifiers, no beam steering)
ESA = electronically-scanned array (no distributed amplifiers, beam steering)
AESA = active electronically-scanned array (distributed amplifiers, beam steering)

****FB = frequency band**

*****N = no electronic beam steering**
AZ = electronic beam steering in azimuth
EL = electronic beam steering in elevation

Table 2-3 Spaceborne SAR systems planned for the future.

In the polarization column the following definitions apply. HH polarization denotes transmit on horizontal polarization and then receive on horizontal polarization. VV polarization denotes transmit on vertical polarization and then receive on vertical polarization. Single polarization means either HH or VV. Dual polarization implies the ability to select between HH and VV. Quad polarization denotes the ability to transmit on both polarizations, either simultaneously or sequentially, and then receive on both polarizations simultaneously.

Envisat. Envisat is a multi-sensor satellite for the monitoring of environmental and climatic change being developed by the European Space Agency for launch in 2001. Its ASAR microwave sensor is a C-Band radar system that will provide continuity with the SAR data library generated by ERS-1 and ERS-2 since 1991. It will include in addition radar performance enhancements in the areas of spatial coverage and polarization sensitivity. It is a polarimetric, electronically-scanned array with beam steering in elevation and distributed transmit/receive (T/R) modules [69].

Radarsat-2. Radarsat-2 is the updated SAR that will extend the Canadian Space Agency's C-Band commercial remote sensing heritage upon its 2003 launch. Radarsat-2 will provide all of the modes currently implemented in Radarsat-1 along with higher-resolution and polarimetric modes. The antenna features the same aperture size as Radarsat-1 but is a 100-MHz electronically-scanned array with distributed T/R modules and beam steering in elevation. The satellite is being developed as a cooperative venture between MacDonald Dettwiler and CSA [70].

ALOS. ALOS is Japan's Advanced Land Observing Satellite that will continue the remote sensing heritage of JERS and the Advanced Earth Observing Satellite (ADEOS) with its launch in 2003. With its primary applications being cartography, disaster monitoring, and resource surveying, the Phased Array type L-Band SAR (PALSAR) will feature elevation beam steering and polarimetric capability. The L-Band antenna is a modest-bandwidth (30 MHz) electronically-scanned array with distributed T/R modules [71][72].

TerraSar. TerraSar is a European public/private partnership with the goal of establishing a self-sustaining geo-information business built on Europe's strength in SAR technology. TerraSar plans to launch two satellites in 2005, one providing 1m-resolution coverage at X-Band and the other providing polarimetric L-Band coverage over a larger field of view. Both antennas are active electronically-scanned arrays with beam steering in elevation [73].

Discoverer II. Discoverer II is a multi-satellite space-based radar concept designed to provide "real-time" surveillance data directly to the warfighter in support of military operations. Its development has been jointly sponsored by the U.S. Air Force, the National Reconnaissance Office (NRO), and the Defense Advanced Research Projects Agency (DARPA) since 1997. It is a multi-function X-Band radar providing both high-resolution SAR imaging and ground moving target detection. The baseline antenna design is an active electronically-scanned array, the development of which has been supported by investment in low-mass, low-cost T/R modules [74].

2.3 SAR Antenna Technology Application

Airborne and spaceborne SAR systems are not unique in the fact that certain types of antennas are better suited to fulfill certain mission requirements. Each type of antenna has advantages and disadvantages that may or may not be particularly significant in the context of a given mission. No single antenna technology is the optimal choice for all missions. This implies a multi-dimensional trade space of requirements wherein the available antenna technologies reside, each being an optimal or at least acceptable choice for only a subset of that space. While such a mapping would certainly reflect the types of antennas that should be considered for various SAR jobs, it would also indicate the improvements necessary to make the various antenna technologies applicable to a larger subset of mission requirements. Based on the legacy and future SAR systems noted in the previous sections, one can *qualitatively* build such a requirement space and determine the subsets occupied by the available antenna technologies.

2.3.1 Technology Preference Without Beam Steering

Probably the most obvious distinction between different subsets of requirements is the need for electronic beam steering. If electronic beam steering is not needed, the active or passive electronically-scanned arrays are certainly not needed. This leaves the reflector, horn, and planar array as the traditional antenna candidates. The advantages of the planar array for both airborne and spaceborne SAR applications are 1) its flexibility in achieving aperture aspect ratios that are long in azimuth and narrow in elevation and 2) its planar, two-dimensional nature. This contributes to ease of mounting in non-deployed cases and ease of stowage/deployment in those cases where the antenna must be deployed. This is evident in the heritage airborne and spaceborne SAR systems described earlier. The majority of airborne systems not requiring electronic beam steering use planar arrays for ease of mounting on the aircraft fuselage. Reflectors and horns are used when their volumes can be accommodated in a hanging pod. With the exception of the planetary missions, all spaceborne SARs not requiring electronic beam steering use planar arrays. This is because of the aspect ratios and the stowage volume/ease of deployment issue when attached to a spacecraft. It is interesting that all three planetary SAR missions used non-deployable reflector antennas. This was apparently due to the facts that the aperture sizes were smaller in relative terms and the larger spacecrafts required for planetary travel could accommodate the three-dimensional reflector volumes. The latter also eliminated the need for reflector deployment and its associated risk.

2.3.2 Technology Preference With Beam Steering

When electronic beam steering of any kind is required, the state-of-the-art heritage antenna is the electronically-scanned array (ESA). The selection between a passive ESA and an active ESA (AESA) is not so obvious, however. It comes down to the efficiency (mass, power, cost) with which the requirements are met and/or any additional qualitative benefit provided such as the demonstration of evolving technology. NASA's desire to demonstrate distributed-amplifier technology in space was a big reason that the L-Band and C-Band antennas for SIR-C were AESAs. The success of SIR-C in turn drove SRTM to utilize AESA technology. The SRTM follow-on scenario suggests that the risk of doing something new and different is a critical issue, especially in space. After the risk associated with distributed amplifiers was reduced as a result of the success of the SIR-C mission, it was easier to select the AESA architecture for SRTM. This is also illustrated with Radarsat-1 and the group of future spaceborne SARs collected in Table 2-3. At the time of the Radarsat-1 development, SIR-C was yet to fly, and the AESA risk may have been too great for this first commercial microwave remote sensing instrument. Radarsat-1 used the passive ESA, while the other contemporary systems (ERS, JERS) chose to not attempt electronic beam steering at all. With the space experience gained from their initial efforts and with the success of SIR-C, all three of these space agencies (Canada, Europe, and Japan) are building follow-on systems based on AESA architecture. The following sections present some arguments guiding the choice between ESA and AESA architectures.

2.3.2.1 ESA/AESA Characteristic Differences

The most obvious architectural difference between the two is the presence of T/R modules in the AESA which serve to distribute the transmit and receive amplifiers to the array-element level. Figure 2-16 compares top-level ESA and AESA block diagrams. Considering this alone, the ESA appears to be less expensive and complex. There are other characteristic differences, not apparent in Figure 2-16 that can make the AESA the better choice, depending on the requirements imposed by the particular mission.

The characteristic differences between the ESA and the AESA are summarized in Table 2-4. For a given set of antenna requirements, the ESA and the AESA will have the same number of phase shifters. The phase shifter technology used, however, will likely be different due to the criticality of the phase shifter insertion loss in the ESA. Since the ESA phase shifters come after the HPA on transmit, they imply the need for higher RF power out of the HPA. Since the ESA phase shifters come before the LNA on receive, they imply an increase in the receiver noise floor with which the receive signal must compete for detection.

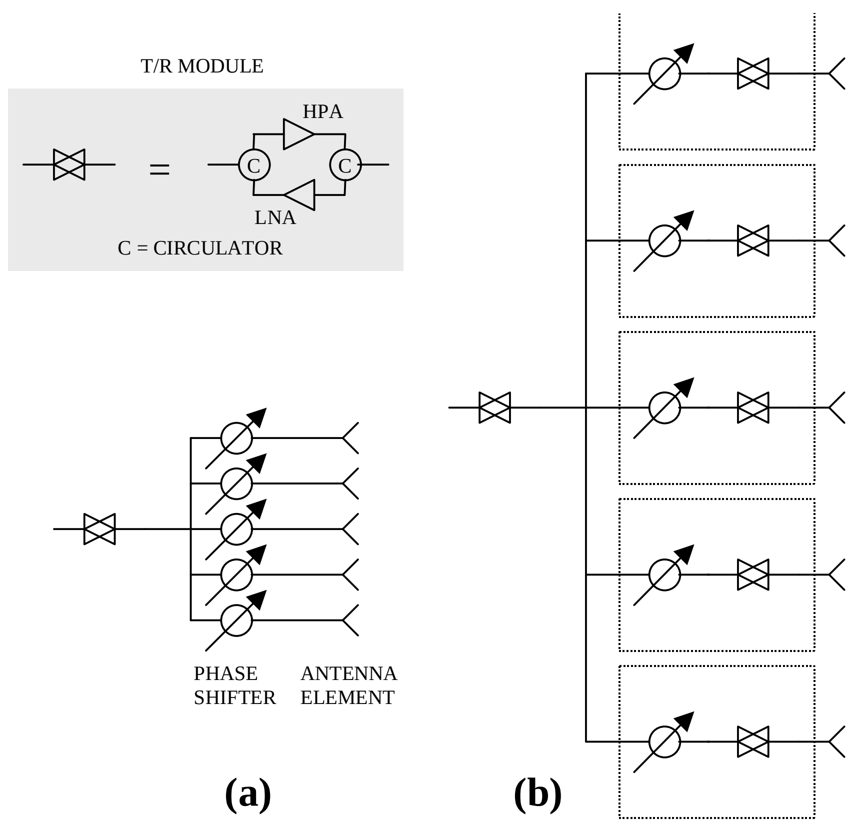

Figure 2-16 The most obvious difference between the ESA (a) and the AESA (b) is the presence of the element-level T/R modules.

Architecture Characteristic	ESA	AESA
Phase Shifter Implementation	**Need Low Loss** **Loss Increases Noise Temp**	**Need Low Mass** **Loss Does Not Increase Noise Temp**
Size and Number of Transmit HPAs	**Single HPA** **Larger RF Power** **Higher Efficiency**	**Distributed HPAs** **Smaller RF Power per HPA** **Lower Efficiency**
Size and Number of Receive LNAs	**Single LNA** **Larger Input RF Power**	**Distributed LNAs** **Smaller Input RF Power per LNA**
Beamforming Network	**Need Low Loss** **Loss Increases Noise Temp**	**Need Low Mass** **Loss Does Not Increase Noise Temp**

Table 2-4 Summary of the characteristic differences between the ESA and AESA antenna architectures.

The AESA has distributed amplifiers on both transmit and receive as opposed to single transmit and receive amplifiers for the ESA. Because of the distributed nature of the AESA HPAs, the peak RF power needed per HPA to produce a given radiated power is much less than that of the ESA. This can affect the distribution of heat to be dissipated, the likelihood of RF breakdown in vacuum (multipaction), and the amplifier technology used. The latter in turn has implications on DC-to-RF efficiency along with physical size and mass. On the receive side, the single ESA LNA must be able to handle a much larger receive signal amplitude than each of the distributed AESA LNAs. This fact can similarly enable the use of different amplifier technologies to reduce AESA LNA DC power and/or mass. While the DC power required to run the total quantity of AESA HPAs does not directly depend on the number of HPAs (since the total RF power generated does not change), the DC power required to run the total number of AESA LNAs is directly proportional to the number of LNAs. Usually the DC power drawn by the LNAs in an AESA is much less than that drawn by the HPAs. As the antenna size and frequency increase, however, one can find a point beyond which the LNA DC power dominates.

Finally, the beamforming network (BFN), exclusive of the ESA phase shifters or AESA T/R modules, is likely to be implemented differently in the two architectures. As with the ESA phase shifters, the ESA BFN insertion loss is critical since it proportionally degrades both transmit and receive performance. ESA BFN technology, therefore, strives for minimal loss often at the expense of other attributes such as mass and cost. Since the AESA BFN resides before the HPAs and after the LNAs, its insertion loss is at worst a second-order impact. As a result the AESA BFN can be implemented in a relatively low-mass and low-cost fashion.

2.3.2.2 Significance of ESA/AESA Characteristic Differences

In order to compare the ESA and AESA for a given set of requirements, one must assume that the RF performance is sufficient and equivalent in both cases. This being the case, the resulting metrics with which to comparatively evaluate the two approaches are DC power, mass, and cost. DC power is the power drawn by the antenna subsystem in order to provide the required RF performance. Mass is the total mass of the components that make up the antenna. Finally, cost includes not only the development and production cost of the antenna hardware but also the cost of providing the DC power required and accommodating the necessary mass. The comparative evaluation using these metrics will be done over the independent variables of antenna size, frequency, and beam steering coverage. These define the three-dimensional coordinate system that will be used to map SAR mission requirements onto the antenna requirement space. Antenna peak RF radiated power and system noise temperature will be treated as dependent variables. The qualitative dependence of the comparison metrics on these independent variables will be developed in the following paragraphs.

DC Power. The amplitude performance of any radar antenna is governed by the radar range equation described in Appendix A. One can summarize the antenna influence on the radar range equation by the product of the equivalent isotropically-radiated power (EIRP) (transmit) and the G/T (receive). EIRP is the product of the peak radiated RF power and the antenna gain, and G/T is the ratio of the antenna gain to the system noise temperature. In comparing an ESA and an AESA for the same set of requirements, including antenna size and frequency which determine antenna gain (see Appendix A), the antenna gain is a given and equal for both. The insertion losses of the ESA phase shifters and BFN, however, make the ESA noise temperature greater than that of the AESA. If the ESA is to provide the same two-way performance (EIRP x G/T), it must make up for the higher noise temperature by increasing its radiated power. This in turn requires more DC power.

Figure 2-16 highlights the relative positions of the phase shifter and BFN losses for the ESA and AESA. The pre-LNA losses in the ESA will exceed those in the AESA by a factor equal to the product of the phase shifter loss and the BFN loss. Appendix A shows that increased pre-LNA loss is proportional to increased system noise temperature. With the ESA and AESA antenna gains the same, one must increase the ESA radiated RF power ($P_{t\text{-}esa}$) by the product of the phase shifter loss ($L_{p\text{-}esa}$) and the BFN loss ($L_{b\text{-}esa}$) to make up for the noise temperature (T) increase. This means that the ESA HPA must generate more RF power ($P_{h\text{-}esa}$) than the total number (n) of the AESA HPAs ($n\,P_{h\text{-}aesa}$) by a factor equal to the square of the product of the phase shifter loss and the BFN loss:

$$
\begin{aligned}
given: &\quad T_{esa} = L_{p-esa}\, L_{b-esa} T_{aesa} \\
given: &\quad P_{t-aesa} = n\,P_{h-aesa} \\
then: &\quad P_{t-esa} = L_{p-esa} L_{b-esa} P_{t-aesa} \\
and: &\quad P_{h-esa} = L_{p-esa} L_{b-esa} P_{t-esa} \\
\therefore &\quad P_{h-esa} = \left(L_{p-esa} L_{b-esa}\right)^2 \left(n\,P_{h-aesa}\right) \qquad (2.1)
\end{aligned}
$$

Translating these peak RF powers to average DC powers (P_d), one finds that the ratio of ESA to AESA DC power depends on the respective DC-to-RF efficiencies (η) as well as these insertion losses and the duty cycle (d):

$$P_{d-esa} = \frac{P_{h-esa} d}{\eta_{esa}}$$

$$P_{d-aesa} = \frac{P_{h-aesa} d}{\eta_{aesa}}$$

$$\frac{P_{d-esa}}{P_{d-aesa}} = \left(L_{p-esa} L_{b-esa}\right)^2 \frac{\eta_{aesa}}{\eta_{esa}} \tag{2.2}$$

Even though ESA HPA efficiencies can be greater than AESA HPA efficiencies, due to the peak power levels and amplifier technologies involved, they do not make up for the effect of the phase shifter and BFN losses except for perhaps very small, low-frequency arrays.

Considering the independent variable of antenna size, one concludes that it affects the BFN loss by virtue of the lengths of the transmission lines and the necessary power splits along the way. The BFN loss will increase with increasing antenna size. The phase shifter loss is not affected by the size of the antenna since each path through the antenna will still contain only one phase shifter. The increasing BFN loss causes the ESA HPA RF power to increase by the square of the BFN loss, which in turn causes the ESA HPA DC power to similarly increase (see Equations (2.1) and (2.2)). The ESA DC power increase may be moderated somewhat by an increase in HPA efficiency with increasing RF output power. The AESA HPA DC power is unaffected by the BFN loss increase to the first order, but it will increase due to the DC-to-RF efficiency reduction that comes with decreasing RF power per HPA (the result of increasing numbers of HPAs with increasing antenna size).

At the lower limit of antenna size (one element), the only difference between ESA and AESA is the location of the phase shifter. This will cause the ESA HPA DC power to exceed that of the AESA by a factor equal to the square of the phase shifter loss, assuming that the DC-to-RF efficiencies are the same. As antenna size increases, the ESA HPA DC power increases faster than that of the AESA due to the square of the BFN loss.

On the receive side, the DC power required by the ESA's single LNA is unaffected to the first order by increasing antenna size. The same is not true for the AESA LNA DC power. Since the number of AESA LNAs increases linearly with antenna size, the total AESA LNA DC power also increases linearly with antenna size. As noted earlier, total AESA LNA DC power has usually been much smaller than total AESA HPA DC power, but there is a point for very large antennas where the two become comparable. It is only at very large antenna sizes that the LNA DC power has any impact for the AESA.

The AESA has the DC power advantage over the ESA, an advantage that increases with increasing antenna size. This is due primarily to the phase shifter and BFN losses that the ESA must overcome with increased HPA RF power. It is noted that for these purposes all other DC power requirements for the two types of antennas are assumed to be equal.

Increasing frequency for a particular antenna size increases the total DC power for each antenna type. For the ESA the total DC power is increased by virtue of 1) increased phase shifter and BFN losses with frequency and 2) decreased DC-to-RF efficiency with frequency. For the AESA the total DC power is increased by virtue of 1) decreased DC-to-RF efficiency with frequency, 2) decreased DC-to-RF efficiency with decreasing RF power per HPA (due to increased numbers of HPAs), and 3) increased LNA DC power due to an increasing number of LNAs. The effect of the increased phase shifter and BFN losses is assumed to dominate the other impacts until one approaches the higher frequencies where solid-state amplifier technology becomes more inefficient. Therefore, the AESA DC power advantage increases with increasing frequency to a point where AESA implementation is no longer practical. Increasing beam steering coverage requires more phase shifters for the ESA and more T/R modules for the AESA for a given antenna size and frequency. More ESA phase shifters impacts ESA DC power only if more phase shifters mean more antenna elements, in which case the BFN loss will increase marginally due to additional power splits. The impact on DC power is greater for the AESA since more T/R modules mean 1) lower RF power per HPA and correspondingly lower HPA DC-to-RF efficiency and 2) more LNAs which increase the LNA DC power proportionally. Although the impact of increased steering coverage on AESA power is greater than that for the ESA, neither impact is particularly significant in relative terms.

Mass. The characteristic ESA/AESA difference that drives antenna mass is the AESA need for T/R modules versus the ESA need for phase shifters. Not only do the T/R modules include HPAs and LNAs in addition to phase shifters, they require DC power supplies and HPA energy storage facilities (capacitors) in close proximity. This is a mass comparison that the AESA loses as a result. The ESA mass advantage increases with antenna size.

There are other architectural differences that have marginal moderating impacts on the AESA T/R module mass disadvantage. First, the ESA HPA and LNA will have more mass than their AESA counterparts (transmit driver amplifiers and receive post-amplifiers) due to the power levels involved. Figure 2-17 shows these AESA components that are distributed as needed to compensate for AESA BFN losses. This ESA disadvantage is compounded by the fact that the ESA HPA and LNA probably each need to be redundant for reliability. As the antenna size increases both sides get heavier, but the marginal AESA advantage is assumed to be maintained. The same thing is expected to happen with increasing beam steering coverage. Second, the ESA BFN will likely be heavier than that of the AESA due to the relative importance of BFN insertion loss. This loss is not important for the AESA, and as a result the emphasis can be on minimizing mass. On the other hand, this loss is crucial for the ESA and must be the highest priority, often requiring a sacrifice of mass. This AESA advantage increases with increasing antenna size and beam steering coverage but probably decreases with increasing frequency. The latter claim reflects the stronger inverse mass-frequency relationship of low-loss transmission-line media (e.g., waveguide) to low-mass media (e.g., coaxial cable) along with the problems associated with the use of coaxial components at the very high frequencies.

Despite these moderating influences, the AESA still has a mass disadvantage that increases with antenna size. For a given antenna size, this disadvantage also increases with increasing frequency due to the corresponding increase in the number of T/R modules. Similarly, the AESA mass disadvantage increases with increasing beam steering coverage due to the increasing number of T/R modules.

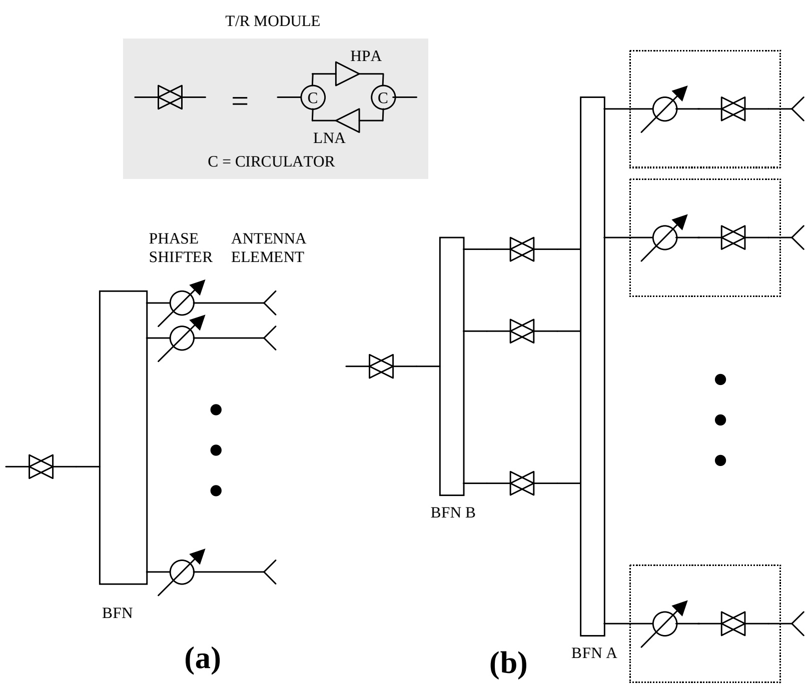

Figure 2-17 ESA (a) and AESA (b) block diagrams highlighting ESA amplifiers and AESA transmit driver amplifiers and receive post-amplifiers.

Cost. Cost is driven by the same characteristic architectural differences as mass, the most significant of which being the comparison of AESA T/R modules and associated electronics to ESA phase shifters. Specifically, since the total cost (non-recurring and recurring) of the combination of the AESA T/R modules, power supplies, and energy storage is higher than the corresponding cost of the ESA phase shifters, the AESA is at a cost disadvantage that will increase with increasing antenna size. The recurring (materials, fabrication, assembly, test) cost disadvantage (due to materials and testing) is linear with the number of T/R modules (phase shifters) as is the corresponding AESA mass disadvantage. The non-recurring (design and qualification) cost disadvantage (due to design, procurement, and test set-up) is more significant for smaller antennas.

The other two architectural differences, single versus distributed amplifiers and low-loss versus low-mass BFN, are expected to temper the ESA cost advantage but not eliminate it. The recurring cost of the single (or dual if redundant) ESA HPA and LNA will likely exceed that of the AESA transmit driver amplifiers and receive post-amplifiers (see Figure 2-17) due to the power levels involved as well as the fact that either AESA element-level T/R modules or other off-the-shelf amplifiers are often used for this purpose in the AESA. Any non-recurring engineering cost associated with the ESA single amplifiers only increases the ESA disadvantage. The cost of the BFN is also a disadvantage for the ESA since it is often a custom design with a lot of engineering behind it to achieve its low-loss performance. In contrast, the AESA BFN can be fabricated using off-the-shelf components with negligible design cost.

The radar platform incurs additional costs associated with the provision of high antenna DC power and the accommodation of high antenna mass. These costs are incurred because of the antenna DC power and mass and should be attributed to the antenna. In this case the AESA has a general advantage in DC power while the ESA has the advantage in mass. For these purposes the "impact" costs for DC power and mass are assumed to offset each other.

It is therefore assumed that the AESA is at an overall cost disadvantage driven by the higher total cost of the T/R modules (and associated electronics) but moderated by lower total costs for the driver/post amplifiers and the BFN. This disadvantage increases with the number of T/R modules and as a result increases with increasing antenna size, frequency, and beam steering coverage.

Summary/Evaluation. In general the AESA requires less DC power for all antenna sizes. The ESA requirement is driven by the square of the increasing BFN losses with antenna size. At the lower limit of antenna size (i.e., a one-element "array"), the ESA DC power exceeds that of the AESA by the square of the loss of the ESA phase shifter. The AESA requirement changes with antenna size due only to decreasing efficiency with decreasing RF power per HPA and the increasing impact of LNA DC power at the high end. With increasing frequency more power is needed, and its slope with antenna size is steeper. With increasing beam steering coverage, the AESA advantage is reduced somewhat since the AESA DC power will increase faster due to more T/R modules.

The AESA has a mass disadvantage, driven by T/R modules and associated DC power electronics, that increases with increasing antenna size, frequency, and beam steering coverage. The AESA has a cost disadvantage, driven by T/R modules and associated DC power electronics, that increases with increasing antenna size, frequency, and beam steering coverage.

2.3.2.3 ESA/AESA Technology Preference

Using antenna size, frequency, and beam steering coverage as independent variables, one can indicate the "efficiency" of each architecture within the resulting three-dimensional space, where “efficiency” in this context refers to the total amount of DC power, mass, and cost needed to deliver the required performance. The lower this amount the better.

Considering the metrics of DC power, mass, cost, and risk, the following conclusions can be drawn for the ESA and AESA architectures:

- ESA is preferred for smaller antenna sizes due to cost
  - All frequencies
  - All steering coverages
- ESA is preferred for larger antenna sizes and lower frequencies due to cost
  - All steering coverages
- AESA is preferred for larger antenna sizes and higher frequencies due to DC power
  - Becomes problematic due to cost as antenna size increases
  - Becomes problematic due to DC power as frequency increases
  - Becomes problematic due to cost and mass as steering coverage increases

These conclusions are presented graphically in Figure 2-18. The cross-hatching in the figure shows where each antenna type is preferred over the other, and the question marks show when even the preferred approach becomes problematic due to one or more of the metrics. Not surprisingly, there is no practical solution to the large-antenna-size, high-frequency, wide-steering problem (see 1 in Figure 2-18) using traditional antenna technology. Neither, however, is there a practical solution to the problem of moderate-size, high-frequency, and moderate steering (see 2 in Figure 2-18). Here the AESA that is preferred over the ESA due to power as a result of the larger antenna size becomes problematic due to the cost and mass associated with the additional T/R modules required to achieve the beam steering. Clearly, these are areas where there is opportunity for new, non-traditional antenna technologies to provide better solutions.

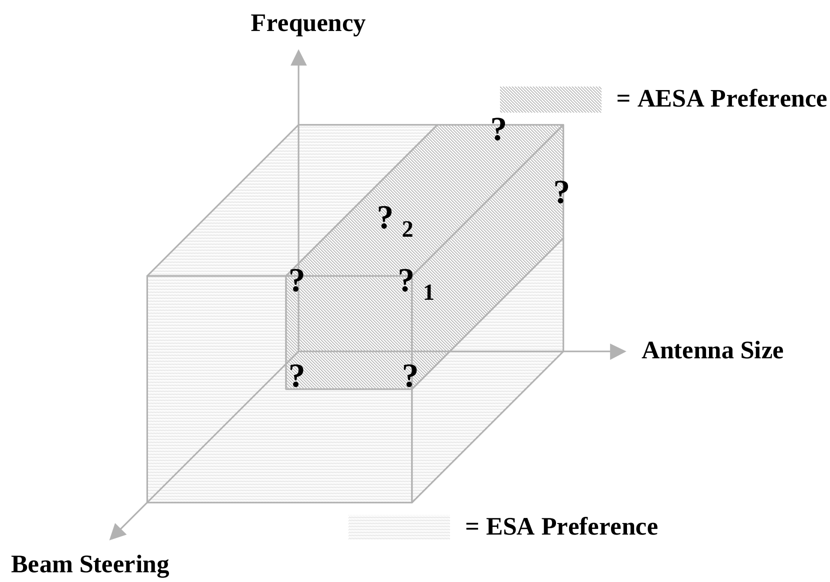

Figure 2-18 SAR antenna technology preference with electronic beam steering.

CHAPTER 3

SAR MISSION REQUIREMENT FLOWDOWN RESULTS

With the emphasis on sizing the radar antenna rather than the details of the radar electronics or digital data processing, Appendix A provides the system-level traceability from SAR mission requirements to SAR antenna requirements. The relationships developed in Appendix A that are key to the requirement allocation process are reproduced here. These relationships are indicative of the fact that the antenna is generally the most important component of the SAR system. All references utilized in the derivation of these relationships are cited in Appendix A.

3.1 Cross-Track Resolution

Image resolution in the dimension perpendicular to the direction of platform movement (i.e., cross-track) is the projection of radar resolution in the slant range dimension onto the surface being imaged (i.e., the Earth). Slant range resolution is typically provided by the bandwidth of the transmit pulse. Cross-track resolution is determined by Equation (A.4):

$$\delta_{ct} = R_e\left[\phi - \cos^{-1}\left(\frac{ck_f}{2B_rR_e} + \cos(\phi)\right)\right] \tag{A.4}$$

where δ_{ct} is cross-track resolution, R_e is the Earth's radius, ϕ is the incidence angle, c is the speed of propagation, k_f is the frequency weighting factor for the transmit pulse, and B_r is the bandwidth of the transmit pulse. One notices that cross-track resolution is independent of radar altitude or slant range.

3.2 Along-Track Resolution

The SAR processing technique provides image resolution in the dimension parallel with the direction of platform movement (i.e., along-track). Not only does the SAR technique synthesize a longer along-track aperture (and therefore narrower along-track beamwidth) over time, using the movement of the platform, but the resulting resolution is also independent of the slant range. Equation (A.15), under the assumption of sinc function beamwidths, provides the well-known result that the best along-track resolution available is roughly equal to one-half of the effective length of the real aperture in the along-track dimension:

$$\delta_{at} = \frac{k_r \pi L_e}{4(1.3915)} \approx 1.13 k_r \frac{L_e}{2} \qquad \text{(A.15)}$$

where δ_{at} is the along-track resolution, k_r is resolution degradation factor, and L_e is the effective along-track real aperture length.

3.3 Swath Width

Swath width is the cross-track width of the strip or swath covered by the radar's field of view as it moves by. Swath width is easily visualized by considering a single, fixed beam that paints a strip of Earth as the platform moves, the width of which is often the antenna's elevation beamwidth projected onto the curved Earth. Specifically, the swath width is calculated as the difference between the ground ranges corresponding to the boundaries of that portion of the antenna's elevation mainlobe being processed:

$$SW_p = R_e \left[\sin^{-1}\left(\frac{R_e + h_r}{R_e} \sin(\theta_n + \Delta\theta_p) \right) - \sin^{-1}\left(\frac{R_e + h_r}{R_e} \sin(\theta_n) \right) - \Delta\theta_p \right] \qquad \text{(A.22)}$$

where SW_p is the processed swath width, h_r is the altitude of the radar, θ_n is the look (elevation) angle at the beginning of the swath, and $\Delta\theta_p$ is the elevation portion of the mainlobe pattern processed beyond θ_n.

3.4 Range Ambiguity

The slant ranges of interest to imaging radars usually occupy a contiguous but small subset of the entire slant range domain. For this reason imaging radars can operate ambiguously in slant range as long as the slant range interval of interest does not exceed the maximum unambiguous range. The upper limit on the radar's pulse repetition frequency is based on the difference between the ambiguous slant ranges at the swath boundaries:

$$PRF \le \frac{c}{2\left(\Delta R_s + c\tau_t\right)} \tag{A.25}$$

where PRF is the pulse repetition frequency, ΔR_s is the slant range interval of interest (a function of the swath width and the incidence angle), and τ_t is the transmit pulsewidth.

3.5 Azimuth Ambiguity

In a manner analogous to slant range ambiguities, the radar's pulse repetition frequency also controls ambiguities in the doppler frequency domain. Platform motion in the azimuth direction (along-track) establishes the link between the instantaneous doppler frequency interval of interest and the antenna azimuth beamwidth. In this case the pulse repetition frequency must be greater than the maximum doppler frequency interval of interest to control azimuth ambiguities:

$$PRF \geq \frac{4v}{\lambda}\sin(\gamma_b)\left(\frac{1.3915\lambda}{\pi L_e}\right) \approx \frac{1.77v}{L_e}\sin(\gamma_b) \tag{A.26}$$

where v is the speed of the platform, λ is the radar wavelength, γ_b is the along-track angle of the beam relative to the velocity vector, and L_e is the effective length of the aperture in azimuth.

3.6 Radar Range Equation

Implied in the descriptions of resolution, swath width, and ambiguities is the detectability of the power levels of the target return echoes relative to the noise level in the radar electronics. The target signal-to-noise ratio that is calculated by the radar range equation is indicative of the detectability of a discrete target or the image quality of a distributed target. The radar range equation customized for imaging radars produces the following relationship for the integrated signal-to-noise ratio including the effects of range compression (pulse compression) and azimuth compression (SAR processing):

$$SNR_{ra} = \frac{P_t \tau_t PRF G_t G_r \lambda^3 \sigma^0 \delta_{ct} B_r}{(4\pi)^3 R_s^{\,3} k T_s k_f \, 2v B_{rx} l} \tag{A.38}$$

where SNR_{ra} is the integrated signal-to-noise ratio, P_t is the peak transmit power, τ_t is the transmit pulsewidth, PRF is the pulse repetition frequency, G_t is the transmit antenna gain, G_r is the receive antenna gain, λ is the wavelength, σ^0 is the mean backscatter coefficient of the Earth, δ_{ct} is the cross-track resolution, B_r is the transmit bandwidth, R_s is the slant range, T_s is the system noise temperature, k_f is the frequency weighting factor for the transmit pulse, v is the platform speed, B_{rx} is the receiver bandwidth, and l is a collection of losses. The integrated signal-to-noise ratio is usually adequate when it is greater than unity. This threshold is the basis for the noise-equivalent sigma zero parameter ($\sigma_{ne}{}^{0}$) which is the mean backscatter coefficient for which the integrated signal-to-noise ratio is unity:

$$\sigma_{ne}{}^{0} = \frac{(4\pi)^3 R_s{}^3 k T_s k_f \, 2 v B_{rx} l}{P_t \tau_t PRF G_t G_r \lambda^3 \delta_{ct} B_r} \tag{A.40}$$

3.7 Prime Power

The largest users of prime power in the SAR antenna are usually the HPAs on transmit and the LNAs on receive. For each individual HPA the average prime power consumed while the radar is operating ($P_{h\text{-}p}$) is proportional to the product of the peak RF power out of the amplifier ($P_{h\text{-}r}$), the transmit pulsewidth (τ_t), and the pulse repetition frequency (PRF):

$$P_{h-p} = \frac{\tau_t PRF}{\eta_{DC}} \left(\frac{P_{h-r} - \dfrac{P_{h-r}}{g}}{\eta_{PAE}} \right) = \frac{\tau_t PRF}{\eta_{DC}} \frac{P_{h-r}}{\eta_{PAE}} \left(1 - \frac{1}{g} \right) \tag{A.42}$$

where η_{DC} is the DC/DC conversion efficiency, η_{PAE} is the power-added efficiency of the amplifier, and g is the amplifier gain. The LNAs in the receive path are “on” longer (between pulses) than the HPAs but typically consume less power per amplifier. Assuming that the LNAs are “on” for the entire time between pulses, one calculates the average prime power per amplifier ($P_{l\text{-}p}$) as a function of the DC power required when the amplifier is on ($P_{l\text{-}d}$).

$$P_{l-p} = \frac{(1 - \tau_t PRF)}{\eta_{DC}} P_{l-d} \tag{A.44}$$

The total average prime power required by the radar when operating is the summation of all of the transmit amplifier, receive amplifier, and control electronics (phase shifters, switches, controller, etc.) requirements.

3.8 Data Rate

Imaging radars must eventually get their data to Earth for use. Where the missions are limited in time and the platform returns to Earth, the data are typically recorded on board and processed after the mission. For satellite-based radars or airborne radars producing time-critical data, the data must eventually be downlinked over a communication channel. The availability and capacity of this channel define the amount of on-board data storage required. The rate of SAR data produced by the radar is driven by the digital-sampling rate (f_s), which is a function of the signal bandwidth (B_r) required to achieve the necessary resolution:

$$f_s = k_s B_r \tag{A.48}$$

where k_s is the bandwidth oversampling factor. The SAR data sampling time period (t_s) is a function of the radar coverage:

$$t_s = \sum_i \left(\frac{2\Delta R_{si}}{c} + \tau_{ti} \right) \tag{A.49}$$

where i includes all of the pulses processed during the particular operational event, ΔR_s is the slant range interval processed between pulses, and τ_t is the transmit pulsewidth. Finally, the amount of SAR data produced during the operational event (e.g., orbit, sortie) determines the maximum on-board data storage requirement (D_r):

$$D_r = k_o\left(b_t + f_s b_s t_s\right) \tag{A.50}$$

where b_s is the number of bits per data sample, b_t is the total number of telemetry bits for the entire operational event, and k_o is the communication channel overhead factor.

3.9 Airborne vs Spaceborne Platforms

Subsequent chapters will consider representative SAR missions from either airborne or spaceborne platforms. In addition to the signal-to-noise ratio disadvantage due to the much longer slant ranges involved, the spaceborne platform has fundamental differences in achievable performance due to its higher speed. One can manipulate the expressions for along-track resolution (δ_{at}) and the slant-range interval (ΔR_s) that corresponds to the swath width to conclude that higher platform speed (v) necessarily implies either degraded resolution or a reduced swath:

$$\frac{\delta_{at}}{\Delta R_s} \geq \frac{1.77\pi}{2(1.3915)c} v \tag{A.51}$$

On the other hand the higher speed of the spaceborne platform positively impacts the area coverage rate (ACR). For the same swath width (SW) and azimuth footprint (FP_{az}), regardless of resolution, the spaceborne platform has a much shorter observation time (T_o), due to the speed (v), that translates to a higher area coverage rate:

$$ACR = \frac{SW\ FP_{az}}{T_o} \qquad ; \qquad T_o = \frac{FP_{az}}{v}$$

$$ACR = SW\ v \tag{A.52}$$

3.10 Antenna Parameter Selection

The complex relationships indicated in the previous paragraphs and developed in Appendix A must be carefully integrated to systematically allocate the mission-level requirements down to the antenna level. This integration task is shown in flow-diagram form in Figure 3-1. The mission-level SAR performance requirements (in the shaded boxes on the left-hand side of the figure) are used to generate constraints from which antenna-level requirements are chosen (boxes in italics). Subsequent calculations are integrated with the chosen antenna requirements to determine the transmit power required. The Excel model described in Appendices A and B is a guide through the SAR antenna requirement allocation process that will be used in later chapters to evaluate antenna solutions to representative SAR missions.

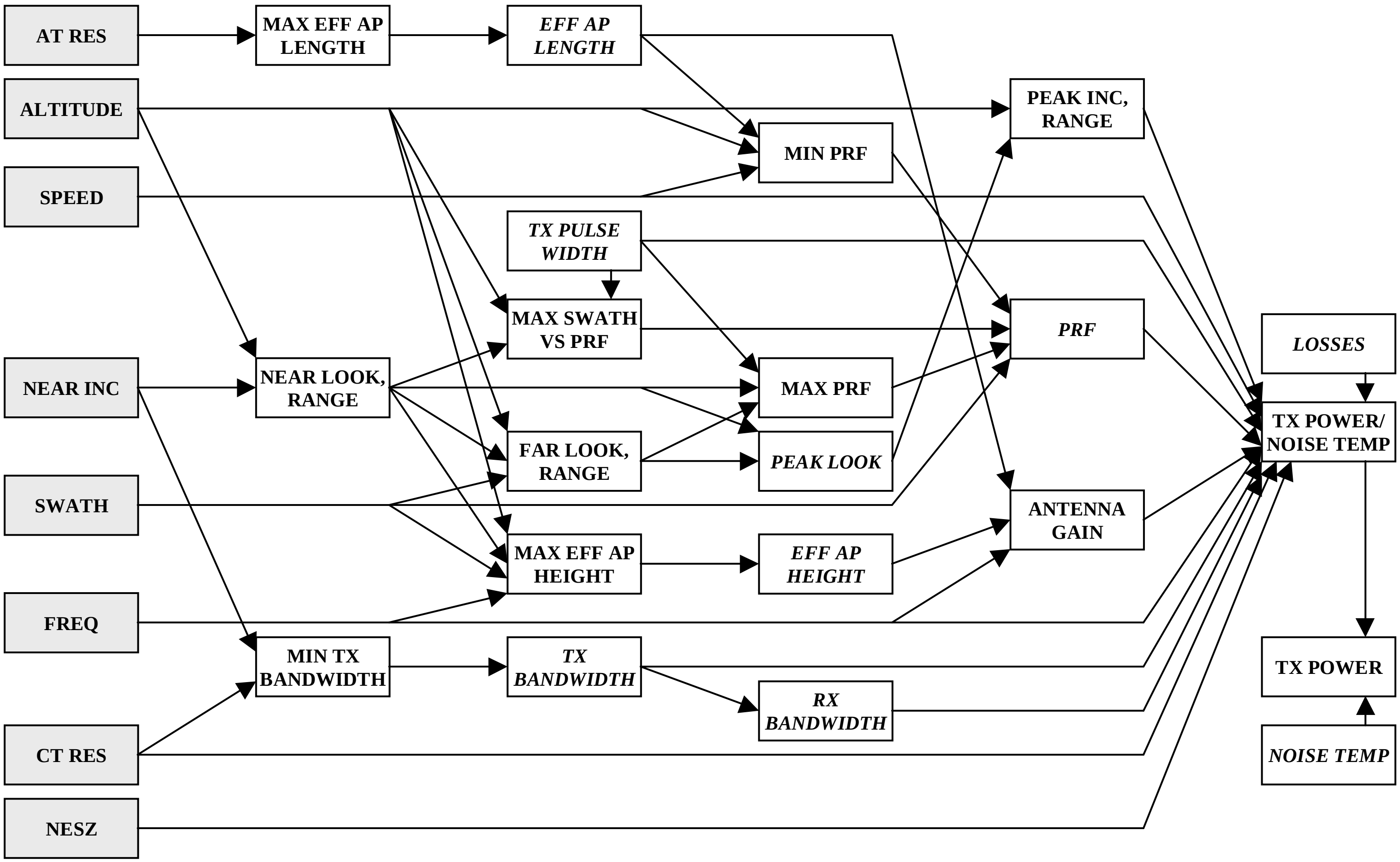

Figure 3-1 SAR mission-level performance requirement flowdown to antenna performance requirements.

CHAPTER 4

QUASI-OPTICAL ANTENNA TECHNOLOGY

This chapter introduces an alternative antenna technology known as Quasi-Optical (QO). This chapter summarizes the QO technology development to date and emphasizes its suitability for radar applications. As it pertains to antennas, QO technology uses spatial combining techniques to implement the transmit and receive BFN. In reference to Figure 4-1, spatial power combining is done, as with any ESA or AESA, with the RF signals radiating from the planar aperture on transmit. What distinguishes the QO radar antenna is that spatial combining is also done in the implementation of the BFN. The QO planar aperture is a discrete microwave lens that has antenna elements on the beamforming side to focus the receive signals to a common feed. On transmit, this common feed distributes the transmit signal to the lens via this same spatial beamforming network. The traditional ESAs or AESAs implement this BFN function via transmission lines and distribution networks that are electromagnetically constrained (e.g., coaxial cables, waveguides, microstrip/stripline circuits) as shown functionally in Figure 4-2.

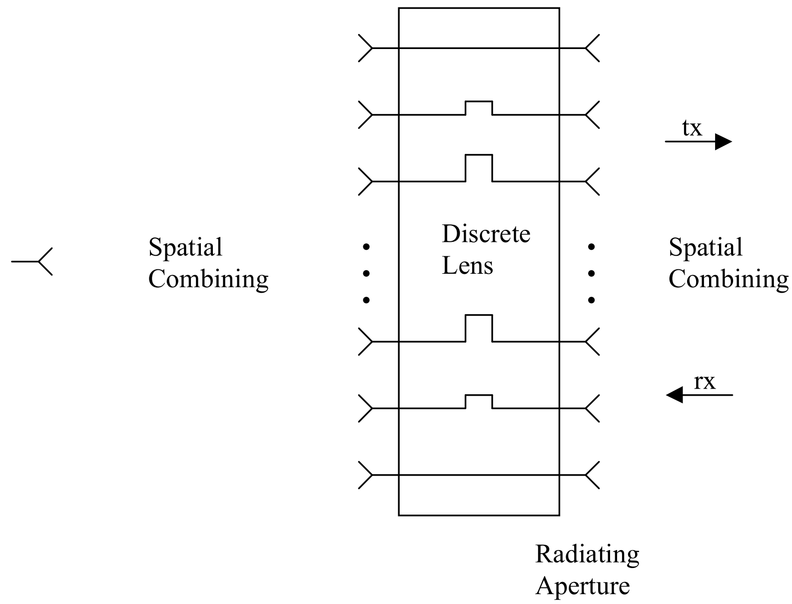

Figure 4-1 Quasi-Optical Antenna Functionality. Spatial combining/distribution techniques are used in antenna beamforming as well as radiation.

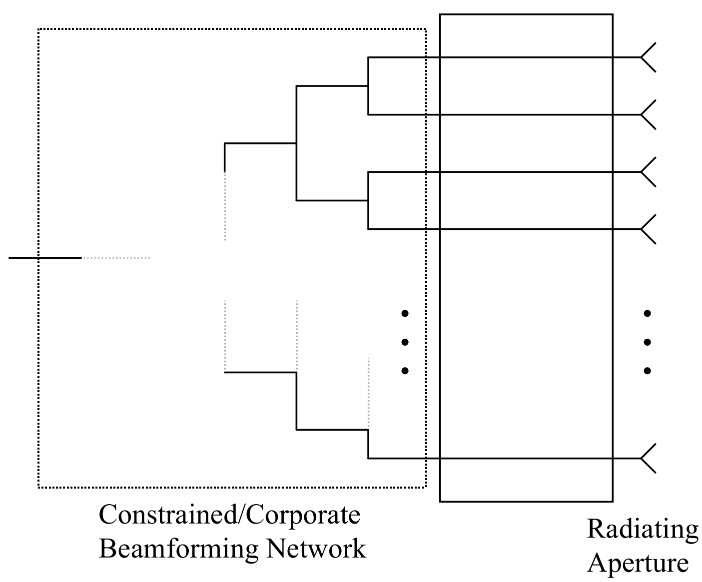

Figure 4-2 Traditional ESA or AESA antennas use constrained beamforming networks.

The passive QO lens shown in Figure 4-1 is analogous to a reflector that uses spatial beamforming to produce a plane wave from a common feed (see Figure 4-3). The reflector shape converts the spherical wave from the feed to a plane wave by virtue of its geometry.

The QO lens does this conversion electrically through the use of progressive delay lines (see Figure 4-4). The QO lens feeds the signals through its planar structure from one side to the other while the reflector reflects its incident energy back. The implementation is different, but the function is the same.

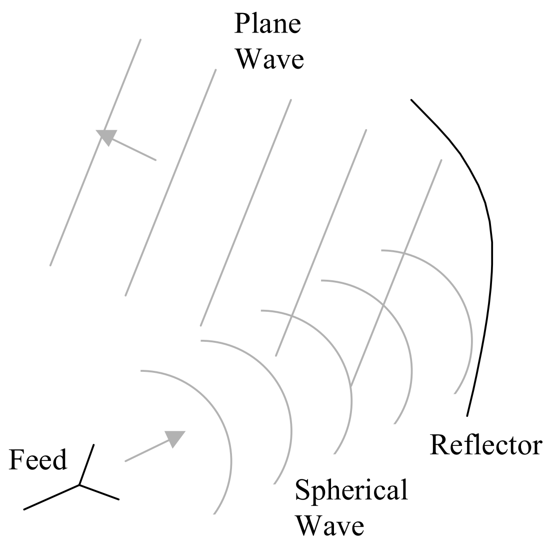

Figure 4-3 The offset-fed reflector is a geometric analog to the QO antenna.

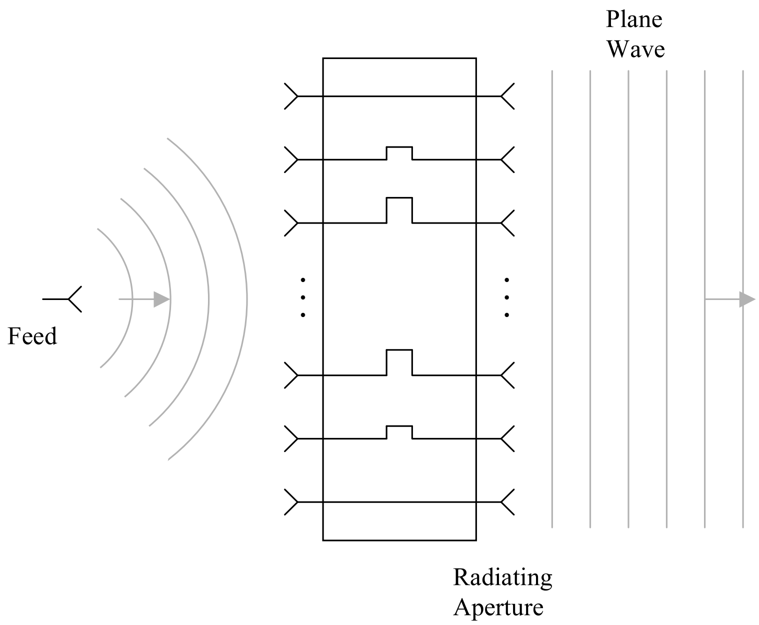

Figure 4-4 The planar QO antenna transforms a spherical wave to a plane wave electrically.

Given that the QO lens is the electrical analog of the reflector, it follows that plane waves at slightly different angles can be produced by moving the feed along the arc defining the location of the lens focus at different angles. In this way the QO antenna can produce steered beams without phase shifters. A switched-feed assembly with various feed ports along the focal arc (or a mechanically movable feed) coupled with a fixed, passive QO lens is the QO equivalent of the ESA (see Figure 4-5). One could go a step further and distribute the transmit and receive amplifiers within the passive QO lens to produce the QO equivalent of the AESA (see Figure 4-6).

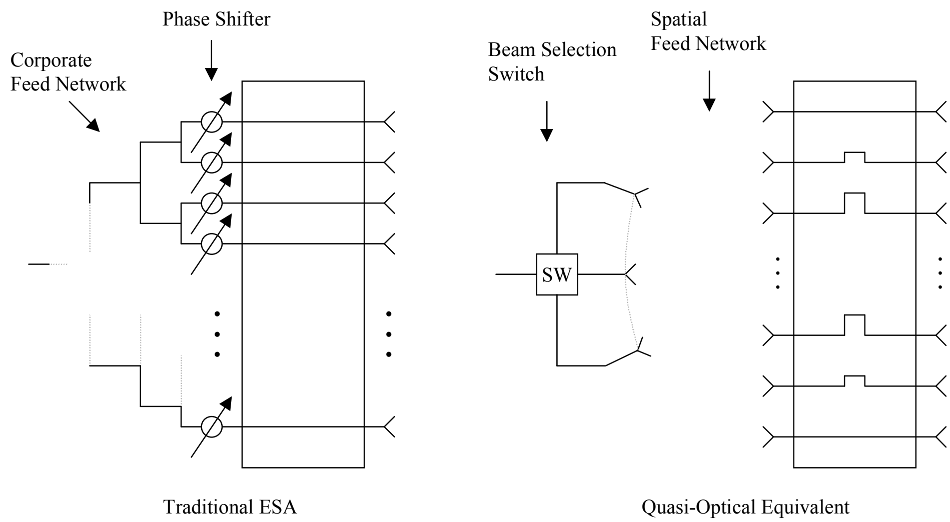

Figure 4-5 Traditional ESA vs QO equivalent.

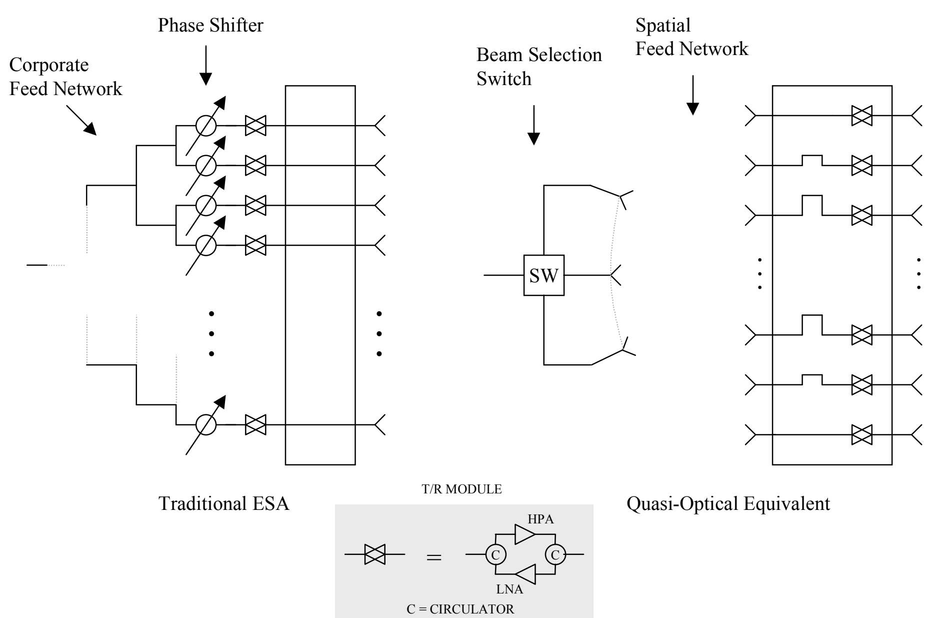

Figure 4-6 Traditional AESA vs QO equivalent.

QO antenna technology, therefore, includes analogous features of reflectors, passive electronically-scanned arrays, and active electronically-scanned arrays. Considering that each of these three traditional antenna technologies has its place for a given class of SAR applications, it is reasonable to expect that there will be SAR applications for which QO antenna approaches are attractive as well. The remainder of this chapter will describe QO antenna technology in more detail.

4.1 QO Technology Development To Date

The fact that active phased array antennas used in radar systems are efficient output (transmit) power combiners is the basis for the study of QO power combining [100]. As compared to traditional circuit power combining techniques, spatial power combining benefits from the elimination of lossy constrained transmission lines. It also has the advantage that its efficiency does not degrade with the number of active amplifiers being combined [101]. These features make QO power combining most promising at the millimeter-wave frequencies above 30 GHz where transmission-line losses are high and individual solid-state amplifier output power is low [102]. Today's era of research into active QO power combining was initiated in 1986 by James Mink [103]. True active QO power combiners are also spatially fed [104], leading to the consideration of open Gaussian-beam and closed-waveguide QO amplifier components [105].

Many QO array components have been designed with applications ranging from amplifier arrays to oscillator arrays, frequency-multiplier arrays, and beam-scanning/switching arrays, most of which can be classified either as grids or active arrays [106]. It is the active array architecture that is of interest here in applying QO technology to SAR due to its basis in classical phased array theory. The QO antenna for SAR applications would incorporate both spatial combining for aperture radiation and a spatial beamforming network, where the array aperture acts like a lens and used delay lines and element locations to collimate the spherical wave emanating from the feed [107]. Previous examples of this type of antenna are the Blass reflectarray [108] and the Rotman lens [109]. The Rotman lens is a multiple-beam implementation of the array formulation of the microwave lens originally introduced by Gent [110]. The planar array structure of the lens with printed elements on either side connected by delay lines was subsequently proposed by McGrath [111]. This planar implementation enables the integration of active amplifiers into the lens for efficiency in transmit power generation and dynamic range and noise figure improvement on receive [112].

While much work has been documented in passive and active discrete lens array development [113], two recent examples are illustrative. Stein Hollung [114] has designed and built the active X-Band transmit/receive lens amplifier shown in Figure 4-7. It is a 24-element aperture incorporating MESFET and PHEMT amplifiers on transmit and receive, respectively. The unit cell layout in Figure 4-8 shows the physical relationships between the amplifiers, the RF and DC circuitry, and the slot apertures for each of the 24 elements. Darko Popović [115] has designed and built the 3 x 15 element passive cylindrical lens shown in Figure 4-9. This lens is also X-Band but has dual-polarized patch elements on each side of the planar lens. At a focal length to diameter ratio (F/D) of 1.5 a directivity of 23 dB with beamwidths of 7° and 21° has been measured. Steered beams (see Figure 4-10) have also been measured out to 45° from aperture boresight via movement of the lens feed.

Figure 4-7 Active, transmit/receive, X-Band lens.

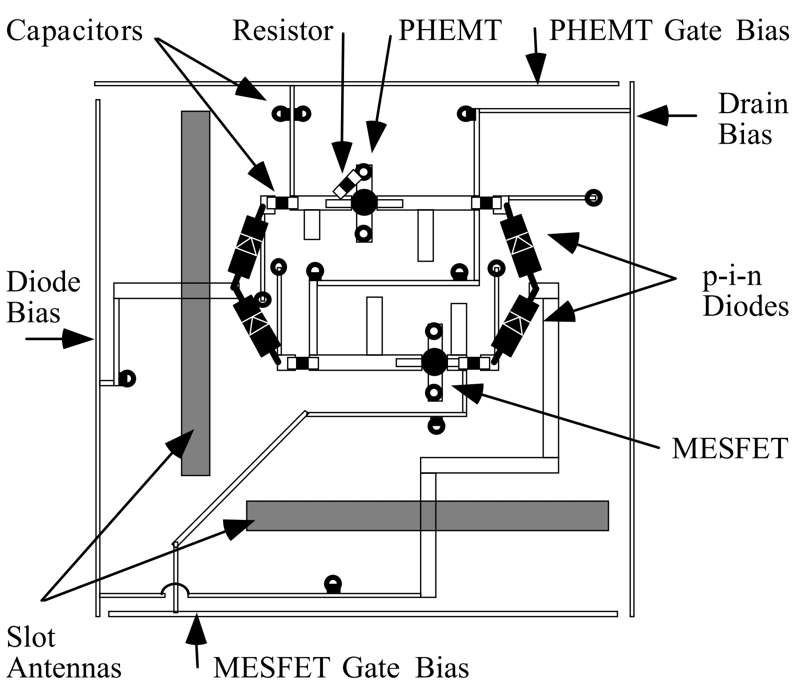

Figure 4-8 Active X-Band lens unit cell layout.

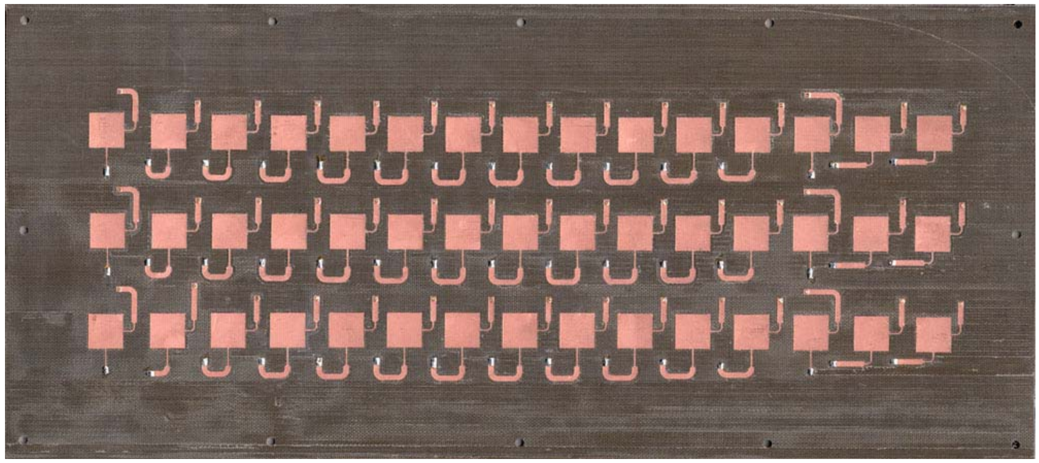

Figure 4-9 Passive, dual-polarized, X-Band, cylindrical lens.

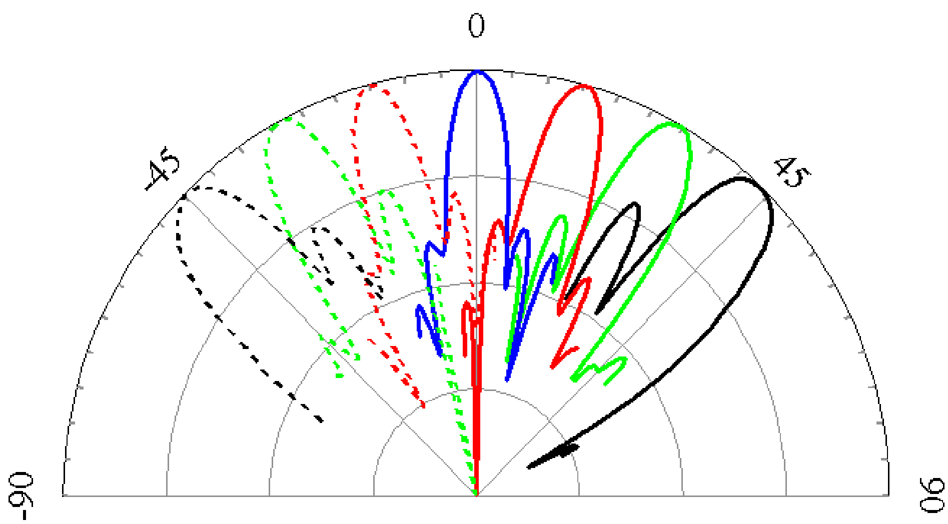

Figure 4-10 Cylindrical lens steered beams.

4.2 QO Antenna Uniqueness

The uniqueness of the generic QO antenna for radar applications lies not in its individual characteristics but rather in its combination of characteristics. The QO radar antenna has characteristic features of both reflectors and planar arrays. It has the spatial beamforming network of the reflector that offers low loss, low mass, and low cost. The spatial beamforming network does require a three-dimensional operational volume like the reflector along with precise location of the feed(s). The QO antenna can easily support multiple-beam operation via the implementation of additional feeds appropriately positioned. Efficient illumination of the lens by the feed(s) has to be balanced against spillover loss like the reflector. Limited beam steering can be provided without the use of phase shifters by moving the feed along the focal arc like the reflector. The QO lens has the aspect-ratio flexibility of the AESA and can implement distributed transmit and receive amplifiers if appropriate to achieve performance or maximize efficiency.

4.3 QO Antenna Parameters for SAR

Because of its unique implementation, some QO antenna SAR performance parameters are calculated in a slightly different way. This section describes how the SAR parameters of interest are determined for the QO antenna.

Antenna Gain. The gain or directivity of the QO aperture is calculated the same way as the AESA. Gain is proportional to the effective area of the radiating aperture and inversely proportional to the square of the wavelength. This applies to both transmit and receive antenna gain.

Radiated Power. The product of transmit antenna gain and radiated power is the EIRP which describes the antenna transmit contribution to the radar range equation. The radiated power (P_t) is the total power radiated from the aperture and is calculated the same as the AESA:

$$P_t = \sum_{i=1}^{N} \frac{PE_i}{LT_i} \tag{4.1}$$

where LT_i is the total ohmic-plus-mismatch loss of the ith element and PE_i is the transmit RF power at the input to the ith element. Relating PE_i back to the single-port transmit input to the

QO antenna involves the ohmic-plus-mismatch loss of the feed element (L_f), the transmit gain of the feed (GF_i) in the direction of the ith beamforming element, the range from the feed to the ith beamforming element on the lens (R_i), the receive gain of the ith beamforming element of the lens in the direction of the feed (GB_i), and the ohmic-plus-mismatch loss through the ith beamforming element to the input to the ith radiating element (LB_i) – see Figure 4-11. Assuming P_{in} at the input to the feed, one can use the Friis formula [13] to calculate PE_i:

$$PE_i = P_{in} \frac{GF_i}{L_f} \frac{1}{4\pi R_i^{\,2}} \frac{GB_i \lambda^2}{4\pi} \frac{1}{LB_i} \tag{4.2}$$

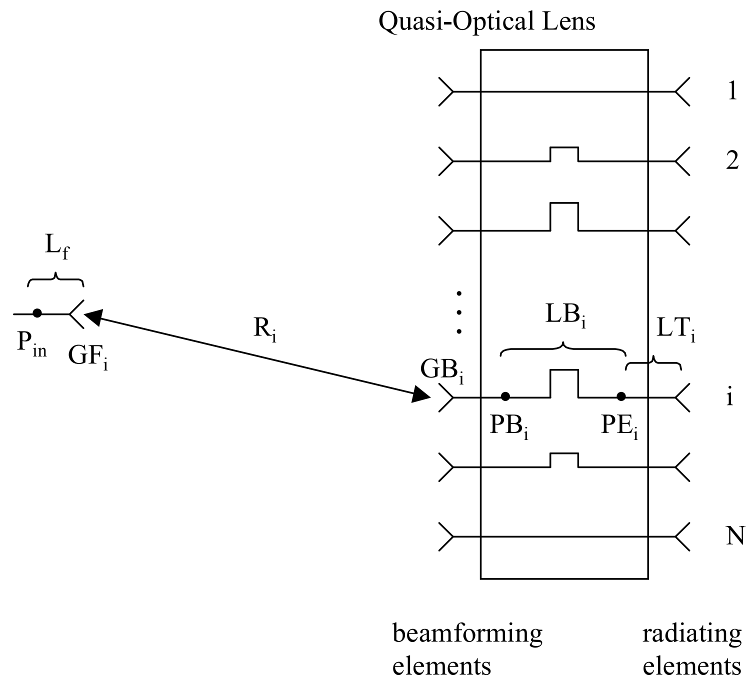

Figure 4-11 Parameters involved in calculation of gain of QO spatial beamforming network.

The transmit gain of the spatial beamforming network of the QO antenna can be determined by summing PB_i (see Figure 4-11) over all of the lens elements and dividing by P_{in}:

$$G_{BFN} = \frac{\sum_{i=1}^{N} PB_i}{P_{in}} \tag{4.3}$$

The calculation of the individual values of PB_i takes into account the radiation patterns of the feed and the lens elements as well as the location of the feed relative to the lens dimension (F/D) via the Friis formula:

$$PB_i = PE_i \, LB_i = P_{in} \frac{GF_i}{L_f} \frac{1}{4\pi R_i^{\,2}} \frac{GB_i \lambda^2}{4\pi} \tag{4.4}$$

Just as with a reflector one needs to consider both spillover loss and illumination loss [99] when evaluating the QO BFN gain. Since the beamwidths of the SAR aperture are as tightly coupled to system performance aspects (along-track resolution and swath) as to radar sensitivity (antenna gain), one can make the simplifying assumption that the feed illumination of the lens be kept as close to uniform as possible. This will minimize the broadening of the aperture beamwidths due to amplitude taper. This means a low illumination loss (relative to uniform illumination). The cost of this simplifying assumption is an increased spillover loss. To achieve near-uniform lens illumination, the feed must broaden its beam to over-illuminate the lens. With a broader feed beam, the lens intercepts less power thereby increasing the spillover loss.

Considering the example of a square lens, 0.14 m on a side, one calculates via Equation (4.3) a spillover loss of 3.9 dB along with an illumination loss of 0.7 dB. This assumes a horn feed located at an F/D of 1.4 producing a lens-edge amplitude taper of 2 dB. This total transmit gain of –4.6 dB is representative in that comparable gains can be obtained via different combinations of the available degrees of freedom. This representative gain will remain representative as the lens increases in size since the spillover and illumination geometries remain the same with constant F/D.

Noise Temperature. The ratio of the receive antenna gain to the system noise temperature describes the antenna receive contribution to the radar range equation. The QO antenna system noise temperature (T_s) has four distinct components: external noise seen by the QO radiating aperture, noise generated internal to the QO lens, external noise seen by the QO feed, and noise generated internal to the feed and the rest of the receive chain [87]. These are combined, assuming that the receive reference point is the (receive) input to the radiating elements of the QO aperture (see Figure 4-12), according to:

$$T_s = \left(T_{ea} + T_a\right) + \left(T_{ef} + T_f\right)\frac{1}{G_{af}} \tag{4.5}$$

where T_{ea} is the external noise input to the QO aperture, T_a is the internal noise generated by the QO lens at the receive reference point, T_{ef} is the external noise input to the QO feed, T_f is the internal noise generated by the feed and the rest of the receive chain referenced at the input to the feed, and G_{af} is the net gain from the receive reference point to the input of the QO feed. T_s in Equation (4.5) is referenced at the input to the QO aperture (the receive reference point).

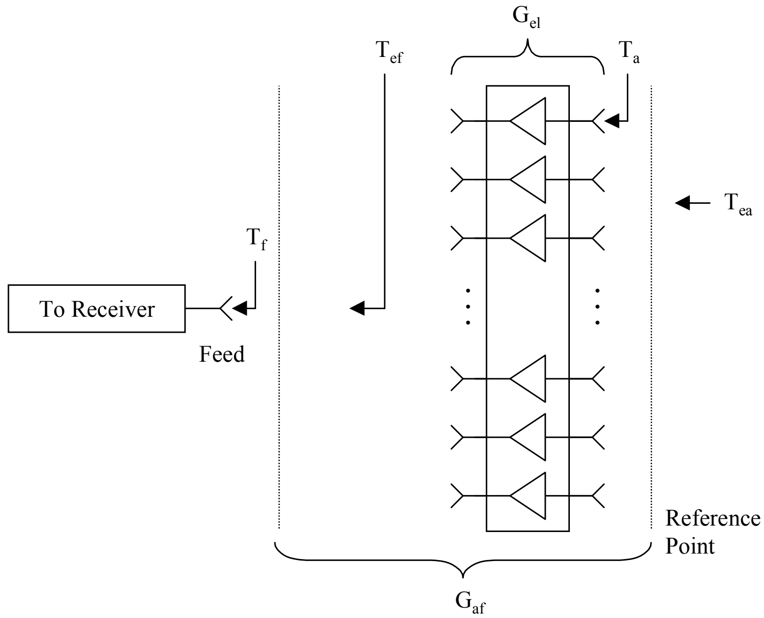

Figure 4-12 Generic QO Block Diagram Showing Noise Temperature Components and Reference Points.

The external noise input to the QO array is a directivity-weighted ($D(\theta,\phi)$) sum of all of the external noise temperatures ($T_n(\theta,\phi)$) in the array's field of view (Ω) [88]:

$$T_{ea} = \frac{1}{4\pi}\int_{4\pi} D(\theta,\phi)T_n(\theta,\phi)d\Omega \tag{4.6}$$

For earth-imaging antennas, the Earth temperature of 290K fills the main beam and thereby drives T_{ea} to 290K.

The internal noise generated by the QO lens (T_a) is a weighted average of the internal noise generated by each discrete path (TA_i) through the lens, where the weight is the relative contribution of each string (c_i):

$$T_a = \frac{\sum_{i=1}^{N} TA_i \, c_i}{\sum_{i=1}^{N} c_i} \qquad (4.7)$$

For the ideal case where all paths are identical and contribute identically, T_a equals TA_i for all i. TA_i is calculated at the input to the i^{th} aperture element using standard terms:

$$TA_i = T_{PREi}\left(L_{PREi} - 1\right) + T_o\left(NF_i - 1\right)L_{PREi} + T_{POSTi}\left(L_{POSTi} - 1\right)\frac{L_{PREi}}{G_i} \qquad (4.8)$$

where T_{PREi} is the temperature of the element and transmission line preceding the i^{th} LNA (if present), L_{PREi} is the ohmic loss of that element and transmission line, T_o is 290K, NF_i is the noise figure of the i^{th} LNA (if present), G_i is the gain of the i^{th} LNA (if present), T_{POSTi} is the temperature of the element and transmission line following the i^{th} LNA (if present), and L_{POSTi} is the ohmic loss of that element and transmission line.

The external noise input to the QO feed is the background noise that enters the QO feed pattern outside the angular region occupied by the QO lens. As such, it is calculated using Equation (4.6) excluding the angular region occupied by the lens. The worst-case assumption is that the Earth temperature of 290K is seen at all angles outside the lens region. This results in an external noise temperature input to the QO feed of 290K weighted by an average feed-pattern sidelobe level outside the lens region.

The internal noise generated by the QO feed and all of the downstream receive components (switches, circulators, transmission lines, post-amplifiers, receivers) referenced at the input to the QO feed (T_f) is:

$$T_f = T_r\left(L_r - 1\right) + T_r\left(NF_r - 1\right)L_f \tag{4.9}$$

where T_r is the temperature of the feed and the downstream receive components, L_f is the ohmic loss of the feed, and NF_r is the equivalent noise figure looking into the downstream receive components.

Finally, the net gain between the receive reference point and the input to the QO feed (G_{af}) is necessary to properly sum all of these noise components as indicated in Equation (4.5). This gain is the product of the electronic gain of the QO lens (G_{el}) and the gain of the spatial beamforming network (G_{BFN}):

$$G_{af} = G_{el}\ G_{BFN} \tag{4.10}$$

The electronic gain of the QO lens is an average of the electronic gains of the individual receive paths:

$$G_{el} = \frac{1}{N}\sum_{i=1}^{N}\frac{G_i}{L_{PREi}\ L_{POSTi}} \tag{4.11}$$

If all of the receive strings in the QO array are identical, G_{el} equals the electronic gain of any individual receive string. The receive gain of the beamforming network (G_{BFN}) is the same as the transmit gain of the QO BFN calculated in Equation (4.3).

4.4 QO Technology Promise for SAR

Relative to the reflector, the QO antenna can have the advantages and disadvantages listed in Table 4-1. Relative to the AESA, the QO antenna appears to have the advantages and disadvantages listed in Table 4-2.

Advantage	Disadvantage
2D vs 3D aperture – less deployed volume, easier stowage/deployment	**Cost and mass of distributed RF amplifiers**
Low-power feed	**More complicated DC power distribution**
Low-power feed switching for beam steering	
No blockage	
More efficient in terms of DC power	
Higher reliability through graceful degradation	

Table 4-1 Apparent QO Antenna Advantages and Disadvantages Relative to Reflectors.

Advantage	Disadvantage
No phase shifters required for beam steering	**3D volume required for operation**
Low-loss BFN – higher DC power efficiency	**More complicated deployment due to feed**
Low-mass BFN	**Less inherent beam steering granularity, extent**
Wide-bandwidth BFN	
Simple accommodation of multiple beams	

Table 4-2 Apparent QO Antenna Advantages and Disadvantages Relative to AESAs.

The significance of these advantages and disadvantages depends on the particular set of performance requirements. The next chapter will perform a detailed extrapolation of evolving SAR requirements and will suggest an area in the multi-dimensional SAR requirement space where QO antenna technology may be competitive. Corresponding future SAR missions will be subsequently configured so that their requirements can be used for comparative evaluations of QO antenna approaches and traditional SAR antenna approaches.

CHAPTER 5

REPRESENTATIVE SAR MISSIONS FOR QO EVALUATION

This chapter will describe in detail the representative SAR mission characteristics that will be used to evaluate the use of QO antenna technology relative to those traditionally used. The idea is to identify a class of SAR missions for which QO antenna technology is competitive or even preferable. These representative SAR missions will be determined according to the distinguishing features of QO antenna technology. Detailed antenna requirements for these missions will then be allocated according to the procedure summarized in Chapter 3.

5.1 Mission Requirements

Given the potential advantages and disadvantages of QO antenna technology, relative to the traditional antenna approaches, noted in Section 4.4, what types of SAR missions should be considered for detailed evaluation?

Relative to the reflector, the QO antenna still requires a three-dimensional space for operation but provides a planar aperture for ease of deployment and aspect-ratio flexibility. It can be more efficient in terms of RF power radiation but at the cost of transmit and receive amplifier distribution. It can have higher reliability and better accommodation of beam steering requirements since the feed does not have to handle as much RF power. It is noted that both approaches can practically support only limited electronic beam steering requirements. SAR missions for which these characteristics would be important are those requiring high RF radiated power, exaggerated azimuth/elevation aperture aspect ratios, high reliability, and limited beam steering.

Relative to the AESA, the QO antenna can offer equally-efficient RF power radiation with a beamforming network that has wider bandwidth capability and lower mass and loss. It features electronic beam steering without the need for phase shifters, thereby reducing complexity and cost, but its beam steering capability is limited in terms of extent and/or granularity. While it does provide the same aperture aspect ratio flexibility of the AESA, it requires a three-dimensional space for operation and a different deployment sequence. SAR missions for which these relative advantages would be important are those requiring high RF radiated power, wide bandwidth, and limited beam steering while allowing a three-dimensional operational structure.

Table 5-1 combines these selected mission characteristics. The need for high radiated RF power can imply the use of small apertures (in terms of wavelengths) and/or high-resolution (small resolution cells) operation. The need for rectangular apertures can imply wide-swath coverage and/or high-resolution stripmap operation. The need for high reliability is more critical to operational success of a space instrument versus an airborne instrument, but reliability is also critical to the maintenance costs of an airborne instrument. Limited beam steering can imply a sensor that is used more for either scientific monitoring or strategic (versus tactical) surveillance. Sensors with limited beam steering probably have wide instantaneous-swath coverage and provide high-resolution (small resolution cells) along-track performance in the stripmap mode. The need for wide bandwidths can imply high-resolution (small resolution cells) operation and/or spaceborne operation at widely-spaced frequencies to correct for ionospheric perturbations of radar performance. Finally, the accommodation of a three-dimensional operational space can imply either a spaceborne antenna of any size or a relatively-small airborne antenna. These possible mission implications are collected in Table 5-2.

Characteristic	Relative to Reflector	Relative to AESA
High radiated RF power	**X**	
Rectangular apertures	**X**	
High reliability	**X**	
Limited beam steering		**X**
Wide bandwidth		**X**
3D operational space		**X**

Table 5-1 Favorable mission characteristics for QO antenna technology.

Characteristic	Mission Implication
High radiated RF power	**Small apertures**
	High resolution
Rectangular apertures	**Wide instantaneous swaths**
	High-resolution stripmap coverage
High reliability	**Space (fault tolerance)**
	Airborne (minimal maintenance cost)
Limited beam steering	**Scientific, strategic**
	Wide instantaneous swaths
	High-resolution stripmap coverage
Wide bandwidth	**High-resolution cross-track performance**
	Space (atmospheric calibration)
3D operational space	**Space**
	Small airborne apertures

Table 5-2 Implications for mission characteristics favorable to QO antenna technology.

QO antennas would seem to be attractive in high-resolution (small resolution cells) SAR missions from the standpoints of the instantaneous bandwidth needed for cross-track resolution and the high radiated RF power needed given the small resolution cells and the short azimuth aperture needed for along-track stripmap resolution. High-resolution (small resolution cells) stripmap operation is also consistent with limited beam steering in the along-track dimension. Limiting electronic beam steering in the cross-track dimension requires relatively-wide instantaneous swaths which in turn limit the elevation aperture. Coupled with high-resolution operation this requires high RF radiated power.

High-resolution, wide-swath SAR operation from airborne or spaceborne platforms would therefore appear to afford QO antenna technology its best chance of success relative to the traditional antenna technologies. In the context of the past, present and future SAR missions noted in Chapter 2, example requirements for such a mission are developed below.

For a space application, resolution on the order of 1 m with a swath on the order of 25 km would seem attractive. Alternatively, wider swaths (~100 km) at the expense of poorer resolution (~10 m) are also desirable. For systems such as this, a low-earth orbit (LEO) seems appropriate, and the range of incidence angles over which the performance is provided is of secondary importance.

From an airborne platform, better resolution should be achievable (0.3 m) at the cost of some swath (~10 km). Altitudes in the range of 12-18 km seem reasonable. For scientific purposes the incidence angle coverage may be of secondary importance, but strategic military applications likely prefer larger incidence angles from the standpoint of survivability.

5.2 Antenna Requirements

In postulating future SAR missions for which QO antenna technology may be applicable, one naturally considers performance improvements relative to previous or current missions. These often come down to improvements in the two fundamental SAR performance parameters – resolution and swath width. While the combination of finer resolution (smaller resolution cells) and wider swath is attractive, the two turn out to be mutually exclusive.

These two fundamental performance parameters are linked by the selection of the PRF. Appendix A develops the equations for the minimum (Equation (A.26)) and maximum (Equation (A.25)) PRFs as a function of the effective azimuth aperture length (L_e) and the equivalent swath width interval in slant range (ΔR_s):

$$PRF_{\min} = \frac{1.77v}{L_e}\sin(\gamma_b) \approx \frac{2v}{L_e}$$

$$PRF_{\max} = \frac{c}{2(\Delta R_s + c\tau_t)} \approx \frac{c}{2\Delta R_s} \tag{5.1}$$

With the best available along-track resolution (δ_b) being approximated by half the effective aperture length and with the slant range interval being approximately translated to swath width according to Figure 5-1, Equations (5.1) are put together to form the approximate PRF inequality:

$$\delta_b \approx \frac{L_e}{2} \quad , \quad SW \approx \frac{\Delta R_s}{\sin(\phi)}$$

$$PRF_{\min} \approx \frac{2v}{L_e} \approx \frac{v}{\delta_b}$$

$$PRF_{\max} \approx \frac{c}{2\Delta R_s} \approx \frac{c}{2SW\sin(\phi)}$$

$$\frac{v}{\delta_b} \leq PRF \leq \frac{c}{2SW\sin(\phi)} \tag{5.2}$$

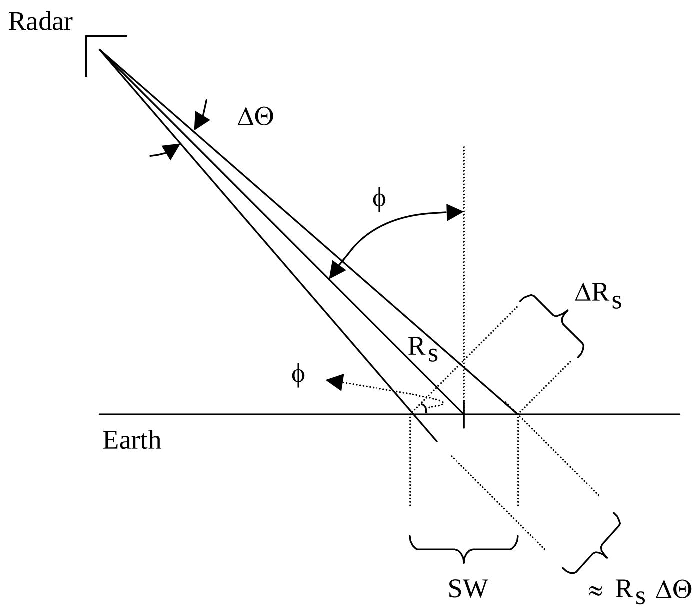

Figure 5-1 Approximate (flat-earth) relationships between swath (SW), slant range interval (ΔRs), and look angle interval (RΔΘ).

By assuming that the maximum PRF is greater than or equal to the minimum PRF, one can relate resolution and swath:

$$\frac{v}{\delta_b} \le \frac{c}{2SW\sin(\phi)}$$

$$SW \le \delta_b \left(\frac{c}{2v\sin(\phi)} \right) \tag{5.3}$$

Equation (5.3) indicates that swath and best available resolution are linearly related and the achievable swath is less than the straight line relating the two parameters. For small resolution cells the maximum swath achievable is also small. For larger resolution cells (poorer resolution), wider swaths are possible.

This relationship can be examined in another light by relating the approximate inequality in Equation (5.2) to antenna aperture dimensions (L_e, H_e) rather than SAR performance parameters:

$$PRF_{\min} \approx \frac{2v}{L_e} \quad , \quad PRF_{\max} \approx \frac{c}{2\Delta R_s}$$

$$\Delta R_s \approx R_s \Delta\theta \tan(\phi) \quad , \quad \Delta\theta \approx \frac{\lambda}{H_e} \quad , \quad \lambda = \frac{c}{f}$$

$$\therefore \ \frac{2v}{L_e} \leq PRF \leq \frac{c}{2\Delta R_s} \approx \frac{fH_e}{2R_s \tan(\phi)}$$

$$and \quad \frac{2v}{L_e} \leq \frac{fH_e}{2R_s \tan(\phi)} \quad or \quad H_e L_e \geq \frac{4vR_s \tan(\phi)}{f} \qquad (5.4)$$

H_e is inversely proportional to L_e, and acceptable values of H_e are above the curve described in Equation (5.4). The interpretation is that for short azimuth aperture lengths (L_e) the only acceptable aperture heights (H_e) are much larger. Short aperture lengths mean high resolution, and large aperture heights mean narrow swaths. For long aperture lengths both small and large aperture heights are possible, meaning that poorer resolution can be achieved with either narrow or wide swaths.

Equation (5.3) indicates that the slope of the swath-versus-resolution line is inversely proportional to the speed of the platform and the sine of the incidence angle. It follows that wider swaths can be achieved for given resolution from slower platforms and/or at small incidence angles. As a result, wider swaths for given resolution and incidence angle can be had from airborne platforms as opposed to spaceborne platforms, and wider swaths for given resolution and platform speed can be achieved nearer nadir than the horizon.

Equation (5.4) indicates that the curve relating effective antenna height to effective antenna length depends on platform speed, slant range, incidence angle, and frequency of operation. As platform speed increases the curve moves up, meaning that larger aperture heights (narrower swaths) are needed for given resolution. Slant range and incidence angle both increase as the image location moves away from nadir, also moving the curve up. Finally, increasing frequency brings the curve back down.

When considering the narrow swaths that come with high-resolution operation, one should determine the beam pointing accuracy required to image the target area of interest. While wide swaths can be somewhat forgiving, narrow swaths leave little room for beam pointing error. Assuming a flat-earth model and a maximum beam pointing error of half the elevation beamwidth, that maximum error can be shown to be inversely proportional to the platform altitude for a given swath and incidence angle. The result is that a narrow swath can be more easily located from an airborne platform, and the use of a narrow swath from a spaceborne platform requires much more accurate beam pointing.

These relationships contribute to the following observations:

1) One can do high-resolution, narrow-swath stripmap processing from airborne platforms more easily than from spaceborne platforms. One may have to rely on spotlight operation to achieve comparably-high resolution from space.
2) Rectangular antenna aspect ratios (long in the along-track dimension and short in the cross-track dimension) are popular for SAR. For airborne platforms, such antennas are physically compatible with fuselage mounting. For spaceborne platforms, such antennas are necessary to achieve wide instantaneous swaths.
3) Square antenna aspect ratios are more practical for airborne platforms. Because of the slant range difference, a square antenna from space must have a much larger aperture

area. In addition to the cost and deployment issues associated with the large antenna, the large aperture height produces a narrow swath that is difficult to accurately locate.

Airborne Antenna Requirements. The first airborne reference case is postulated with both high resolution and wide swath access in mind. In this case electronic beam steering in elevation provides enhanced elevation field of view. High along-track resolution is provided via stripmap operation using a short antenna with no azimuth beam steering. These stripmap reference-case parameters are listed in Table 5-3. Another possible airborne reference case utilizes electronic beam steering in azimuth to achieve high-resolution coverage via spotlight operation. Mechanical pointing of the antenna in elevation (via aircraft attitude) provides area access in the range dimension. This is the Joint STARS mission as briefly described in Chapter 2.

Parameter	Airborne Stripmap Requirement
Frequency (GHz)	9.6
Polarization	HH
Swath Width (km)	4-8
Altitude (km)	12
Speed (m/s)	300
Aperture Size (m x m) (el x az)	0.14 x 0.48
Pulsewidth (μsec)	12
PRF (Hz)	5000
Bandwidth (MHz)	800
Elevation Beam Steering (deg)	+/- 8.5
Azimuth Beam Steering (deg)	None
Avg Sensitivity (dB Wm^4/K)	-39.7
Resolution (m)	0.3
Noise Equiv Sigma Zero (dB)	-21
Incidence Angles (deg)	40-65

Table 5-3 Reference case antenna requirements for high-resolution stripmap performance from an airborne platform.

Spaceborne Antenna Requirements. There are two spaceborne reference cases, one featuring one-meter-class resolution and the other offering wide instantaneous swath capability and elevation field of view. The wide-swath mission uses a long azimuth aperture for wide-swath coverage at moderate resolution. Electronic beam steering in elevation enables wider elevation access or field of view. The high-resolution mission provides stripmap coverage of a narrower instantaneous swath through use of a smaller azimuth aperture. Elevation beam steering can similarly position the narrow instantaneous swath in the range dimension. Antenna parameters for these two spaceborne missions are shown in Table 5-4.

Parameter	Space Wide-Swath Mission	Space High-Res Mission
Frequency (GHz)	9.6	9.6
Polarization	HH	HH
Swath Width (km)	70-88	15
Altitude (km)	800	800
Speed (m/s)	7450	7450
Aperture Size (m x m) (el x az)	0.5 x 13	1.85 x 1.85
Pulsewidth (μsec)	30	8
PRF (Hz)	1850	9905
Bandwidth (MHz)	60	400
Elevation Beam Steering (deg)	+/- 6.7	+/- 6.7
Azimuth Beam Steering (deg)	None	None
Avg Sensitivity (dB Wm^4/K)	11.5	17.7
Resolution (m)	7	1
Noise Equiv Sigma Zero (dB)	-21	-21
Incidence Angles (deg)	21-41	24-40

Table 5-4 Reference case antenna requirements for dual-mode performance from a spaceborne platform

CHAPTER 6

QUASI-OPTICAL ANTENNA EVALUATION FOR AIRBORNE SAR

This chapter documents the comparative evaluation of QO antenna solutions for the airborne SAR mission described in Chapter 5. QO antenna solutions are compared to the traditional AESA antenna solution in terms of the power, mass, and cost resources required to achieve the required RF performance. The AESA and QO antenna design work is high level in nature and not intended to be a thorough electromagnetic analysis. Its purpose is to describe the antenna approaches in sufficient detail to estimate the fundamental characteristics of mass, power, and cost. The antenna requirements for the airborne SAR mission used as the basis for this comparison are listed in Table 5-3.

6.1 AESA Antenna Solution

To achieve the ±8.5° electronic beam steering required in elevation without grating lobes, the AESA must have phase control at a spacing of 0.87λ or less according to the following [90]:

$$spacing \leq \frac{\lambda}{1+\left|\sin(8.5)\right|} = 0.87\lambda \tag{6.1}$$

Considering a 0.15m elevation dimension, this spacing results in 5.5 phase control points in elevation. Increasing this to the next-higher integer number of 6 results in a spacing of 0.8λ, which is acceptable for beam steering. The 800 MHz instantaneous bandwidth will cause the beam to squint in elevation by about 0.7° if non-true-time-delay phase shifters are used for steering. This is acceptable considering the elevation beamwidth is about 10.6°.

Using this 0.8λ spacing for the antenna radiating elements in both dimensions, one determines that 120 total elements are needed, 6 in elevation and 20 in azimuth. Solving for total radiated power from the absolute sensitivity requirement (RS_{abs} - see Equation (A.58)), one concludes that the necessary peak transmit power per element is roughly 2 W:

$$RS_{abs} = \frac{P_t \tau_t PRF A_e^{\ 2}}{T_s} \quad or \quad P_t = \frac{RS_{abs} T_s}{\tau_t PRF A_e^{\ 2}} \tag{6.2}$$

given the RS_{abs}, τ_t, PRF, and A_e requirements in Table 5-3 and an estimate of 650K for T_s. Given this value and the current state-of-the-art in solid-state power amplifiers at X-Band, the traditional distributed-amplifier approach is to have an HPA at each element. A pulsed-radar application like this one does not usually have significant HPA linearity requirements. As a result a power-added efficiency of 35% is used for these distributed HPAs [116]. One does not need a phase shifter at each element, however, since electronic beam steering is required only in elevation. This leads to an architecture where the 20 elements in azimuth are combined per row followed by a MMIC phase shifter per row. Considering the loss of the MMIC phase shifter and the 20-way combiner, distributed LNAs are needed at each element to minimize the system noise temperature. Figure 6-1 also shows an HPA driver amplifier and an LNA post-amplifier at the input to the antenna, primarily to provide the necessary transmit drive level to the distributed HPAs.

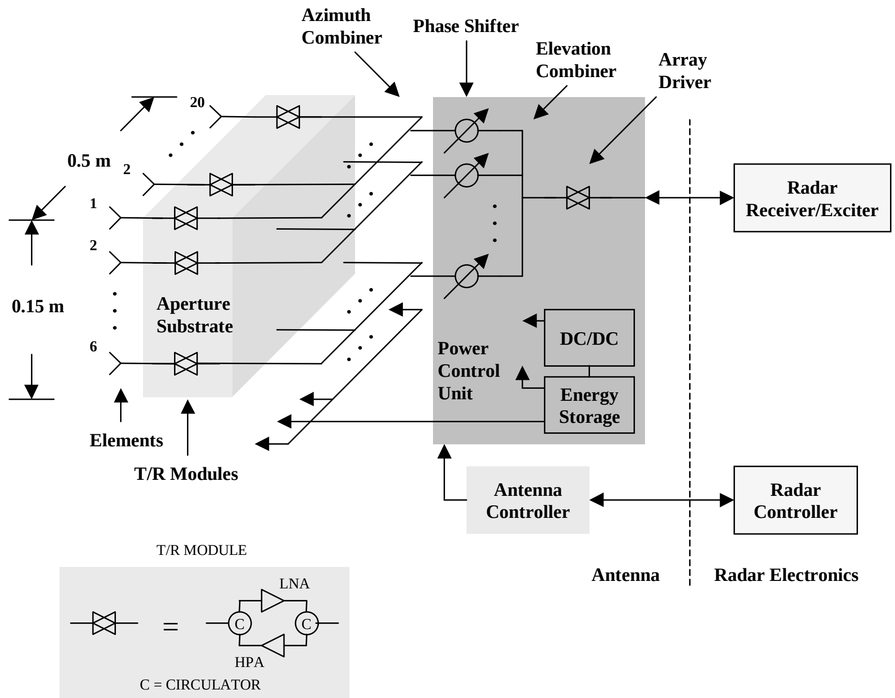

Figure 6-1 AESA antenna block diagram for airborne high-resolution stripmap reference SAR mission.

Given an external input noise temperature of 290K, representative of looking directly at the Earth, Figure 6-2 calculates the actual system noise temperature, an estimate of which was used in Equation (6.2) to estimate the per-element radiated power. Figure 6-2 also shows transmit signal levels throughout the antenna and estimates the prime power required by the antenna amplifiers to produce the required RF performance. It is not surprising that the prime power is driven by that needed for the element-level HPAs for which a power-added efficiency of 35% is assumed.

Sensitivity (dB Wm4/K)	-39.7
Effective Elevation Aperture (m)	0.1425
Effective Azimuth Aperture (m)	0.475
Pulsewidth (ms)	12
PRF (Hz)	5000
HPA Duty Cycle (%)	6
LNA Duty Cycle (%)	50
number of elements	120
ambient temperature (C)	0
DC/DC conversion efficiency (%)	75
System Noise Temperature (K)	630
Array Transmit Power (W)	246
Element Transmit Power (W)	2.0

Component	Receive Ohmic Loss (dB)	Receive Amp Gain (dB)	Receive Amp NF (dB)	Receive Combine (ways)	CW DC Power (mW)	Transmit Ohmic Loss (dB)	Transmit Amp Gain (dB)	Transmit Eff (%)	Sys Noise (K)	Transmit Loss (dB)	Input Power (dBm)	Output Power (dBm)	Quantity	Receive Prime Power (W)	Transmit Prime Power (W)
external									290.0						
element	0.3	na	na	na	na	0.3	na	na	19.5	0.3	33.4	33.1	120		
feedthrough	0.2	na	na	na	na	0.2	na	na	13.8	0.2	33.6	33.4	120		
amplifier interface	1	na	na	na	na	0.8	na	na	79.3	0.8	34.4	33.6	120		
amplifier	na	20	1.5	na	50	na	30	35	169.0	-30.0	4.4	34.4	120	4.0	75.6
amplifier interface	0.8	na	na	na	na	0.8	na	na	0.8	0.8	5.2	4.4	120		
transmission line	0.5	na	na	na	na	0.5	na	na	0.6	0.5	5.7	5.2	120		
az combine/divide	2	na	na	20	na	2	na	na	3.0	15.0	20.7	5.7	6		
transmission line	0.5	na	na	na	na	0.5	na	na	1.0	0.5	21.2	20.7	6		
phase shifter	5	na	na	na	na	5	na	na	20.0	5.0	26.2	21.2	6		
el combine/divide	0.8	na	na	6	na	0.8	na	na	5.9	8.6	34.8	26.2	1		
amplifier interface	0.8	na	na	na	na	0.8	na	na	7.1	0.8	35.6	34.8	1		
amplifier	na	20	1.5	na	50	na	20	35	18.5	-20.0	15.6	35.6	1	0.0	0.8
amplifier interface	0.8	na	na	na	na	0.8	na	na	0.1	0.8	16.4	15.6	1		
transmission line	1	na	na	na	na	1	na	na	0.1	1.0	17.4	16.4	1		
receiver interface	0.5	na	na	na	na	na	na	na	0.1				1		
receiver	na	na	4	na	na	na	na	na	1.2				1		
													subtotals	4.0	76.5
													total		80.5

Figure 6-2 AESA antenna RF performance for airborne high-resolution stripmap reference SAR mission.

Figures 6-3 and 6-4 in turn estimate the antenna mass and cost. The element-level HPAs and LNAs are assumed to be integrated into the antenna substrate without the individual packaging that often drives mass and cost. The DC/DC converters and energy storage capacitors are housed in the 6-way divider/phase shifter unit. One sees that the beamforming network behind the element-level amplifiers is significant to both mass and cost.

	Unit Mass (g)	**Qty**	**Total Mass (kg)**
aperture length (m)		*0.5*	
aperture height (m)		*0.15*	
number of panels		*1*	
radiating element density (g/sqm)		3138	
structural panel density (g/sqm)		*6858*	
radiating element substrate	235	1	0.2
structural panel	514	1	0.5
Beamforming Network			
element T/R modules	*10*	*120*	1.2
T/R RF cables	*15*	*120*	1.8
20-way	*100*	*6*	0.6
20-way RF cables	*10*	*6*	0.1
6-way, PS, driver, PCU	1100	*1*	1.1
panel RF cables	*110*	*1*	0.1
PCU DC cables	*40*	*1*	0.0
controller	*3500*	*1*	3.5
controller DC cables	*1290*	*1*	1.3
		subtotal	10.4
		20% contingency	2.1
		total	12.5

Substrate Layup	**g/sqm**
paint - 2 mil	*107*
elements - 50%, 1/2 oz Cu	*79*
substrate - 50 mil Duroid	*2794*
ground plane - 1/2 oz Cu	*158*
	3138

PCU Mass	
number of power supplies	*20*
power supply unit mass (g)	*20*
capacitor mass factor	*1.5*
	g
substrate + housing	*500*
power supplies + caps	*600*
	1100

Figure 6-3 AESA antenna mass for airborne high-resolution stripmap reference SAR mission.

	Unit Cost (k$)	Qty	Total Parts Cost (k$)
radiating element substrate	*0.3*	*1*	0
structural panel	*0.3*	*1*	0
Beamforming Network			
element T/R modules	*0.5*	*120*	60
element T/R RF cables	*0.05*	*120*	6
20-way	*0.75*	*6*	5
20-way RF cables	*0.05*	*6*	0
6-way, PS, driver, PCU	12.3	*1*	12
panel RF cables	*0.3*	*1*	0
PCU DC cables	*0.5*	*1*	1
controller	*5*	*1*	5
controller DC cables	*1*	*1*	1
		subtotal	91
		20% contingency	18
		total	109

PCU Cost	
unit T/R ($)	*500*
unit phase shifter ($)	*200*
unit power supply ($)	*500*
number of phase shifters	*6*
number of power supplies	*20*
capacitor cost factor	*1.01*
housing + substrate	*500*
T/R + phase shifter parts	1700
power supplies + caps	10100
	12300

Figure 6-4 AESA antenna cost for airborne high-resolution stripmap reference SAR mission.

6.2 Fully-Distributed QO Antenna Solution

This alternative antenna approach is an active microwave lens with HPAs and LNAs at each lens element. Refer to Chapter 4 for an operational description. To achieve the ±8.5° electronic beam steering in elevation without grating lobes, the QO antenna has the same element spacing requirements as the AESA. Section 6.1 concludes that 6 elements spaced 0.8λ apart are sufficient in elevation for beam steering coverage. The 800 MHz instantaneous bandwidth will cause no squint in elevation since no phase shifters are used for beam steering.

Using the 0.8λ spacing for the antenna radiating elements in both dimensions, one determines that 120 total elements are needed, just like the AESA. Solving for total radiated power from the absolute sensitivity requirement, one concludes that the necessary peak power per element is on the order of 2W.

Beam steering or beam switching is provided in elevation by the implementation of a separate feed horn at the end of the QO space feed for each beam. Using the viewing geometry noted in Table 5-3, one concludes that the required incidence angle range can be covered with a collection of three separate beams at different angles. The QO antenna will operate by selecting one of three fixed elevation beam positions rather than “steering” a given beam to different positions. Figure 6-5 shows the functional block diagram of the fully-distributed QO antenna approach. With a 3:1 aspect ratio for the radiating aperture, it is reasonable to consider a single horn as the feed element for each of the three beams. A calculation similar to the one done for the square (1:1) aspect ratio lens in Section 4.3 confirms that the representative BFN loss determined there (4.6 dB, including spillover and non-uniform illumination effects) is indeed representative. By adjusting the degrees of freedom available (F/D, feed gain, and feed pattern), one can achieve a comparable total loss for this 3:1 aspect ratio. It is noted that the illumination loss increases slightly with the rectangular lens but can be offset with a slight reduction in spillover loss.

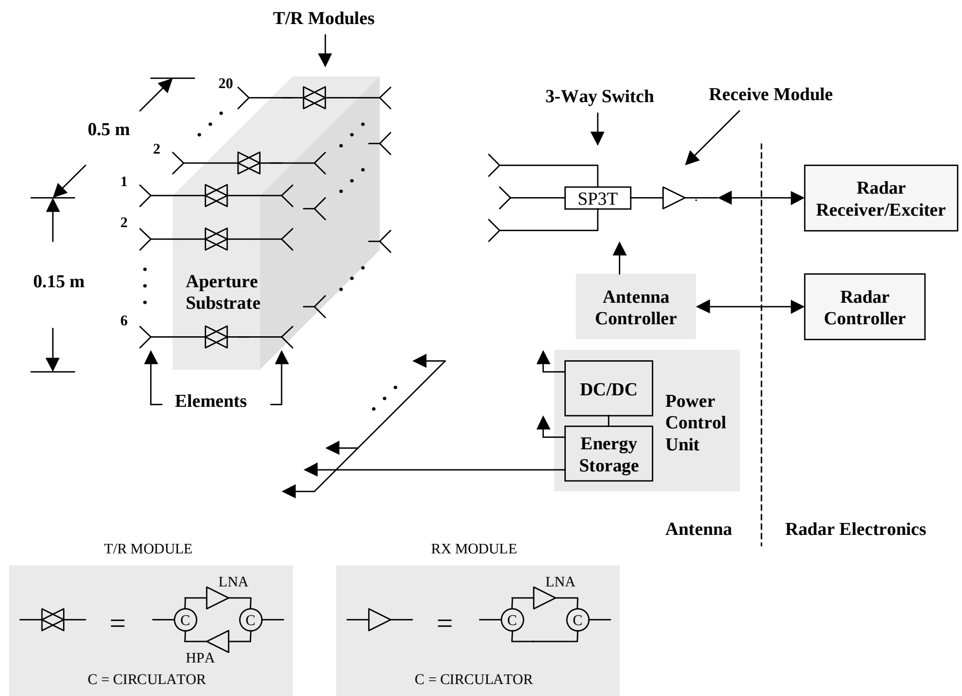

Figure 6-5 Fully-distributed QO antenna block diagram for airborne high-resolution stripmap reference SAR mission.

Given the external input noise temperature of 290K, representative of looking directly at the Earth, Figure 6-6 calculates the actual system noise temperature. This calculation is customized for the QO antenna according to the relationships described in Section 4.3. The unique features of this calculation are 1) the addition of an external noise input to the feed horn and 2) the net gain of the spatial BFN. As described in Section 4.3 the external noise input that enters the feed horn by bypassing the lens is calculated like any normal external noise input but with the appropriate parameter assignments. The worst-case assumption is that the feed horn is looking at 290K outside the perimeter of the lens aperture, where the feed horn radiation pattern is decreasing with angle. The result is an external noise input at the input to the feed horn equal to the product of 290K and the average radiation pattern of the feed outside the angular extent of the lens aperture. The assumption in Figure 6-6 is that this average radiation pattern is –10 dB.

Sensitivity (dB Wm4/K)	-39.7				
Effective Elevation Aperture (m)	0.14				
Effective Azimuth Aperture (m)	0.48				
Pulsewidth (ms)	12	avg spillover level (dB)	-10		
PRF (Hz)	5000	spillover loss (dB)	3.8	System Noise Temperature (K)	610
HPA Duty Cycle (%)	6	illumination loss (dB)	1		
LNA Duty Cycle (%)	50				
				Array Transmit Power (W)	241
number of elements	120			Element Transmit Power (W)	2.0
ambient temperature (C)	0				
DC/DC conversion efficiency (%)	75				

	Receive Ohmic Loss (dB)	Receive Amp Gain (dB)	Receive Amp NF (dB)	Receive Combine (ways)	CW DC Power (mW)	Transmit Ohmic Loss (dB)	Transmit Amp Gain (dB)	Transmit Eff (%)	Sys Noise (K)	Transmit Loss (dB)	Input Power (dBm)	Output Power (dBm)	Quantity	Receive Prime Power (W)	Transmit Prime Power (W)
external primary									290						
outer element	0.3	na	na	na	na	0.3	na	na	19.5	0.3	33.3	33.0	120		
feedthrough	0.2	na	na	na	na	0.2	na	na	13.8	0.2	33.5	33.3	120		
amplifier interface	1.0	na	na	na	na	0.8	na	na	79.3	0.8	34.3	33.5	120		
amplifier	na	20	1.5	na	50	na	30	35	169.0	-30.0	4.3	34.3	120	4.0	74.2
amplifier interface	0.8	na	na	na	na	0.8	na	na	0.8	0.8	5.1	4.3	120		
transmission line	0.2	na	na	na	na	0.2	na	na	0.2	0.2	5.3	5.1	120		
inner element	0.3	na	na	na	na	0.3	na	na	0.3	0.3	5.6	5.3	120		
space feed	na	-4.8	0	120	na	na	-25.6	na	0.0	25.6	31.2	5.6	1		
external secondary									1.7						
feed	1.2	na	na	na	na	1.2	na	na	5.0	1.2	32.4	31.2	1		
transmission line	0.3	na	na	na	na	0.3	na	na	1.5	0.3	32.7	32.4	1		
beam switch	0.8	na	na	na	na	0.8	na	na	4.5	0.8	33.5	32.7	1		
transmission line	0.3	na	na	na	na	0.3	na	na	1.9	0.3	33.8	33.5	1		
amplifier interface	0.8	na	na	na	na	0.8	na	na	5.8	0.8	34.6	33.8	1		
amplifier	na	20	1.5	na	50	na	30	35	15.1	-30.0	4.6	34.6	1	0.0	
amplifier interface	0.8	na	na	na	na	0.8	na	na	0.1	0.8	5.4	4.6	1		
transmission line	1.0	na	na	na	na	1.0	na	na	0.1	1.0	6.4	5.4	1		
receiver interface	0.5	na	na	na	na	0.5	na	na	0.1				1		
receiver	na	na	4	na	na	na	na	na	0.9				1		
													subtotals	4.0	74.9
													total		78.9

Figure 6-6 Fully-distributed QO antenna RF performance for airborne high-resolution stripmap reference SAR mission.

The net gain of the spatial beamforming network is used to translate noise temperature values between the lens components and the feed components as described in Section 4.3. The spatial BFN does not contribute its own noise temperature component since no power is dissipated as heat. Figure 6-6 uses Equation (4.2) to determine the average transmit gain from the feed element to the *N* individual elements of the lens. The figure shows transmit signal levels throughout the antenna and estimates the prime power required by the antenna amplifiers to produce the required RF performance. The same assumptions regarding amplifier gains, noise figures, and efficiencies made for the AESA are made here for the QO approach to normalize the comparison. While one might argue with particular assumptions or question their continued applicability over time, it is the relative consistency that is more important for this comparison.

Figures 6-2 and 6-6 show that the prime power requirements for the AESA and the fully-distributed QO antenna, for this airborne SAR mission, are comparable. Even though the QO spatial BFN has less loss than the AESA BFN (9.1 dB versus 10.3 dB, both without amplifiers), the distribution of transmit and receive amplifiers in both cases equalizes their efficiencies.

This is justified via reference to the generic calculations in Figure 6-7 for the AESA. The upper equation shows that the loss of the AESA BFN (with amplifiers) is reduced by the gain of the HPA. Without the gain of the HPA, the BFN loss would not be reduced from the total of the BFN ohmic losses (10.3 dB in this airborne case). System noise temperature can be shown to be proportional to the noise figure of the distributed LNA and the portion of the BFN loss preceding the LNA (assuming the gain of the LNA is sufficiently large). Without the presence of the LNA, the system noise temperature is instead proportional to the product of the receiver noise figure and the entire BFN loss. This is significant for the following two reasons. The distributed-LNA noise figures can be lower than the receiver noise figure (1.5 dB versus 4 dB for this airborne case) since they do not have to accommodate as large an input power level. Also, the pre-LNA loss is often only a small portion of the entire BFN loss (1.5 dB versus 10.3 for this airborne case). The system noise temperature is therefore reduced due to the distribution of LNAs by 11.3 dB. Given a two-way sensitivity requirement allocated down from the SAR mission requirements and essentially equal to the product of the antenna EIRP and G/T, one concludes that the DC power necessary to deliver the required performance is proportional to the noise figure of the LNA and the square of the pre-LNA BFN loss.

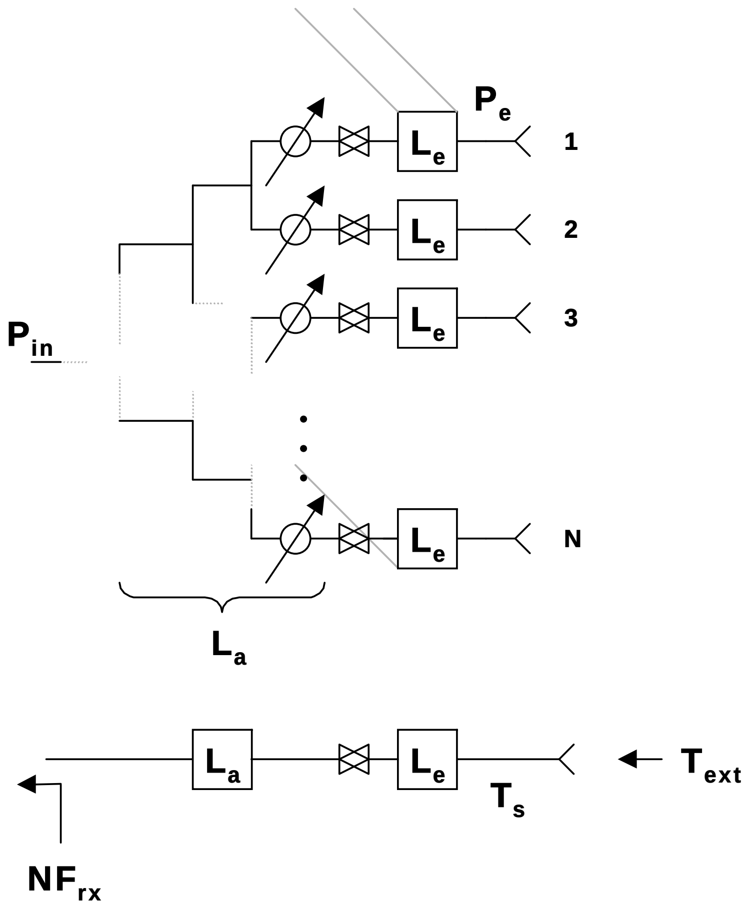

$$\frac{P_{in}}{\sum P_e} = \frac{L_a L_e}{G_{HPA}}$$

- **Distributed HPAs generate transmit power**

$$T_s = T_0 NF_{LNA} L_e$$

- **T_0 = 290K**

- **Assume G_{LNA} is sufficiently large**
- **LNA NF can be lower than receiver**
- **L_e is only pre-LNA loss**

$$S = \frac{\sum P_e d A^2}{T_s}$$

- **2-way sensitivity**

$$P_{dc} = \left(\frac{L_a}{G_{HPA}} + 1\right)\frac{S\,T_0\,NF_{LNA} L_e{}^2}{\eta_{dc} A^2} + P_{LNA}$$

- **DC power reduced due to L_e and NF_{LNA}**

Figure 6-7 Generic beamforming network efficiency calculations for the AESA.

With reference to Figure 6-7, the assumptions are that the gain of the HPA is much greater than the pre-HPA BFN loss and that the DC power required for the collection of distributed LNAs is small relative to that required by the HPAs. Without the presence of the distributed LNAs and HPAs, the total DC power is instead proportional to the noise figure of the receiver and the square of the loss of the entire BFN. Figure 6-8 shows these calculations for the passive ESA.

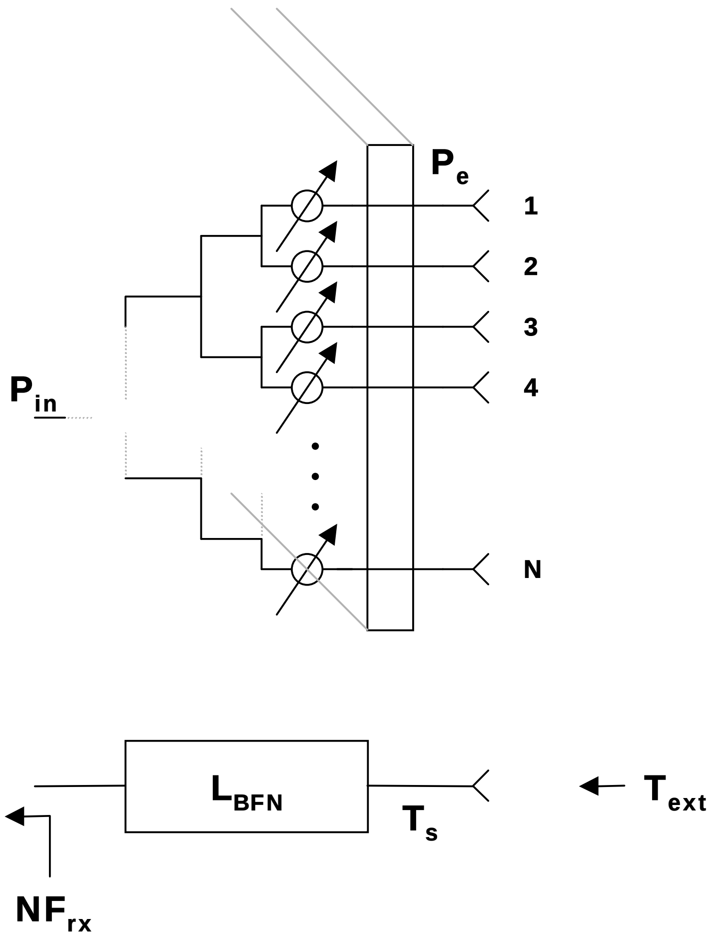

$$\frac{P_{in}}{\sum P_e} = L_{BFN}$$

- **Transmission lines, phase shifters**
- **Lost power dissipated as heat**

$$T_s = T_0 NF_{rx} L_{BFN}$$

- **$T_0 = 290$K**

- **Earth-facing**
- **BFN losses produce noise**

$$S = \frac{\sum P_e dA^2}{T_s}$$

- **2-way sensitivity**

$$P_{dc} = \sum P_e L_{BFN} \frac{d}{\eta_{dc}} = \frac{S\, T_0\, NF_{rx} L_{BFN}{}^2}{\eta_{dc} A^2}$$

- **DC power depends on $L_{BFN}{}^2$**

Figure 6-8 Generic beamforming network efficiency calculations for the passive ESA.

Figure 6-9 shows the functional architecture of the fully-distributed QO antenna. Just like the AESA, the transmit gain is increased by the gain of the distributed HPA. As for noise temperature, even though the calculation is different for the QO antenna (see Section 4.3), it can be approximately reduced to the same form as the AESA. Given that both transmit and receive performance are similarly derived for the AESA and the fully-distributed QO antennas, the same DC power requirement will result if consistent noise figures, losses, and DC efficiencies are used.

HPA and LNA Distribution

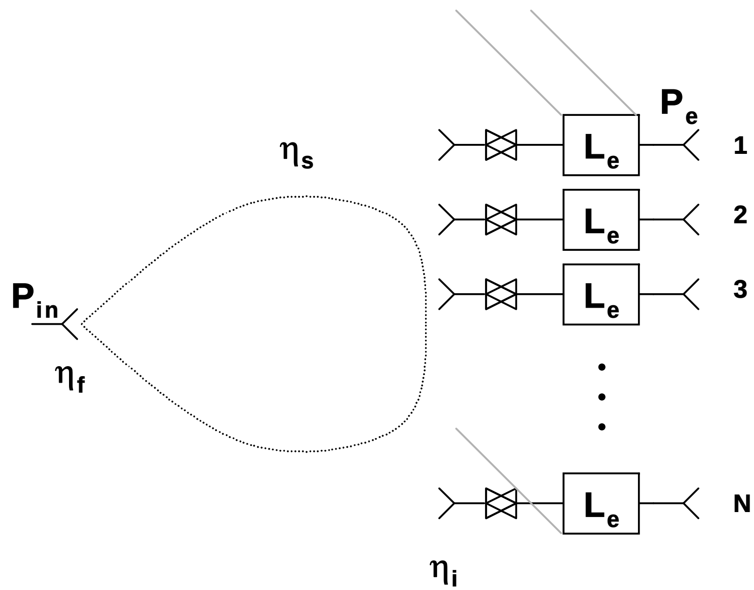

$$T_s \leq T_0 NF_{LNA} L_e$$

$$P_{in} = \frac{S T_0 NF_{LNA} L_e^{\ 2}}{dA^2}$$

$$P_{dc} = \left(\frac{L_a}{G_{HPA}} + 1 \right) \frac{S\, T_0\, NF_{LNA} L_e^{\ 2}}{\eta_{dc} A^2} + P_{LNA}$$

- **DC power reduced <u>to AESA level</u>**

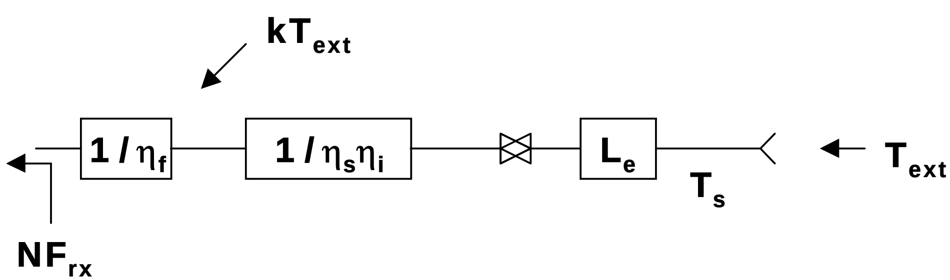

Figure 6-9 Generic beamforming network efficiency calculations for the fully-distributed QO antenna.

Figures 6-10 and 6-11 estimate the QO antenna mass and cost in the same level of detail as the AESA in Section 6.1. One concludes that the trade of a multiple-feed structure for phase shifters and a corporate feed network (AESA) does not significantly affect mass or cost for this case. The element-level HPAs and LNAs are assumed to be integrated into the antenna substrate without the individual packaging that often drives mass and cost. The DC/DC converters and energy storage capacitors are housed remotely, from where they supply DC power to the amplifiers via a distribution network integrated into the aperture substrate. This substrate is assumed to be roughly twice as heavy as that of the AESA due to its two-sided nature.

aperture length (m)	*0.5*		
aperture height (m)	*0.15*		
number of panels	*1*		
radiating element density (g/sqm)	6011		
structural panel density (g/sqm)	*6858*		
	Unit Mass (g)	**Qty**	**Total Mass (kg)**
radiating element substrate	451	1	0.5
structural panel	514	1	0.5
Beamforming Network			
element T/R modules	*10*	*120*	1.2
PCU	1100	*1*	1.1
feed	*500*	*3*	1.5
feed RF cable	*10*	*3*	0.0
beam switch	*100*	*1*	0.1
array post-amp	*50*	*1*	0.1
panel RF cables	*110*	*1*	0.1
PCU DC cables	*40*	*1*	0.0
controller	*3500*	*1*	3.5
controller DC cables	*1290*	*1*	1.3
feed structure	*1000*	*1*	1.0
		subtotal	10.9
		20% contingency	2.2
		total	13.1

Substrate Layup	**g/sqm**
paint - 2 mil	*107*
elements - 50%, 1/2 oz Cu	*79*
substrate - 50 mil Duroid	*2794*
ground plane - 1/2 oz Cu	*158*
substrate - 50 mil Duroid	*2794*
elements - 50%, 1/2 oz Cu	*79*
	6011

PCU Mass	
number of power supplies	*20*
power supply unit mass (g)	*20*
capacitor mass factor	*1.5*
	g
substrate + housing	*500*
power supplies + caps	*600*
	1100

Figure 6-10 Fully-distributed QO antenna mass for airborne high-resolution stripmap reference SAR mission.

	Unit Cost (k$)	Qty	Total Parts Cost (k$)
radiating element substrate	*0.6*	*1*	1
structural panel	*0.3*	*1*	0
Beamforming Network			
element T/R modules	*0.5*	*120*	60
PCU	10.6	*1*	11
feed	*1*	*3*	3
feed RF cable	*0.05*	*3*	0
beam switch	*0.3*	*1*	0
array T/R module	*2*	*1*	2
panel RF cables	*0.3*	*1*	0
PCU DC cables	*0.5*	*1*	1
controller	*5*	*1*	5
controller DC cables	*1*	*1*	1
feed structure	*0.5*	*1*	1
		subtotal	84
	20% contingency		17
		total	101

PCU Cost	
unit T/R ($)	*0*
unit phase shifter ($)	*200*
unit power supply ($)	*500*
number of phase shifters	*0*
number of power supplies	*20*
capacitor cost factor	*1.01*
housing + substrate	*500*
T/R + phase shifter parts	0
power supplies + caps	10100
	10600

Figure 6-11 Fully-distributed QO antenna cost for airborne high-resolution stripmap reference SAR mission.

6.3 Partially-Distributed QO Antenna Solution

Since the majority of the fully-distributed QO cost and power dissipation resides in the HPAs at the aperture-element level (see Figures 6-6 and 6-11), the most obvious QO architecture modification to consider is the removal of the element-level HPAs in favor of a centralized HPA at the feed level. This is the partially-distributed QO antenna solution. While a centralized HPA will have to generate higher peak RF power, it may have a cost advantage over 120 distributed HPAs.

Figure 6-12 shows the functional architecture of this partially-distributed QO antenna. Only LNAs are distributed at the lens-element level. While the LNAs maintain the system noise temperature, more RF power must be generated to overcome the entire loss of the QO BFN rather than just the element-level loss (L_e) in Figure 6-9. Accordingly, the total DC power requirement should increase roughly by a factor equal to the difference between the entire QO BFN loss and L_e for the same efficiency. The centralized array driver amplifier would probably be implemented as a Traveling Wave Tube Amplifier (TWTA), however, which can operate at higher efficiencies [117]. Assuming an efficiency of 50% rather than 35%, Figure 6-13 predicts an increase in DC power of roughly 8 dB.

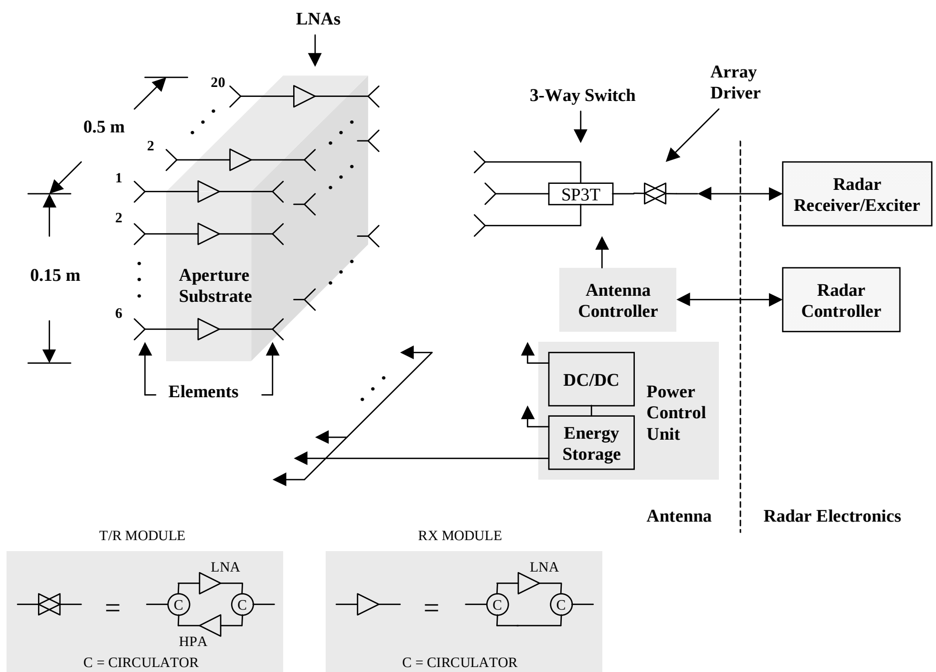

Figure 6-12 Partially-distributed QO antenna block diagram for airborne reference SAR mission.

Sensitivity (dB Wm4/K)	-39.7				
Effective Elevation Aperture (m)	0.14				
Effective Azimuth Aperture (m)	0.48				
Pulsewidth (ms)	12	avg spillover level (dB)	-10		
PRF (Hz)	5000	spillover loss (dB)	3.8	System Noise Temperature (K)	610
HPA Duty Cycle (%)	6	illumination loss (dB)	1		
LNA Duty Cycle (%)	50				
				Array Transmit Power (W)	241
number of elements	120			Element Transmit Power (W)	2.0
ambient temperature (C)	0				
DC/DC conversion efficiency (%)	75				

	Receive Ohmic Loss (dB)	Receive Amp Gain (dB)	Receive Amp NF (dB)	Receive Combine (ways)	CW DC Power (mW)	Transmit Ohmic Loss (dB)	Transmit Amp Gain (dB)	Transmit Eff (%)	Sys Noise (K)	Transmit Loss (dB)	Input Power (dBm)	Output Power (dBm)	Quantity	Receive Prime Power (W)	Transmit Prime Power (W)
external primary									290						
outer element	0.3	na	na	na	na	0.3	na	na	19.5	0.3	33.3	33.0	120		
feedthrough	0.2	na	na	na	na	0.2	na	na	13.8	0.2	33.5	33.3	120		
amplifier interface	1.0	na	na	na	na	0.8	na	na	79.3	0.8	34.3	33.5	120		
amplifier	na	20	1.5	na	50	na	0	0	169.0	0.0	34.3	34.3	120	4.0	0.0
amplifier interface	0.8	na	na	na	na	0.8	na	na	0.8	0.8	35.1	34.3	120		
transmission line	0.2	na	na	na	na	0.2	na	na	0.2	0.2	35.3	35.1	120		
inner element	0.3	na	na	na	na	0.3	na	na	0.3	0.3	35.6	35.3	120		
space feed	na	-4.8	0	120	na	na	-25.6	na	0.0	25.6	61.2	35.6	1		
external secondary									1.7						
feed	1.2	na	na	na	na	1.2	na	na	5.0	1.2	62.4	61.2	1		
transmission line	0.3	na	na	na	na	0.3	na	na	1.5	0.3	62.7	62.4	1		
beam switch	0.8	na	na	na	na	0.8	na	na	4.5	0.8	63.5	62.7	1		
transmission line	0.3	na	na	na	na	0.3	na	na	1.9	0.3	63.8	63.5	1		
amplifier interface	0.8	na	na	na	na	0.8	na	na	5.8	0.8	64.6	63.8	1		
amplifier	na	20	1.5	na	50	na	30	50	15.1	-30.0	34.6	64.6	1	0.0	
amplifier interface	0.8	na	na	na	na	0.8	na	na	0.1	0.8	35.4	34.6	1		
transmission line	1.0	na	na	na	na	1.0	na	na	0.1	1.0	36.4	35.4	1		
receiver interface	0.5	na	na	na	na	0.5	na	na	0.1				1		
receiver	na	na	4	na	na	na	na	na	0.9				1		
													subtotals	4.0	463.2
													total		467.3

Figure 6-13 Partially-distributed QO antenna RF performance for airborne reference SAR mission.

Figure 6-14 calculates the mass of this partially-distributed QO antenna solution to be greater than the fully-distributed QO solution by virtue of the expected mass of the centralized high-power amplifier. This effect is doubled in the interests of providing redundancy. Also, in terms of cost, the partially-distributed QO solution (see Figure 6-15) is higher than the fully-distributed case due to the expected cost of the array driver amplifier(s).

aperture length (m)		0.5		***Substrate Layup***	
aperture height (m)		0.15			**g/sqm**
number of panels		1		paint - 2 mil	107
radiating element density (g/sqm)		6011		elements - 50%, 1/2 oz Cu	79
structural panel density (g/sqm)		6858		substrate - 50 mil Duroid	2794
				ground plane - 1/2 oz Cu	158
				substrate - 50 mil Duroid	2794
	Unit		**Total**	elements - 50%, 1/2 oz Cu	79
	Mass	**Qty**	**Mass**		6011
	(g)		**(kg)**		
radiating element substrate	451	1	0.5		
structural panel	514	1	0.5		
Beamforming Network				***PCU Mass***	
element T/R modules	5	120	0.6		
PCU	3600	1	3.6	number of power supplies	10
feed	500	3	1.5	power supply unit mass (g)	140
feed RF cable	10	3	0.0	capacitor mass factor	1.5
beam switch	100	1	0.1		**g**
array transmit amp	5000	2	10.0	substrate + housing	1500
panel RF cables	110	1	0.1	power supplies + caps	2100
PCU DC cables	40	1	0.0		3600
controller	3500	1	3.5		
controller DC cables	1290	1	1.3		
feed structure	1000	1	1.0		
		subtotal	22.7		
		20% contingency	4.5		
		total	27.3		

Figure 6-14 Partially-distributed QO antenna mass for airborne reference SAR mission.

	Unit Cost (k$)	Qty	Total Parts Cost (k$)		
radiating element substrate	0.6	1	1	***PCU Cost***	
structural panel	0.3	1	0		
				unit T/R ($)	0
Beamforming Network				unit phase shifter ($)	200
element T/R modules	0.25	120	30	unit power supply ($)	500
PCU	6.05	1	6	number of phase shifters	0
feed	1	3	3	number of power supplies	10
feed RF cable	0.05	3	0	capacitor cost factor	1.01
beam switch	0.3	1	0		
array transmit amp	30	2	60	housing + substrate	1000
panel RF cables	0.3	1	0	T/R + phase shifter parts	0
PCU DC cables	0.5	1	1	power supplies + caps	5050
					6050
controller	5	1	5		
controller DC cables	1	1	1		
feed structure	0.5	1	1		
		subtotal	108		
	20% contingency		22		
		total	129		

Figure 6-15 Partially-distributed QO antenna cost for airborne reference SAR mission.

6.4 Centralized QO Antenna Solution

The final member of the family of QO antenna solutions to the airborne SAR mission is the centralized QO antenna. This antenna centralizes the LNA function as well as the HPA function (see Figure 6-16). Since the LNA will see higher RF power levels in its centralized location, its noise figure degrades. Assuming a 4-dB noise figure rather than 1.5 dB, Figure 6-17 predicts an additional increase in DC power of about 8 dB due to the corresponding increase in system noise temperature.

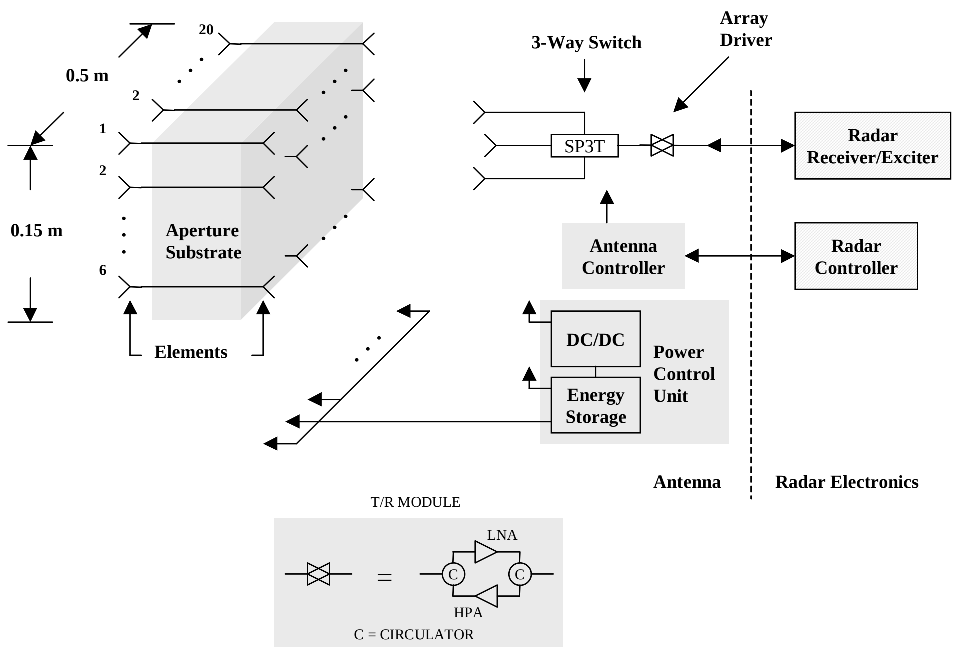

Figure 6-16 Centralized QO antenna block diagram for airborne reference SAR mission.

Sensitivity (dB Wm4/K)	-39.7
Effective Elevation Aperture (m)	0.14
Effective Azimuth Aperture (m)	0.48
Pulsewidth (ms)	12
PRF (Hz)	5000
HPA Duty Cycle (%)	6
LNA Duty Cycle (%)	50
number of elements	120
ambient temperature (C)	0
DC/DC conversion efficiency (%)	75
avg spillover level (dB)	-10
spillover loss (dB)	3.8
illumination loss (dB)	1
System Noise Temperature (K)	5428
Array Transmit Power (W)	2147
Element Transmit Power (W)	17.9

	Receive Ohmic Loss (dB)	Receive Amp Gain (dB)	Receive Amp NF (dB)	Receive Combine (ways)	CW DC Power (mW)	Transmit Ohmic Loss (dB)	Transmit Amp Gain (dB)	Transmit Eff (%)	Sys Noise (K)	Transmit Loss (dB)	Input Power (dBm)	Output Power (dBm)	Quantity	Receive Prime Power (W)	Transmit Prime Power (W)
external primary									290						
outer element	0.3	na	na	na	na	0.3	na	na	19.5	0.3	42.8	42.5	120		
feedthrough	0.2	na	na	na	na	0.2	na	na	13.8	0.2	43.0	42.8	120		
amplifier interface	0.0	na	na	na	na	0.0	na	na	0.0	0.0	43.0	43.0	120		
amplifier	na	0	0	na	0	na	0	0	0.0	0.0	43.0	43.0	120	0.0	0.0
amplifier interface	0.0	na	na	na	na	0.0	na	na	0.0	0.0	43.0	43.0	120		
transmission line	0.2	na	na	na	na	0.2	na	na	14.4	0.2	43.2	43.0	120		
inner element	0.3	na	na	na	na	0.3	na	na	22.9	0.3	43.5	43.2	120		
space feed	na	-4.8	0	120	na	na	-25.6	na	0.0	25.6	69.1	43.5	1		
external secondary									110.3						
feed	1.2	na	na	na	na	1.2	na	na	330.3	1.2	70.3	69.1	1		
transmission line	0.3	na	na	na	na	0.3	na	na	97.9	0.3	70.6	70.3	1		
beam switch	0.8	na	na	na	na	0.8	na	na	296.5	0.8	71.4	70.6	1		
transmission line	0.3	na	na	na	na	0.3	na	na	126.1	0.3	71.7	71.4	1		
amplifier interface	0.8	na	na	na	na	0.8	na	na	382.0	0.8	72.5	71.7	1		
amplifier	na	20	4	na	150	na	30	50	3646.8	-30.0	42.5	72.5	1	0.1	
amplifier interface	0.8	na	na	na	na	0.8	na	na	4.6	0.8	43.3	42.5	1		
transmission line	1.0	na	na	na	na	1.0	na	na	7.1	1.0	44.3	43.3	1		
receiver interface	0.5	na	na	na	na	0.5	na	na	4.2				1		
receiver	na	na	4	na	na	na	na	na	61.9				1		
													subtotals	0.1	2854.1
													total		2854.2

Figure 6-17 Centralized QO antenna RF performance for airborne reference SAR mission.

Figure 6-18 shows that the expected mass increases due to the mass of the higher-power TWTAs needed to provide the transmit drive signal. Cost is similarly driven by the expected cost of the two TWTAs (see Figure 6-19).

aperture length (m)	*0.5*
aperture height (m)	*0.15*
number of panels	*1*
radiating element density (g/sqm)	6011
structural panel density (g/sqm)	*6858*

	Unit Mass (g)	**Qty**	**Total Mass (kg)**
radiating element substrate	451	1	0.5
structural panel	514	1	0.5
Beamforming Network			
element T/R modules	*0*	*120*	0.0
PCU	11720	*1*	11.7
feed	*500*	*3*	1.5
feed RF cable	*10*	*3*	0.0
beam switch	*100*	*1*	0.1
array transmit amp	*10000*	*2*	20.0
panel RF cables	*110*	*1*	0.1
PCU DC cables	*40*	*1*	0.0
controller	*3500*	*1*	3.5
controller DC cables	*1290*	*1*	1.3
feed structure	*1000*	*1*	1.0
		subtotal	40.3
		20% contingency	8.1
		total	48.3

Substrate Layup	**g/sqm**
paint - 2 mil	*107*
elements - 50%, 1/2 oz Cu	*79*
substrate - 50 mil Duroid	*2794*
ground plane - 1/2 oz Cu	*158*
substrate - 50 mil Duroid	*2794*
elements - 50%, 1/2 oz Cu	*79*
	6011

PCU Mass	
number of power supplies	*32*
power supply unit mass (g)	*140*
capacitor mass factor	*1.5*
	g
substrate + housing	*5000*
power supplies + caps	*6720*
	11720

Figure 6-18 Centralized QO antenna mass for airborne reference SAR mission.

	Unit Cost (k$)	Qty	Total Parts Cost (k$)
radiating element substrate	0.6	1	1
structural panel	0.3	1	0
Beamforming Network			
element T/R modules	0	120	0
PCU	25.74	1	26
feed	1	3	3
feed RF cable	0.05	3	0
beam switch	0.3	1	0
array transmit driver	50	2	100
panel RF cables	0.3	1	0
PCU DC cables	0.5	1	1
controller	5	1	5
controller DC cables	1	1	1
feed structure	0.5	1	1
		subtotal	137
		20% contingency	27
		total	165

PCU Cost	
unit T/R ($)	0
unit phase shifter ($)	200
unit power supply ($)	750
number of phase shifters	0
number of power supplies	32
capacitor cost factor	1.01
housing + substrate	1500
T/R + phase shifter parts	0
power supplies + caps	24240
	25740

Figure 6-19 Centralized QO antenna cost for airborne reference SAR mission.

Table 6-1 summarizes the estimated resource requirements for the airborne SAR mission.

AIRBORNE Figures of Merit	AESA Solution	Fully-Distributed QO Solution	Partially-Distributed QO Solution	Centralized QO Solution
Prime Power (W)	80	79	467	2854
Mass (kg)	13	13	27	48
Recurring Cost (k$)	109	100	129	165

Table 6-1 Figures of merit for airborne reference SAR mission. Recurring cost includes materials, fabrication, and assembly.

Given that these figures of merit are estimated using assumptions that are considered representative at this point in time, relative comparisons are more meaningful than the absolute values. Based on the analysis in Section 6.2, the similarity between the AESA and fully-distributed QO figures of merit is expected. Even though the QO antenna has a more efficient beamforming network, the significance of the beamforming network loss is eliminated by the distribution of LNAs and HPAs. Distributing LNAs and HPAs in both antenna architectures equalizes their resource requirements. The partially-distributed and centralized QO antenna solutions are expected to require significantly more DC power than the AESA. Due to the size of the airborne antenna, the mass and cost savings provided by centralizing functions is overshadowed by the addition of the centralized high-power amplifier. Although the absolute cost estimates used in each case are indicative of a given point in time, it is reasonable to expect that the various cost estimates would change comparably over time in the short term, leaving the cost ratios the same. Due to the many different types of materials and components in each type of antenna, the cost reduction with technology advancement is expected to be less than that normally attributed to electronic devices.

CHAPTER 7

QUASI-OPTICAL ANTENNA EVALUATION FOR SPACEBORNE SAR

This chapter documents the comparative evaluation of QO antenna solutions for the wide-swath version of the spaceborne SAR mission described in Chapter 5. Appendix C covers the high-resolution version of the spaceborne SAR mission. In both cases QO antenna solutions are compared to the traditional AESA antenna solution in terms of the power, mass, and cost resources required to achieve the required RF performance. As in Chapter 6 the AESA and QO antenna design work is high level in nature and is not intended to be a thorough electromagnetic analysis. Its purpose is to describe the antenna approaches in sufficient detail to estimate the fundamental characteristics of mass, power, and cost. The antenna requirements for the spaceborne SAR mission are listed in Table 5-4.

7.1 AESA Antenna Solution for Wide-Swath Mission

To achieve the ±6.7° electronic beam steering required in elevation without grating lobes, the AESA must have phase control at a spacing of 0.89λ or less. Considering a 0.5m elevation dimension, this spacing results in 17.9 phase control points in elevation. Increasing this to a higher-integer number of 20 results in a spacing of 0.8λ, which is acceptable for beam steering. The 60 MHz instantaneous bandwidth will cause inconsequential beam squint in elevation and will not require true-time-delay phase shifters.

Using 0.81λ element spacing in azimuth, one makes the number of elements in azimuth come out to be 512. This results in the total number of elements being 10240. Solving for total radiated power from the absolute sensitivity requirement, one concludes that the necessary peak power per element is roughly 0.5 W. Given this value an HPA well within the current state-of-the-art can be used at each element for the traditional fully-distributed AESA approach. One does not need a phase shifter at each element, however, since electronic beam steering is again required only in elevation. Given the 13m x 0.5m aperture size, it makes sense to implement the aperture via eight subarrays each measuring 1.62m x 0.5m. This leads to an architecture where the 64 elements in azimuth per row for each subarray are combined followed by a phase shifter and an intermediate amplifier. The intermediate amplifier is needed to properly drive the element-level HPAs. Considering the loss of the 64-way combiner network and the phase shifter, an LNA is also needed at each element to control the noise temperature. The 20 rows per subarray are then combined followed by the combination of the eight subarrays as shown in Figure 7-1. Neither a driver HPA nor a post-amplifier LNA is necessary at the array level due to the transmit and receive gain already distributed in the array.

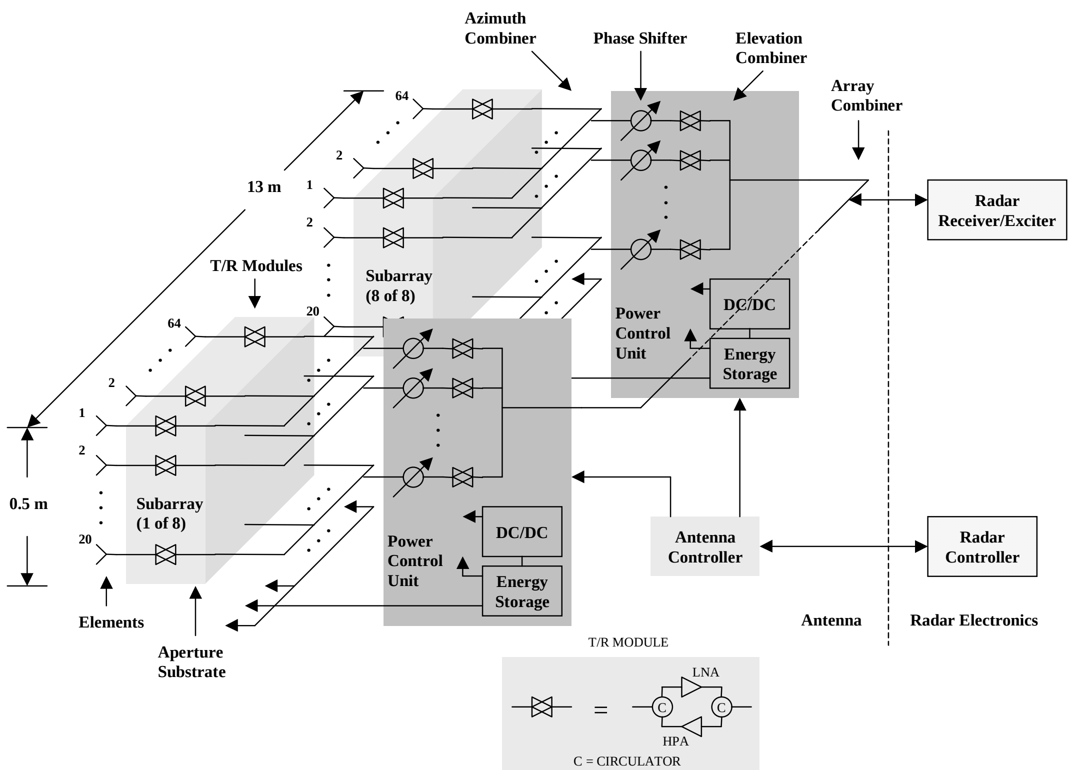

Figure 7-1 AESA antenna block diagram for spaceborne wide-swath reference SAR mission.

Given an external input noise temperature of 290K, Figure 7-2 calculates the actual system noise temperature, an estimate of which was used to determine the per-element radiated power. Figure 7-2 also shows the transmit signal levels throughout the antenna, justifying the need for intermediate HPAs, and estimates the prime power required by the antenna amplifiers to produce the required RF performance. It is again the case that the element-level HPAs drive the average prime power required, but one notices that the total LNA prime power is becoming more significant.

Sensitivity (dB Wm4/K)	11.5
Effective Elevation Aperture (m)	0.45
Effective Azimuth Aperture (m)	12.35
Pulsewidth (ms)	30
PRF (Hz)	1850
HPA Duty Cycle (%)	5.6
LNA Duty Cycle (%)	50
number of elements	10240
ambient temperature (C)	0
DC/DC conversion efficiency (%)	75

System Noise Temperature (K)	652
Array Transmit Power (W)	5376
Element Transmit Power (W)	0.52

Component	Receive Ohmic Loss (dB)	Receive Amp Gain (dB)	Receive Amp NF (dB)	Receive Combine (ways)	CW DC Power (mW)	Transmit Ohmic Loss (dB)	Transmit Amp Gain (dB)	Transmit Eff (%)	Sys Noise (K)	Transmit Loss (dB)	Input Power (dBm)	Output Power (dBm)	Quantity	Receive Prime Power (W)	Transmit Prime Power (W)
external									290						
element	0.3	na	na	na	na	0.3	na	na	19.5	0.3	27.5	27.2	10240		
feedthrough	0.2	na	na	na	na	0.2	na	na	13.8	0.2	27.7	27.5	10240		
amplifier interface	1.0	na	na	na	na	0.8	na	na	79.3	0.8	28.5	27.7	10240		
amplifier	na	20	1.5	na	50	na	30	35	169.0	-30.0	-1.5	28.5	10240	341.3	1531.6
amplifier interface	0.8	na	na	na	na	0.8	na	na	0.8	0.8	-0.7	-1.5	10240		
transmission line	0.7	na	na	na	na	0.7	na	na	0.8	0.7	0.0	-0.7	10240		
az combine/divide	3.2	na	na	64	na	3.2	na	na	5.9	21.3	21.3	0.0	160		
transmission line	0.5	na	na	na	na	0.5	na	na	1.4	0.5	21.8	21.3	160		
phase shifter	5.0	na	na	na	na	5.0	na	na	27.6	5.0	26.8	21.8	160		
transmission line	0.5	na	na	na	na	0.5	na	na	4.9	0.5	27.3	26.8	160		
amplifier interface	0.8	na	na	na	na	0.8	na	na	9.2	0.8	28.1	27.3	160		
amplifier	na	20	1.5	na	50	na	30	35	23.9	-30.0	-1.9	28.1	160	5.3	21.6
amplifier interface	0.8	na	na	na	na	0.8	na	na	0.1	0.8	-1.1	-1.9	160		
el combine/divide	2.0	na	na	20	na	2.0	na	na	0.4	15.0	13.9	-1.1	8		
transmission line	1.5	na	na	na	na	1.5	na	na	0.4	1.5	15.4	13.9	8		
array combine/divide	1.0	na	na	8	na	1.0	na	na	0.4	10.0	25.4	15.4	1		
transmission line	1.0	na	na	na	na	1.0	na	na	0.5	1.0	26.4	25.4	1		
receiver interface	0.5	na	na	na	na	0.5	na	na	0.3				1		
receiver	na	na	4	na	na	na	na	na	4.2						
														346.7	1553.3
															1899.9

Figure 7-2 AESA antenna RF performance for spaceborne wide-swath reference SAR mission.

Figures 7-3 and 7-4 in turn estimate the antenna mass and cost. The element-level HPAs and LNAs are assumed to be integrated into the antenna substrate without the individual packaging that often drives mass and cost. The DC/DC converters and energy storage capacitors are housed in the elevation divider/phase shifter units. This mission requires a large antenna that must be deployed by a sophisticated extendable support structure. One also notices that the beamforming network behind the element-level amplifiers is even more significant to both mass and cost given the physical size of the antenna.

aperture length (m)	13
aperture height (m)	0.5
number of panels	8
radiating element density (g/sqm)	3138
structural panel density (g/sqm)	6858

	Unit Mass (g)	Qty	Total Mass (kg)
radiating element substrate	2550	8	20
structural panel	5572	8	45
Beamforming Network			
element T/R modules	10	10240	102
element T/R RF cables	15	10240	154
64-way	300	160	48
64-way RF cables	10	160	2
20-way, driver, PS, PCU	3420	8	27
20-way RF cables	25	8	0
8-way	75	1	0
panel RF cables	110	1	0
PCU DC cables	40	8	0
controller	6000	1	6
controller DC cables	3300	8	26
deployment structure	80000	1	80
deployment actuators	15000	1	15
		subtotal	526
		20% contingency	105
		total	631

Substrate Layup	**g/sqm**
paint - 2 mil	107
elements - 50%, 1/2 oz Cu	79
substrate - 50 mil Duroid	2794
ground plane - 1/2 oz Cu	158
	3138

PCU Mass	
number of power supplies	64
power supply unit mass (g)	20
capacitor mass factor	1.5
	g
substrate + housing	1500
power supplies + caps	1920
	3420

Figure 7-3 AESA antenna mass for spaceborne wide-swath reference SAR mission.

	Unit Cost (k$)	Qty	Total Parts Cost (k$)		
radiating element substrate	2.8	8	22	**PCU Cost**	
structural panel	2.8	8	22		
				unit T/R ($)	500
Beamforming Network				unit phase shifter ($)	200
element T/R modules	0.5	10240	5120	unit power supply ($)	500
element T/R RF cables	0.05	10240	512	number of phase shifters, T/Rs	20
64-way	1.5	160	240	number of power supplies	64
64-way RF cables	0.05	160	8	capacitor cost factor	1.01
20-way, driver, PS, PCU	48.3	8	387		
20-way RF cables	0.1	8	1	housing + substrate	2000
8-way	0.6	1	1	T/R + phase shifter parts	14000
array RF cables	0.3	1	0	power supplies + caps	32320
PCU DC cables	0.5	8	4		48320
controller	50	1	50		
controller DC cables	1	8	8		
deployment structure	2000	1	2000		
deployment actuators	200	1	200		
		subtotal	8575		
		20% contingency	1715		
		total	10290		

Figure 7-4 AESA antenna cost for spaceborne wide-swath reference SAR mission.

7.2 Fully-Distributed QO Antenna Solution for Wide-Swath Mission

This is an active microwave lens with HPAs and LNAs at each lens element. Refer to Chapter 4 for an operational description. To achieve the ±6.7° electronic beam steering in elevation without grating lobes, the QO antenna has the same element-spacing requirements as the AESA. Section 7.1 shows that these requirements result in a 20 x 512 element array over the 0.5 x 13 m radiating aperture. The 60 MHz instantaneous bandwidth will cause no beam squint in elevation since no phase shifters are used for elevation beam steering. Given the elevation beamwidth and the viewing geometry noted in Table 5-4, one concludes that the required incidence-angle range can be covered by a collection of five separate beams at different elevation angles. Elevation beam steering will be done by switching between five separate feeds located on the focal arc of the lens. Given the exaggerated aspect ratio of the lens, however, multiple feed horns (4) are necessary in azimuth to properly illuminate the lens for each beam.

Solving for total radiated power from the absolute sensitivity requirement, one concludes that the necessary peak power per element remains at roughly 0.5 W. Given this value an HPA well within the current state-of-the-art can be used at each element. The fully-distributed QO antenna architecture also features LNAs at each element to control the noise temperature. Figure 7-5 shows the QO antenna functional block diagram.

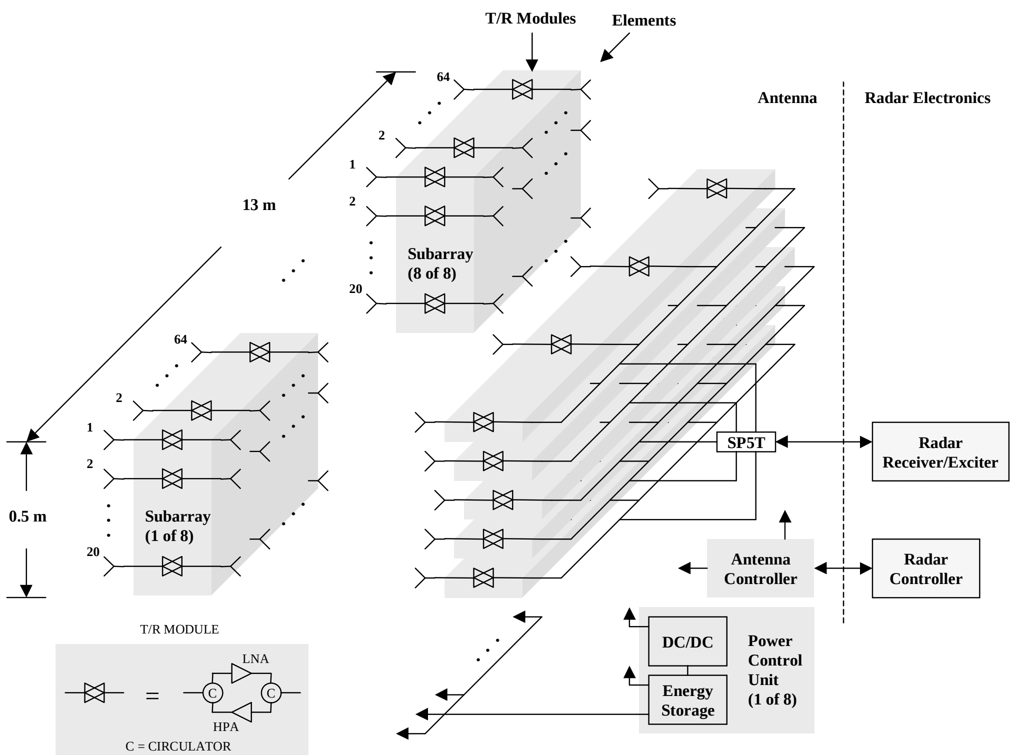

Figure 7-5 Fully-distributed QO antenna block diagram for spaceborne wide-swath reference SAR mission.

Given the external input noise temperature of 290K, Figure 7-6 calculates the system noise temperature. Figure 7-6 also shows the transmit signal levels throughout the antenna and estimates the prime power required by the antenna amplifiers to produce the required RF performance. It is no surprise that these prime power numbers are comparable to the AESA solution given that HPAs and LNAs are distributed at the element level in both cases.

Sensitivity (dB Wm4/K)	11.5				
Effective Elevation Aperture (m)	0.45				
Effective Azimuth Aperture (m)	12.35				
Pulsewidth (ms)	30				
PRF (Hz)	1850	avg spillover level (dB)	-10	System Noise Temperature (K)	599
HPA Duty Cycle (%)	5.6	spillover loss (dB)	3.8		
LNA Duty Cycle (%)	50	illumination loss (dB)	1		
				Array Transmit Power (W)	4937
number of elements	10240			Element Transmit Power (W)	0.5
ambient temperature (C)	0				
DC/DC conversion efficiency (%)	75				

Component	Receive Ohmic Loss (dB)	Receive Amp Gain (dB)	Receive Amp NF (dB)	Receive Combine (ways)	CW DC Power (mW)	Transmit Ohmic Loss (dB)	Transmit Amp Gain (dB)	Transmit Eff (%)	Sys Noise (K)	Transmit Loss (dB)	Input Power (dBm)	Output Power (dBm)	Quantity	Receive Prime Power (W)	Transmit Prime Power (W)
external primary									290						
outer element	0.3	na	na	na	na	0.3	na	na	19.5	0.3	27.1	26.8	10240		
feedthrough	0.2	na	na	na	na	0.2	na	na	13.8	0.2	27.3	27.1	10240		
transmission line	0.0	na	na	na	na	0.0	na	na	0.0	0.0	27.3	27.3	10240		
amplifier interface	1.0	na	na	na	na	0.8	na	na	79.3	0.8	28.1	27.3	10240		
amplifier	na	20	1.5	na	50	na	30	35	169.0	-30.0	-1.9	28.1	10240	341	1407
amplifier interface	0.8	na	na	na	na	0.8	na	na	0.8	0.8	-1.1	-1.9	10240		
transmission line	0.2	na	na	na	na	0.2	na	na	0.2	0.2	-0.9	-1.1	10240		
inner element	0.3	na	na	na	na	0.3	na	na	0.3	0.3	-0.6	-0.9	10240		
space feed	na	-4.8	0	2560	na	na	-38.9	na	0.0	38.9	38.3	-0.6	4		
external secondary									1.7				0		
feed	1.2	na	na	na	na	1.2	na	na	5.0	1.2	39.5	38.3	4		
transmission line	0.3	na	na	na	na	0.3	na	na	1.5	0.3	39.8	39.5	4		
amplifier interface	0.8	na	na	na	na	0.8	na	na	4.5	0.8	40.6	39.8	4		
amplifier	na	20	1.5	na	50	na	30	35	11.7	-30.0	10.6	40.6	4	0	10
amplifier interface	0.8	na	na	na	na	0.8	na	na	0.1	0.8	11.4	10.6	4		
transmission line	0.5	na	na	na	na	0.5	na	na	0.0	0.5	11.9	11.4	4		
az combine/divide	0.6	na	na	4	na	0.6	na	na	0.1	6.6	18.5	11.9	1		
transmission line	0.5	na	na	na	na	0.5	na	na	0.1	0.5	19.0	18.5	1		
beam switch	1.0	na	na	na	na	1.0	na	na	0.1	1.0	19.5	18.5	1		
receiver interface	1.5	na	na	na	na	1.5	na	na	0.2				1		
receiver	na	na	4	na	na	na	na	na	1.3				1		
													subtotals	341	1417
													total		1758

Figure 7-6 Fully-distributed QO antenna RF performance for spaceborne wide-swath reference SAR mission.

Figures 7-7 and 7-8 estimate the QO antenna mass and cost. The element-level HPAs and LNAs are assumed to be integrated into the antenna substrate without the individual packaging that often drives mass and cost. The DC/DC converters and energy storage capacitors are housed remotely from where they distribute DC power to the amplifiers via a distribution network integrated into the aperture substrate. This mission requires a large antenna and a more-complicated feed cluster, both of which must be deployed by sophisticated extendable support structures.

aperture length (m)	12.35
aperture height (m)	0.6
number of panels	8
radiating element density (g/sqm)	6011
structural panel density (g/sqm)	6858

	Unit Mass (g)	Qty	Total Mass (kg)
radiating element substrate	5568	8	45
structural panel	6352	8	51
Beamforming Network			
element T/R modules	12	10240	123
PCU	2920	8	23
feed	500	20	10
array driver modules	50	20	1
feed RF cable	10	20	0
4-way	75	5	0
switch RF cables	15	4	0
beam switch	100	1	0
panel RF cables	110	1	0
PCU DC cables	40	8	0
controller	6000	1	6
controller DC cables	3300	8	26
deployment structure	50000	1	50
feed structure	10000	1	10
deployment actuators	15000	1	15
		subtotal	361
		20% contingency	72
		total	433

Substrate Layup	**g/sqm**
paint - 2 mil	107
elements - 50%, 1/2 oz Cu	79
substrate - 50 mil Duroid	2794
ground plane - 1/2 oz Cu	158
substrate - 50 mil Duroid	2794
elements - 50%, 1/2 oz Cu	79
	6011

PCU Mass	
number of power supplies	64
power supply unit mass (g)	20
capacitor mass factor	1.5
	g
substrate + housing	1000
power supplies + caps	1920
	2920

Figure 7-7 Fully-distributed QO antenna mass for spaceborne wide-swath reference SAR mission.

	Unit Cost (k$)	Qty	Total Parts Cost (k$)
radiating element substrate	*7.0*	*8*	56
structural panel	*3.7*	*8*	30
Beamforming Network			
element T/R modules	*0.6*	*10240*	6144
PCU	33.8	*8*	271
feed	*1*	*20*	20
array driver modules	*1.5*	*20*	30
feed RF cable	*0.05*	*20*	1
4-way	*0.5*	*5*	3
switch RF cables	*0.05*	*5*	0
beam switch	*0.5*	*1*	1
panel RF cables	*0.3*	*1*	0
PCU DC cables	*0.5*	*8*	4
controller	*50*	*1*	50
controller DC cables	*1*	*8*	8
deployment structure	*1250*	*1*	1250
feed structure	*10*	*1*	10
deployment actuators	*150*	*1*	150
		subtotal	8027
		20% contingency	1605
		total	9632

PCU Cost	
unit T/R ($)	*0*
unit phase shifter ($)	*0*
unit power supply ($)	*500*
number of phase shifters	*0*
number of power supplies	*64*
capacitor cost factor	*1.01*
housing + substrate	*1500*
T/R + phase shifter parts	0
power supplies + caps	32320
	33820

Figure 7-8 Fully-distributed QO antenna cost for spaceborne wide-swath reference SAR mission.

7.3 Partially-Distributed QO Antenna Solution for Wide-Swath Mission

The majority of the power dissipation and cost resides in the aperture-element level distributed HPAs and LNAs for the wide-swath mission. This partially-distributed QO architecture trades the DC power increase for the mass and cost savings associated with the elimination of 10240 element-level HPAs. Figure 7-9 shows the block diagram of the partially-distributed QO solution with the 10240 HPAs removed from the aperture and with the centralized HPA function following the beam selection switch. The LNAs remain at the aperture-element level to maintain the noise temperature and the radiated RF power requirement. Figure 7-10 indicates that an 80 kW centralized array driver amplifier is necessary to produce the radiated power required. Even with an increased efficiency of 50%, the resulting prime power requirement is almost 12 kW.

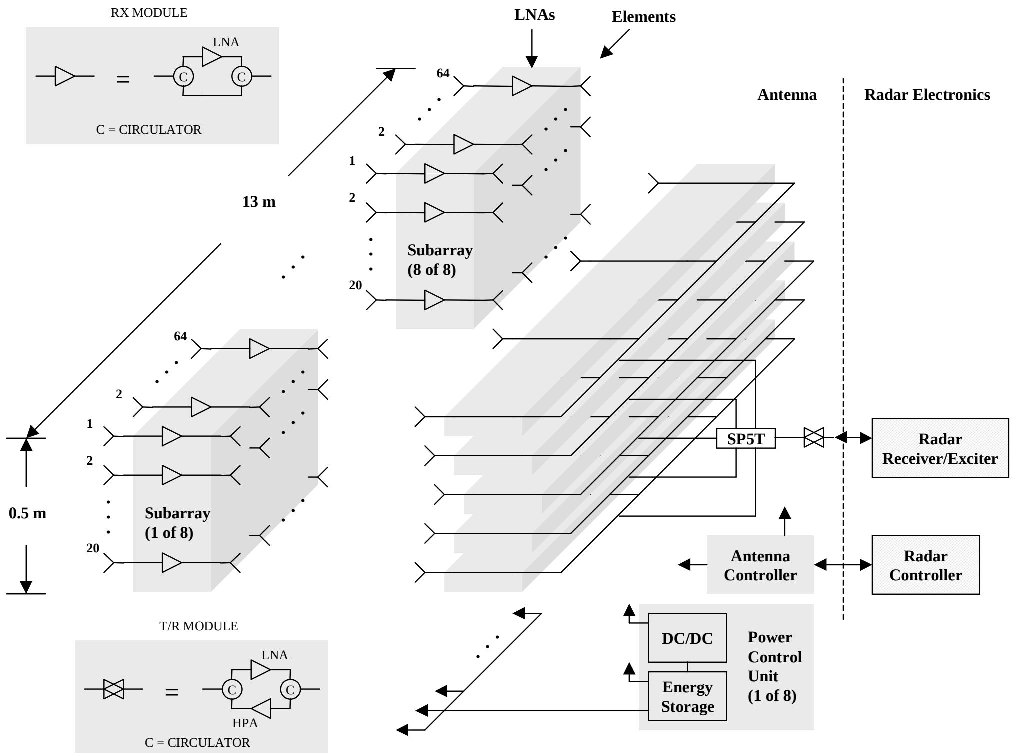

Figure 7-9 Partially-distributed QO antenna block diagram for spaceborne wide-swath reference SAR mission.

Sensitivity (dB Wm4/K)	11.5
Effective Elevation Aperture (m)	0.45
Effective Azimuth Aperture (m)	12.35
Pulsewidth (ms)	30
PRF (Hz)	1850
HPA Duty Cycle (%)	5.6
LNA Duty Cycle (%)	50
number of elements	10240
ambient temperature (C)	0
DC/DC conversion efficiency (%)	75

avg spillover level (dB)	-10
spillover loss (dB)	3.8
illumination loss (dB)	1

System Noise Temperature (K)	623
Array Transmit Power (W)	5133
Element Transmit Power (W)	0.5

Component	Receive Ohmic Loss (dB)	Receive Amp Gain (dB)	Receive Amp NF (dB)	Receive Combine (ways)	CW DC Power (mW)	Transmit Ohmic Loss (dB)	Transmit Amp Gain (dB)	Transmit Eff (%)	Sys Noise (K)	Transmit Loss (dB)	Input Power (dBm)	Output Power (dBm)	Quantity	Receive Prime Power (W)	Transmit Prime Power (W)
external primary									290						
outer element	0.3	na	na	na	na	0.3	na	na	19.5	0.3	27.3	27.0	10240		
feedthrough	0.2	na	na	na	na	0.2	na	na	13.8	0.2	27.5	27.3	10240		
amplifier interface	1.0	na	na	na	na	0.8	na	na	79.3	0.8	28.3	27.5	10240		
amplifier	na	20	1.5	na	50	na	0	0	169.0	0.0	28.3	28.3	10240	341	
amplifier interface	0.8	na	na	na	na	0.8	na	na	0.8	0.8	29.1	28.3	10240		
transmission line	0.2	na	na	na	na	0.2	na	na	0.2	0.2	29.3	29.1	10240		
inner element	0.3	na	na	na	na	0.3	na	na	0.3	0.3	29.6	29.3	10240		
space feed	na	-4.8	0	2560	na	na	-38.9	na	0.0	38.9	68.5	29.6	4		
external secondary									1.7						
feed	1.2	na	na	na	na	1.2	na	na	5.0	1.2	69.7	68.5	4		
transmission line	0.3	na	na	na	na	0.3	na	na	1.5	0.3	70.0	69.7	4		
az combine/divide	0.6	na	na	4	na	0.6	na	na	3.3	6.6	76.6	70.0	1		
transmission line	0.5	na	na	na	na	0.5	na	na	3.1	0.5	77.1	76.6	1		
beam switch	1.0	na	na	na	na	1.0	na	na	7.4	1.0	78.1	77.1	1		
amplifier interface	0.8	na	na	na	na	0.8	na	na	7.3	0.8	78.9	78.1	1		
amplifier	na	20	1.5	na	50	na	30	50	19.0	-30.0	48.9	78.9	1	0	11486
amplifier interface	0.8	na	na	na	na	0.8	na	na	0.1	0.8	49.7	48.9	1		
transmission line	0.5	na	na	na	na	0.5	na	na	0.1	0.5	50.2	49.7	1		
receiver interface	1.5	na	na	na	na	1.5	na	na	0.2				1		
receiver	na	na	4	na	na	na	na	na	1.3				1		
													subtotals	341	11486
													total		11827

Figure 7-10 Partially-distributed QO antenna RF performance for spaceborne wide-swath reference SAR mission.

Figure 7-11 shows that the partially-distributed QO architecture for the spaceborne wide-swath mission also provides a slight mass reduction due to the number of distributed HPAs in the fully-distributed QO solution. The mass of the high-power centralized amplifier and its associated power supplies consume most of the mass savings from the distributed HPAs. Cost is significantly affected due to the large numbers of distributed HPAs in the original QO solution. Figure 7-12 shows that the total cost is reduced by about one-third.

aperture length (m)		*12.35*	
aperture height (m)		*0.6*	
number of panels		*8*	
radiating element density (g/sqm)		6011	
structural panel density (g/sqm)		*6858*	
	Unit Mass (g)	**Qty**	**Total Mass (kg)**
radiating element substrate	5568	8	45
structural panel	6352	8	51
Beamforming Network			
element T/R modules	*7*	*10240*	72
PCU	36880	*1*	37
feed	*500*	*20*	10
feed RF cable	*10*	*20*	0
4-way	*75*	*5*	0
switch RF cables	*15*	*5*	0
beam switch	*100*	*1*	0
array driver amp	*15000*	*2*	30
panel RF cables	*110*	*1*	0
PCU DC cables	*40*	*8*	0
controller	*6000*	*1*	6
controller DC cables	*3300*	*1*	3
deployment structure	*50000*	*1*	50
feed structure	*10000*	*1*	10
deployment actuators	*15000*	*1*	15
		subtotal	329
		20% contingency	66
		total	395

Substrate Layup	
	g/sqm
paint - 2 mil	*107*
elements - 50%, 1/2 oz Cu	*79*
substrate - 50 mil Duroid	*2794*
ground plane - 1/2 oz Cu	*158*
substrate - 50 mil Duroid	*2794*
elements - 50%, 1/2 oz Cu	*79*
	6011

PCU Mass	
number of power supplies	*128*
power supply unit mass (g)	*140*
capacitor mass factor	*1.5*
	g
substrate + housing	*10000*
power supplies + caps	26880
	36880

Figure 7-11 Partially-distributed QO antenna mass for spaceborne wide-swath reference SAR mission.

	Unit Cost (k$)	Qty	Total Parts Cost (k$)		
radiating element substrate	7.0	8	56	***PCU Cost***	
structural panel	3.7	8	30		
				unit T/R ($)	0
Beamforming Network				unit phase shifter ($)	0
element T/R modules	0.35	10240	3584	unit power supply ($)	500
PCU	69.6	1	70	number of phase shifters	0
feed	1	20	20	number of power supplies	128
feed RF cable	0.05	20	1	capacitor cost factor	1.01
4-way	0.5	5	3		
switch RF cables	0.05	5	0	housing + substrate	5000
beam switch	0.5	1	1	T/R + phase shifter parts	0
array driver amp	50	2	100	power supplies + caps	64640
panel RF cables	0.3	1	0		69640
PCU DC cables	0.5	8	4		
controller	50	1	50		
controller DC cables	1	1	1		
deployment structure	1250	1	1250		
feed structure	10	1	10		
deployment actuators	150	1	150		
		subtotal	5329		
		20% contingency	1066		
		total	6395		

Figure 7-12 Partially-distributed QO antenna cost for spaceborne wide-swath reference SAR mission.

7.4 Centralized QO Antenna Solution

Centralizing the LNA function along with the HPA function, as indicated in Figure 7-13, requires a large amount of prime power. Figure 7-14 estimates the prime power requirement to be nearly 90 kW which is clearly impractical for a space application.

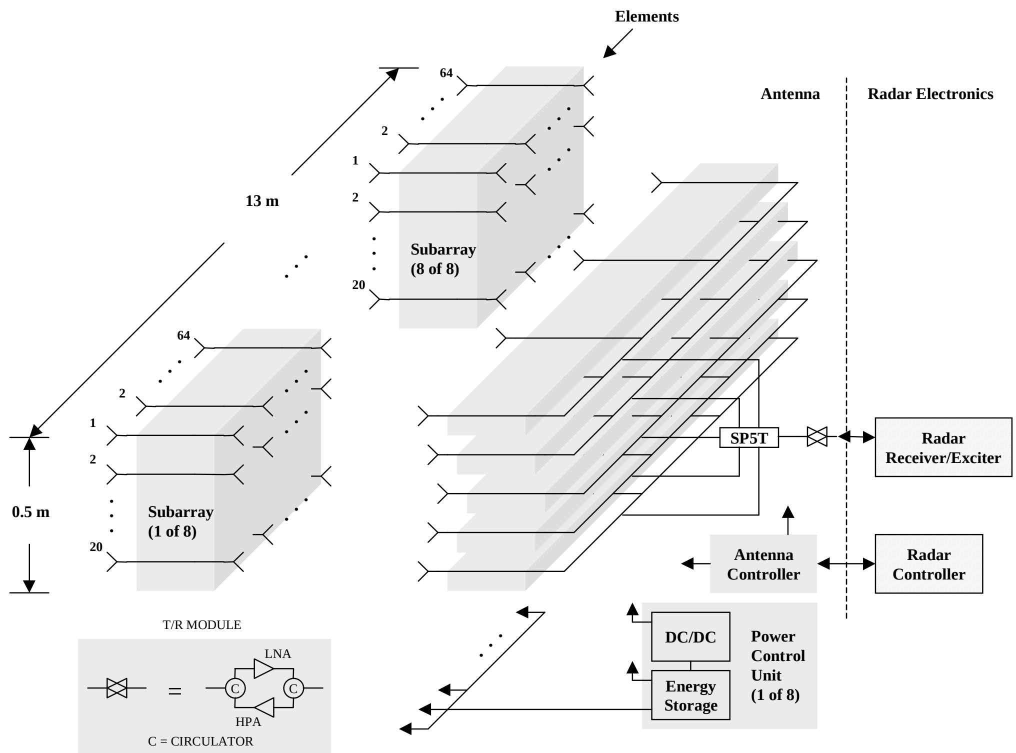

Figure 7-13 Centralized QO antenna block diagram for spaceborne wide-swath reference SAR mission.

Sensitivity (dB Wm4/K)	11.5				
Effective Elevation Aperture (m)	0.45				
Effective Azimuth Aperture (m)	12.35				
Pulsewidth (ms)	30				
PRF (Hz)	1850	avg spillover level (dB)	-10	System Noise Temperature (K)	6996
HPA Duty Cycle (%)	5.6	spillover loss (dB)	3.8		
LNA Duty Cycle (%)	50	illumination loss (dB)	1		
				Array Transmit Power (W)	57651
number of elements	10240			Element Transmit Power (W)	5.6
ambient temperature (C)	0				
DC/DC conversion efficiency (%)	75				

Component	Receive Ohmic Loss (dB)	Receive Amp Gain (dB)	Receive Amp NF (dB)	Receive Combine (ways)	CW DC Power (mW)	Transmit Ohmic Loss (dB)	Transmit Amp Gain (dB)	Transmit Eff (%)	Sys Noise (K)	Transmit Loss (dB)	Input Power (dBm)	Output Power (dBm)	Quantity	Receive Prime Power (W)	Transmit Prime Power (W)
external primary									290						
outer element	0.3	na	na	na	na	0.3	na	na	20	0.3	37.8	37.5	10240		
feedthrough	0.2	na	na	na	na	0.2	na	na	14	0.2	38.0	37.8	10240		
transmission line	0.2	na	na	na	na	0.2	na	na	14	0.2	38.2	38.0	10240		
inner element	0.3	na	na	na	na	0.3	na	na	23	0.3	38.5	38.2	10240		
space feed	na	-4.8	0	2560	na	na	-38.9	na	0	38.9	77.4	38.5	4		
external secondary									110						
feed	1.2	na	na	na	na	1.2	na	na	330	1.2	78.6	77.4	4		
transmission line	0.3	na	na	na	na	0.3	na	na	98	0.3	78.9	78.6	4		
az combine/divide	0.6	na	na	4	na	0.6	na	na	217	6.6	85.5	78.9	1		
transmission line	0.5	na	na	na	na	0.5	na	na	205	0.5	86.0	85.5	1		
beam switch	1.0	na	na	na	na	1.0	na	na	489	1.0	87.0	86.0	1		
amplifier interface	0.8	na	na	na	na	0.8	na	na	481	0.8	87.8	87.0	1		
amplifier	na	20	4	na	150	na	30	50	4591	-30.0	57.8	87.8	1	0	89255
amplifier interface	0.8	na	na	na	na	0.8	na	na	6	0.8	58.6	57.8	1		
transmission line	0.5	na	na	na	na	0.5	na	na	4	0.5	59.1	58.6	1		
receiver interface	1.5	na	na	na	na	1.5	na	na	16				1		
receiver	na	na	4	na	na	na	na	na	87				1		
													subtotals	0	89255
													total		89256

Figure 7-14 Centralized QO antenna RF performance for spaceborne wide-swath reference SAR mission.

Table 7-1 summarizes the resource estimates for the spaceborne wide-swath SAR mission.

SPACEBORNE WIDE-SWATH Figures of Merit	AESA Solution	Fully-Distributed QO Solution	Partially-Distributed QO Solution	Centralized QO Solution
Prime Power (W)	1900	1758	11827	89256
Mass (kg)	631	433	395	-
Recurring Cost (k$)	10290	9632	6395	-

Table 7-1 Figures of merit for spaceborne wide-swath reference SAR mission. Recurring cost includes materials, fabrication, and assembly.

The fully-distributed QO antenna requires comparable prime power and has roughly the same parts cost as the AESA. Due to its spatial beamforming network, however, it has a third less mass. The partially-distributed QO antenna has mass comparable to the fully-distributed QO antenna but provides a one-third cost savings at the expense of a significant increase in prime power. The selection between these three alternatives can depend on which resource requirement is most critical.

With reference to Appendix C, Table 7-2 summarizes the resource estimates for the high-resolution spaceborne mission.

SPACEBORNE HIGH-RESOLUTION Figures of Merit	AESA Solution	Fully-Distributed QO Solution	Partially-Distributed QO Solution	Centralized QO Solution
Prime Power (W)	22445	21715	146960	-
Mass (kg)	392	286	-	-
Recurring Cost (k$)	5483	5674	-	-

Table 7-2 Figures of merit for spaceborne high-resolution reference SAR mission. Recurring cost includes materials, fabrication, and assembly.

While the fully-distributed QO antenna has a modest 25% mass advantage, that advantage is overshadowed by the 23 kW prime power requirement of both the AESA and the QO antennas. The partially-distributed and centralized QO antennas are impractical due to their prohibitive power requirements.

CHAPTER 8

MULTIPLE-BEAM SAR

QO antenna technology is characterized by a lightweight, low-loss BFN that can provide beam steering without the need for phase shifters. The resource advantages and disadvantages attributed to QO antenna technology and described in Chapters 6 and 7 and Appendix C for the missions considered are the direct results of these characteristics. There is another unique characteristic of QO antennas, however, that has not yet been considered for SAR. Due to the linearity of the lens aperture, the QO antenna can implement multiple, simultaneous beams with the same lightweight, low-loss BFN. The addition of another feed, located appropriately on the focal arc of the lens aperture, is all that is necessary to make the QO antenna capable of producing another simultaneous beam. The angular separation between beams is determined by the feed separation along the focal arc. While the use of multiple, simultaneous beams is not normally associated with SAR, it can significantly enhance the attractiveness of QO antenna technology for SAR. SRTM (see Chapter 2) is the only known SAR mission to use a multiple-beam operational mode. SRTM used two simultaneous beams in elevation to double the instantaneous swath width and the area coverage rate as indicated in Figure 8-1. The SRTM AESA antennas generated these two simultaneous beams by utilizing their existing dual-polarization, corporate-feed BFNs. One beam was horizontally polarized (using the horizontal corporate-feed BFNs), and the other was vertically polarized (using the vertical corporate-feed BFNs). Polarization diversity not only enabled the generation of the two simultaneous beams, but it also provided the necessary isolation to distinguish the two returns from each other.

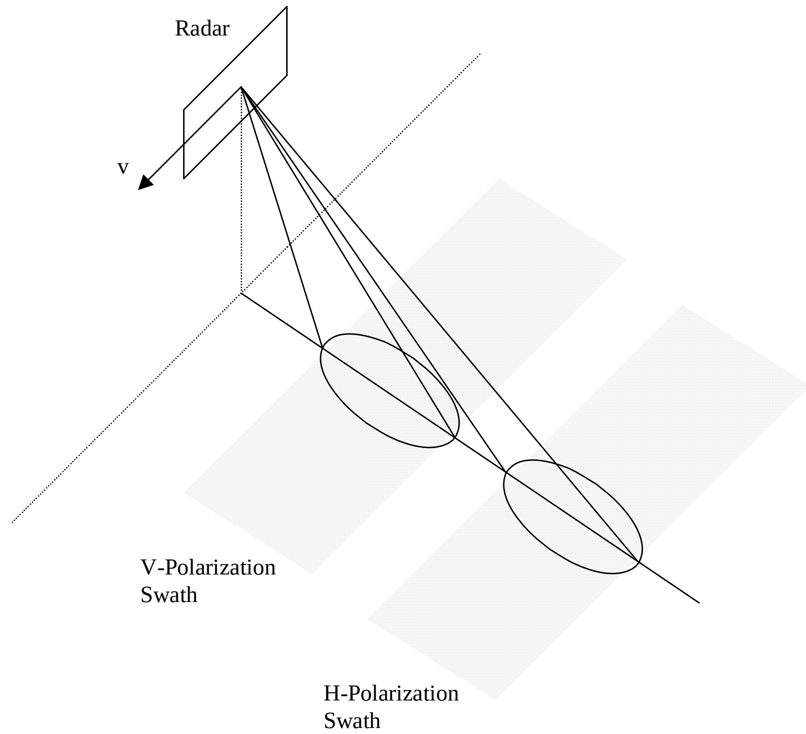

Figure 8-1 The AESA antennas of the SRTM interferometric SAR each utilized two simultaneous beams at different polarizations to increase swath and area coverage rate.

Although multiple-beam SAR processing has not been implemented in the azimuth or along-track dimension, it can provide either increased efficiency or enhanced performance. Specifically, the use of multiple, simultaneous beams in the along-track dimension can either 1) enable finer resolution for the same aperture and same swath, 2) reduce peak and average power for the same resolution and swath, or 3) provide wider swath for the same resolution. The combinations of performance possible in 1) and 3) are not achievable with single-beam antennas. The efficiency with which QO antennas can implement multiple beams makes it the enabling technology for multiple-beam SAR operation.

8.1 Finer Resolution

The idea is to use multiple, simultaneous beams in the along-track dimension as shown in Figure 8-2. In classical, single-beam SAR theory (see Appendix A) the size of the along-track resolution cell is inversely proportional to the length of time the target is in the antenna beamwidth as the single beam passes by. Since the azimuth beamwidth is a function of the length of the antenna in azimuth, resolution in the along-track dimension is linked to antenna length. If one had multiple, simultaneous beams in azimuth, however, one could divide the total “time on target” between the simultaneous beams since a given image area will be sequentially illuminated by each individual beam as the radar flies by. This would mean that the coherently-combined target returns may not be contiguous in time (i.e., the beam mainlobes may not overlap), but that does not appear to be a feasibility problem for SAR digital data processing. For the same antenna length (and same azimuth beamwidth), a collection of three simultaneous beams would triple the “time on target” and therefore produce along-track resolution three times as fine.

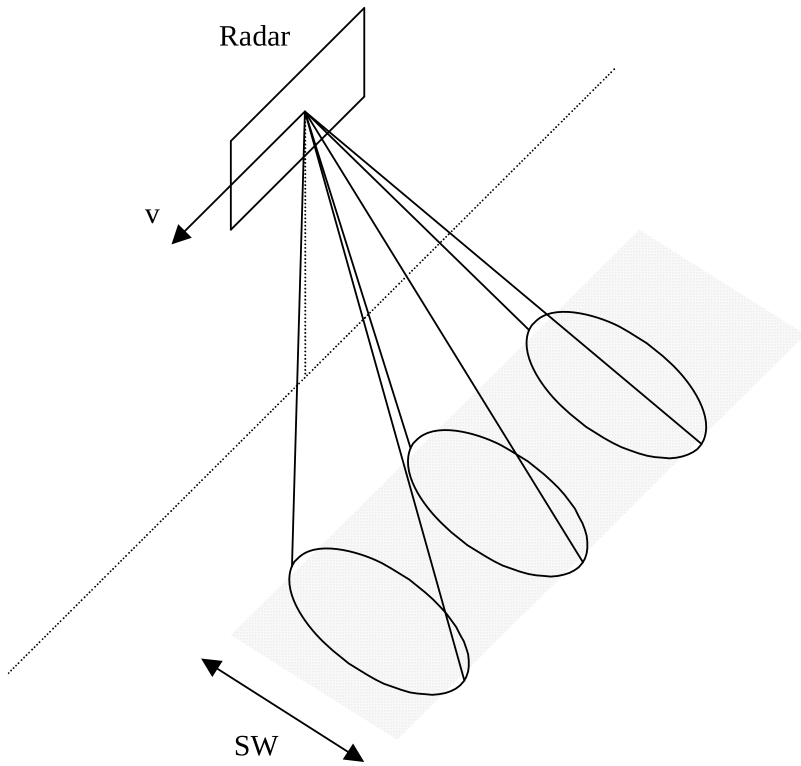

Figure 8-2 The use of multiple, simultaneous beams in the along-track dimension.

While this could be considered a trivial advantage relative to the alternative of a 3x shorter antenna, the implementation of the shorter antenna has negative implications on the swath achievable. For single-beam systems, a shorter antenna implies a higher PRF (see Equation (A.26)) which in turn reduces the maximum swath that can be accommodated. Equation (5.3) describes a positively-sloped line defining the maximum swath achievable for a given resolution. Assuming that the single-beam system used as a reference here is optimized so that it provides the finest resolution for the particular swath, the three-beam system can still deliver three-times-better resolution (along-track resolution cells a third as big). This is a combination of swath and resolution that a single-beam antenna cannot provide.

The implementation of multiple simultaneous beams requires sufficient isolation between those beams. Sections A.5 and A.9 describe the ambiguous-signal issues associated with single-beam SAR processing. Because of the use of multiple pulses transmitted at the PRF, the target return power received in the mainlobe of the single beam must compete with ambiguous power received through the azimuth sidelobes of the single-beam pattern at doppler-frequency intervals spaced PRF apart. The relationship between azimuth angle and doppler frequency developed in Section A.2 maps the two-way azimuth pattern into the doppler-frequency domain. Section A.9 indicates that the goal for the azimuth-ambiguity-to-signal-ratio (AASR) is to be less than –20 dB, in which case the ambiguous power can be ignored. If the AASR is greater than –20 dB, the ambiguous power will begin to degrade the image signal-to-noise ratio (SNR). With reference to Figure 8-3, the AASR is normally calculated as the ratio of the sum of the power received in the ambiguous (sidelobe) doppler intervals to the power received in the unambiguous (mainlobe) doppler interval. For the single-beam case the power in each doppler interval is weighted by the two-way (transmit and receive) azimuth pattern of the particular beam.

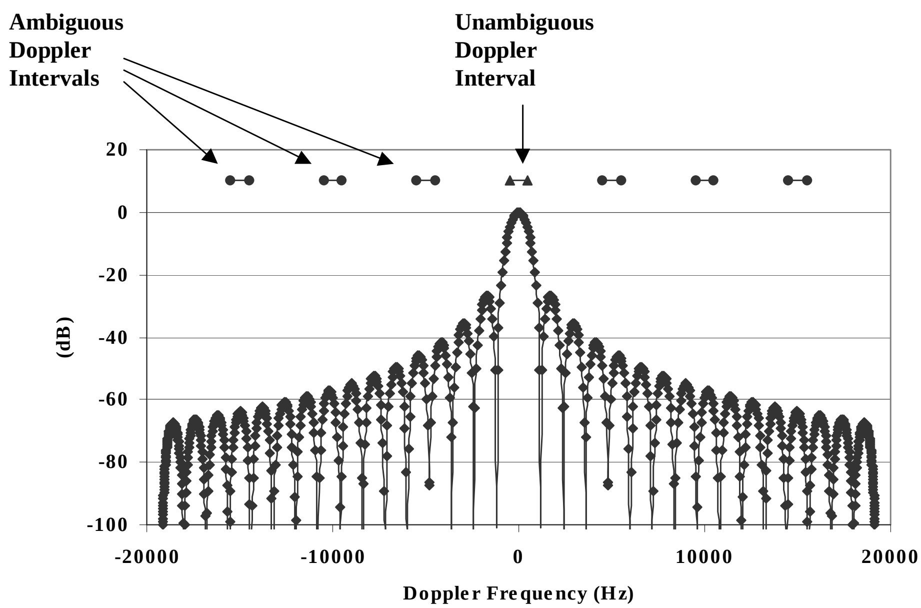

Figure 8-3 The azimuth-ambiguity-to-signal ratio is the ratio of the sum of the power received from the ambiguous doppler intervals to the power received from the unambiguous doppler interval. The two-way beam pattern shown is for a single beam with uniform amplitude distribution.

For the multiple-beam case each receive beam pattern can be treated individually, but, assuming that each of the beams transmits simultaneously, the transmit pattern used must be a composite of the individual transmit beam patterns. The composite transmit pattern will include the mainlobes of all individual transmit beam patterns spaced accordingly (see Figure 8-4). The receive pattern of each individual beam will attenuate the transmit mainlobes of the other beams by virtue of its sidelobe structure. As a result, the two-way pattern used in the calculation of the azimuth ambiguities will be higher than the single-beam case in the regions of the mainlobes of the other beams as indicated in the airborne example shown in Figure 8-5.

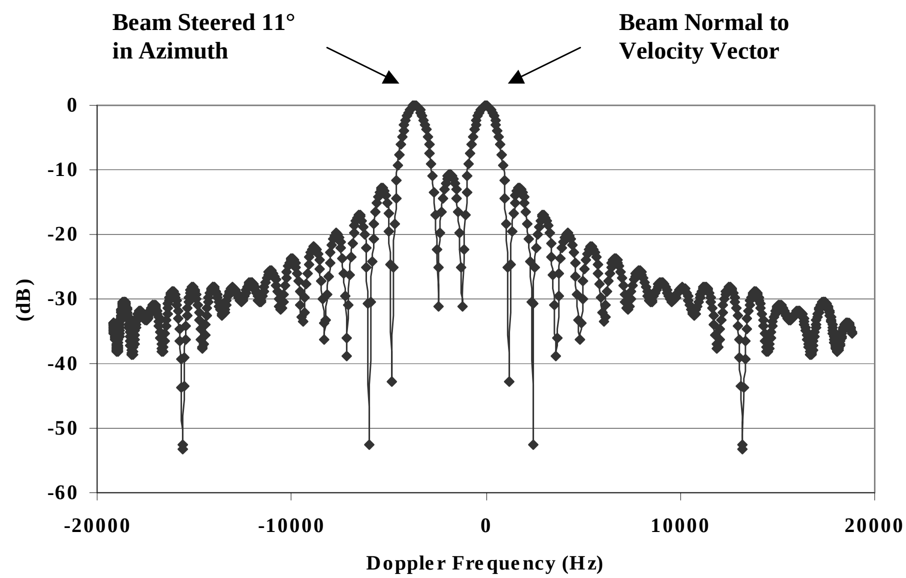

Figure 8-4 Example two-beam composite transmit (one-way) pattern for one beam at zero doppler and the other steered 11 degrees away in the along-track dimension.

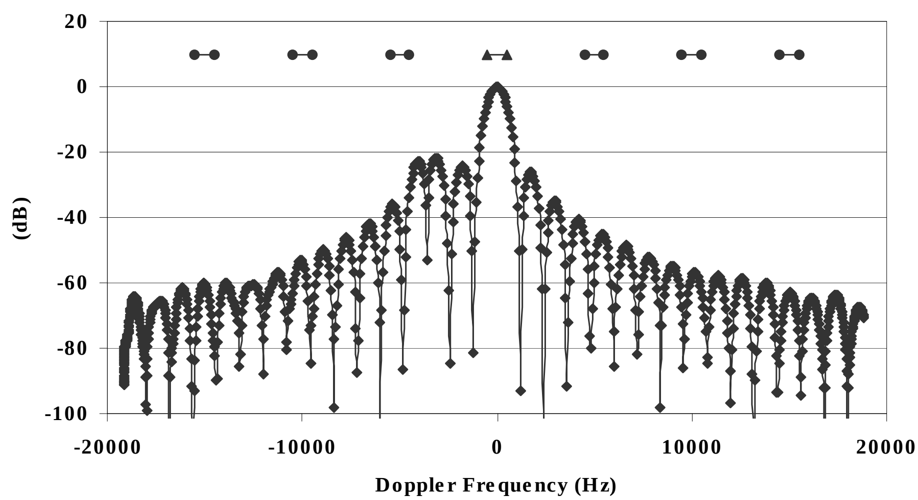

Figure 8-5 Example two-way pattern for zero-doppler beam showing the pattern degradation caused by the second beam steered 11 degrees away in the along-track dimension.

The degree to which this increases the AASR depends on the relative locations of the beam mainlobes and the locations of the ambiguous (by PRF) doppler intervals. In the airborne example shown in Figure 8-5, the AASR degraded from –45 dB to –34 dB (PRF =

5000 Hz, doppler bandwidth = 1000 Hz), but it is still less than –20 dB and therefore still negligible. While this is just one example, there are enough degrees of freedom, most notably the beam locations and the beam receive sidelobe tapers (uniform taper used in Figure 8-5), to conclude that this example is probably nonsingular. On the other hand, there are probably situations where the AASR increase cannot be sufficiently tolerated. For these situations other forms of isolation must be used to further limit the AASR. An example is beam-to-beam diversity in transmit waveform modulation. Something as simple as a downchirp versus an upchirp on adjacent beams may be sufficient to provide the marginal discrimination needed between adjacent-beam returns. The conclusion is that the azimuth ambiguity degradation caused by multiple transmit beams can be accommodated in most cases.

8.2 Reduced Power

Rather than keeping the same antenna length to increase resolution, one can increase the antenna length to save power. In the example of three beams, one would increase the antenna by a factor of three to maintain the same along-track resolution. This would result in a factor-of-three increase in antenna gain which in turn implies a factor-of-nine decrease in average RF power per beam. Keeping the same PRF and pulsewidth, one concludes that the peak RF power per beam is also reduced by a factor of nine. Since there are three individual beams, the total average RF power (and average DC power) is reduced by a factor of three.

8.3 Wider Swath

Rather than using the idea depicted in Figure 8-2 to provide the same resolution and swath performance more efficiently, one can also take advantage of the longer along-track antenna dimension to cover a wider instantaneous swath. The multiple, simultaneous beams are still used to provide the required time-on-target in piecemeal fashion, but here the individual-beam PRF is reduced by a factor equal to the number of simultaneous beams. Lower individual-beam PRFs provide more receive time to accommodate wider swaths, but wider swaths in turn require wider elevation beamwidths. Wider elevation beamwidths require shorter elevation apertures, which reduce the antenna gain. The surprising result is that for the same resolution, wider swaths than are possible with single-beam SAR operation can be provided via the implementation of multiple, simultaneous beams in the along-track dimension.

As an illustration of this logic, consider a reference single-beam SAR system providing resolution δ and swath width *SW* with antenna length *L*, height *H*, gain *G*, bandwidth *B*, average RF power P_{avg}, and pulse repetition frequency *PRF*. To achieve the same along-track resolution with a 3-beam system, where the three beams are spaced in the along-track dimension, one increases the antenna length to *3L*. This not only increases the antenna gain to 3G, but it also decreases the minimum PRF by a factor of 3 (Equation (A.26)). Rather than maintaining the same PRF as in Section 8.2 one now reduces the individual-beam PRF to *PRF/3*. This provides the time between pulses to collect target returns from a wider swath of *3SW*. In order to cover a *3SW* swath with the elevation beamwidth, one must reduce the height of the antenna to *H/3*. This leaves the antenna gain unchanged at *G*, which means that the average RF power per beam remains at P_{avg}. With the reduced individual-beam PRF, either the peak RF power or the transmit pulsewidth must increase by a factor of three to achieve the average RF power of P_{avg}. For the collection of three individual beams the total average RF power would be increased by a factor of 3 to a total of $3P_{avg}$.

As with the pursuit of finer resolution in Section 8.1, the enhanced swath coverage provided here by multiple-beam processing represents a combination of resolution and swath performance that cannot be achieved by any single-beam SAR system. The only way for a SAR having one beam in azimuth to achieve such a combination of swath and resolution is to have multiple beams in elevation. While the total average RF power would be the same at $3P_{avg}$, implementing a *3SW* swath with multiple beams in elevation would require that the multiple beams have overlapping mainlobes, which severely complicates the beam-to-beam isolation problem.

8.4 Hardware Implications

The hardware requirements for implementing multiple, simultaneous beams include longer antennas, multiple BFNs, higher power, and multiple receiver chains. Multiple receiver chains are necessary regardless of the type of antenna, but the hardware implications of multiple BFNs vary greatly with the antenna technology used. Multiple BFNs are most efficiently implemented in QO antennas since the feed network is spatial. The implementation of multiple beams in the AESA is usually an expensive proposition since the BFNs often include active-amplifier and phase-shifter devices and constrained transmission line media (e.g., waveguides, coaxial cables). Multiple-beam implementation in QO antennas requires only multiple feeds appropriately positioned on the focal arc to achieve the beam steering required. The implementation of multiple feeds in azimuth obviously works best when there is only one feed horn or element in azimuth for each beam. Conversely, if there are multiple feeds in azimuth for a single beam (e.g., a cylindrical lens), then the implementation of multiple azimuth beams is problematic due to the possibility of blockage. Also problematic is the implementation of multiple beams in azimuth along with different switched beam positions in elevation. Unless the elevation and azimuth aperture dimensions are comparable, the positioning of feeds along the focal arc in both dimensions will result in conflicts. There are also obvious practical problems associated with increasing an antenna length indefinitely. The conclusion to be drawn is that the implementation of multiple beams in azimuth is most practical for QO antennas that have a single feed in azimuth and that have a limited number of feeds in elevation.

CHAPTER 9

CONCLUSION AND FUTURE WORK

This final chapter summarizes the ability of QO antenna technology to satisfy SAR antenna requirements. Three SAR mission profiles, representative of demonstrated SAR performance evolution, were generated and their mission-level requirements allocated down to the antenna level. These requirement sets were used to evaluate the power, mass, and cost resources required by various QO antenna architectures relative to the traditional AESA architecture. These resource requirement estimates are collected in Table 9-1.

Antenna and Figure of Merit	Airborne Mission	Space Wide-Swath Mission	Space High-Resolution Mission
AESA Prime Power (W)	80	1900	22445
AESA Mass (kg)	13	631	392
AESA Recurring Cost (k$)	109	10290	5483
Fully-Distributed QO Prime Power (W)	73	1758	22715
Fully-Distributed QO Mass (kg)	13	433	286
Fully-Distributed QO Recurring Cost (k$)	100	9632	5674
Partially-Distributed QO Prime Power (W)	467	11827	146960
Partially-Distributed QO Mass (kg)	27	395	-
Partially-Distributed QO Recurring Cost (k$)	129	6395	-
Centralized QO Prime Power (W)	2854	89256	-
Centralized QO Mass (kg)	48	-	-
Centralized QO Recurring Cost (k$)	165	-	-

Table 9-1 Figures of merit for AESA and QO antenna solutions to the reference SAR missions. Recurring cost includes materials, fabrication, and assembly.

Chapter 6 examines the efficiency of the QO beamforming network and finds that it is indeed generally more efficient than the corresponding AESA beamforming network without the amplifiers. The QO BFN efficiency is also relatively constant with increasing aperture size while the AESA BFN efficiency will decrease as the aperture increases.

Chapter 6 also concludes that 1) the passive QO BFN is not as efficient as the AESA BFN with the distributed amplifiers and 2) the efficiencies of the QO and AESA BFNs, both with the distributed amplifiers, are comparable. The distribution of LNAs and HPAs to the element level in either type of antenna essentially overwhelms the losses in the passive portions of the BFNs.

Table 9-1 shows no reason to consider the QO antenna as an alternative to the AESA for the airborne SAR mission. Not enough mass is associated with the AESA BFN, and not enough mass and cost is associated with the distributed amplifiers to give the QO antenna an advantage. The spaceborne high-resolution mission is similar except that the elimination of the AESA BFN is worth a 25% mass savings for the fully-distributed QO antenna. Similarly, the spaceborne wide-swath fully-distributed QO antenna enjoys a 30% mass advantage due to the elimination of the AESA BFN. For this mission the partially-distributed QO antenna provides another trade-off. Mass is maintained while a significant cost reduction is traded against a significant power increase. The identification of the driving requirement will depend on the particular circumstances.

These evaluations lead one to conclude that QO antennas may be attractive for SAR missions requiring passive antennas and for SAR missions with active antennas where the aperture is large and the power requirements are moderate. Traditional AESA technology has been developed, environmentally qualified, and demonstrated both on airborne platforms and in space (see Chapter 2) over the last 15 years. The payoff for all of the development funding spent on AESA antenna technology is that the AESA is a trusted standard for SAR antennas. AESA antenna technology is considered low-risk for SAR applications as long as the prime power, mass, and cost requirements remain reasonable. QO antenna technology for SAR will remain a high-risk alternative until it can be developed, qualified, and demonstrated like AESA technology. QO antenna technology will have to either offer significant efficiencies in prime power, mass, or cost or enable significant enhancements in SAR performance before its development will warrant serious consideration.

QO antenna technology is the enabling technology for multiple-beam SAR operation. The enhancements in efficiency or swath/resolution performance provided by multiple-beam SAR operation certainly make QO antenna technology more attractive. Chapter 8 notes that the enhanced performance possible with multiple-beam SAR cannot be achieved with single-beam antennas. In those cases where the enhanced level of performance is necessary, the N-beam QO antenna will favorably compare with N single-beam antennas.

A limitation of QO antenna technology is that it may not be able to practically provide a large number of different beams, either simultaneously or sequentially, to increase the flexibility and availability of the SAR imaging capability provided. Although blockage from a large feed cluster is not an issue as it can be with a reflector, a large feed cluster becomes unwieldy and complex. As the number of beams and/or the electronic scanning range becomes large in one or both dimensions, the QO solution may get less practical. The antenna innovation that would greatly benefit QO antenna application is a way of implementing more steered beams, especially for the larger apertures. So far this is the exclusive domain of the AESA, but the AESA is not always affordable and often requires too much prime power and mass. The radar development that would further enhance the utility of QO antennas for SAR, relative to AESA technology, is the development of the technology supporting the implementation of multiple-beam SAR processing. Specifically, this could include optimum feed geometries (spillover, illumination, etc.), the accommodation of non-uniform aperture illuminations and variable-gain amplifiers, optimum sidelobe structures, transmit waveform diversity, doppler-frequency sensitivities, and digital processing implications.

BIBLIOGRAPHY

[1] Skolnik, M. I., editor-in-chief, *Radar Handbook*, McGraw-Hill, 1970, p. 23-3.

[2] Curlander, J. C. and McDonough, R. N., *Synthetic Aperture Radar*, Wiley, 1991, p. 17.

[3] Skolnik, p. 19-2.

[4] Curlander, p. 20.

[5] Curlander, p. 20.

[6] Carrara, W. G., Goodman, R. S., Majewski, R. M., *Spotlight Synthetic Aperture Radar: Signal Processing Algorithms*, Artech House, p. 4.

[7] Cantafio, L. J., editor, *Space-Based Radar Handbook*, Artech House, 1989, pp. 123-124.

[8] Blake, L. V., *Antennas*, Artech House, 1984, pp. 295-296.

[9] Skolnik, p. 11-10.

[10] Curlander, p. 121.

[11] Skolnik, p. 17-8.

[12] Oppenheim, A. V. and Schafer, R. W., *Digital Signal Processing*, Prentice-Hall, 1975, pp. 28-29.

[13] Collin, R. E., *Antennas and Radiowave Propagation*, McGraw-Hill, 1985, pp. 303-304.

[14] Oliver, B. M., "Thermal and Quantum Noise", *Proceedings of the IEEE*, May 1965, p. 446.

[15] Curlander, p. 91.

[16] Curlander, p. 93.

[17] Goj, W. W., *Synthetic-Aperture Radar and Electronic Warfare*, Artech House, 1993, p. 4.

[18] Skolnik, M. I., editor-in-chief, *Radar Handbook*, McGraw-Hill, 1990, p. 10.31.

[19] Goj, p. 20.

[20] DiFranco, J. V., Rubin, W. L., *Radar Detection*, Prentice-Hall, 1968, p. 380.

[21] Curlander, p. 121.

[22] Freeman, A., instructor, *Synthetic Aperture Radar: Design, Processing, and Applications*, UCLA University Extension Engineering 867.108, 1991.

[23] Curlander, pp. 298, 303.

[24] Curlander, p. 306.

[25] Milligan, T., *Modern Antenna Design*, McGraw-Hill, 1985, p. 145.

[26] Elliott, R., *Antenna Theory and Design*, Prentice-Hall, 1981, p. 160.

[27] Balanis, C., *Antenna Theory, Analysis, and Design*, Harper & Row, 1982, p. 681.

[28] Harger, R. O., *Synthetic Aperture Radar Systems: Theory and Design*, Academic Press, 1970, p. 30.

[29] Curlander, p. 304.

[31] Curlander, p. 298.

[32] Hovanessian, S. A., *Introduction to Synthetic Array and Imaging Radars*, Artech House, 1980, p. v.

[33] Morris, G. V., *Airborne Pulsed Doppler Radar*, Artech House, 1988, p. 157.

[34] Carrara, p. 3.

[35] Soumekh, M., *Synthetic Aperture Radar Signal Processing*, John Wiley & Sons, 1999, p. xx.

[36] http://airsar.jpl.nasa.gov/

[37] http://irctr.et.tudelft.nl/sector/rs/frames.htm

[38] http://www.ehis.navy.mil/oknews6.htm

[39] http://www.ccrs.nrcan.gc.ca/ccrs/tekrd/satsens/sarbro/sbmaine.html

[40] Gray, A. L., Livingstone, C. E., Hawkins, R. K., Vachon, P., Lukowski, T. I., Lalonde, M., "The CCRS Airborne SAR Systems: Radar for Remote Sensing Research," *Canadian Journal of Remote Sensing*, vol. 21, no. 4, Dec 1995, p. 408.

[41] http://www.cmc.sandia.gov/facts/saros

[42] http://www.emi.dtu.dk/research/DCRS/Emisar/emisar.html

[43] http://infoserv.kp.dlr.de/NE-HF/projects/ESAR/igars96_scheiber.html

[44] http://www2.crl.go.jp/ck/ck521/3d_sar/E/index.html

[45] Shnitkin, H., "A Unique Joint STARS Phased Array Antenna", *Microwave Journal*, vol. 34, no. 1, Jan 1991, pp. 131-141.

[46] http://www.erim-int.com/SDAG/SAR/s_sar_IFSARE.html

[47] http://ltpwww.gsfc.nasa.gov/ISSSR-95/interfer.htm

[48] http://www.eomonline.com/Common/Archives/June 00/ellis.htm

[49] http://www.cc.gatech.edu/slasses/AY2001/cs6235_spring/papers/rasspcon3.html

[50] http://www.atl.external.lmco.com/projects/rassp/RASSP_legacy/casestudies/SAR/CAS-SAR_02.HTM

[51] http://peoiews.monmouth.army.mil/aps/tesar.htm

[52] http://isis.dlr.de/guide/Seasat-SAR.html

[53] http://cassini-radar.jpl.nasa.gov/reports/iwgsar/3_SAR_Development.html

[54] http://nssdc.gsfc.nasa.gov/nmc/tmp/1983-054A.html

[55] http://www.jpl.nasa.gov/magellan/

[56] http://pds.jpl.nasa.gov/mgddf/chap1/chap1.htm

[57] http://www.neosoft.com/Almaz/almaz1/default.htm

[58] http://isis.dlr.de/guide/ERS-SAR.html

[59] http://msl/jpl.nasa.gov/QuickLooks/ersQL.html

[60] http://www.eurimage.com/Products/ERS/Mmissions.html

[61] http://www.infoterra-global.com/japanese_jers.html

[62] http://www.ccrs.nrcan.gc.ca/ccrs/tekrd/satsens/sats/jerse.html

[63] IEEE AES Systems Magazine, vol. 10, no. 11, Nov 95, pp. 15-23.

[64] http://isis.dlr.de/guide/SRL_SIR-C_X-SAR.html

[65] http://www.jpl.nasa.gov/cassini

[66] http://southport.jpl.nasa.gov/radar/bigpicture

[67] http://cassini-radar.jpl.nasa.gov

[68] http://www.jpl.nasa.gov/srtm

[69] http://envisat.esa.int/

[70]
http://www.space.gc.ca/csa_sectors/earth_environment/radarsat2/rad_inf/tec_spe/default.asp#

[71] http://www.nasda.go.jp/Home/Projects/ALOS/index_e.html

[72] http://alos.nasda.go.jp/index-e.html

[73] http://www.infoterra-global.com/terrasar.htm/

[74] http://www.fas.org/spp/military/program/imint/starlight.htm

[75] Skolnik, M. I., "Detection and Ranging: Radar in the Twentieth Century", *IEEE Aerospace & Electronic Systems Magazine*, vol. 15, no. 10, Oct 2000, pp. 27-44.

[76] http://members.nbci.com/082499/aviation/nws002.awst046.htm (from AWST, 6/12/00)

[77] Braybrook, R., Richardson, D., "Ground Surveillance Aircraft," *Armada International*, Mar 2001.

[78] Caro, E., Freeman, A., Jordan, R., Johnson, W., Kim, Y., Rosen, P., Shen, Y., Stuhr, F., van Zyl, J., "Space-Borne Imaging", *IEEE Aerospace & Electronic Systems Magazine*, vol. 15, no. 10, Oct 2000, pp. 118-124.

[79] York, R.A., Popović, Z.B., editors, *Active and Quasi-Optical Arrays for Solid-State Power Combining*, John Wiley & Sons, 1997, pp. xvi-xvii.

[80] Brown, E.R., Harvey, J.F., "Research Focus on Quasi-Optical Technology", *Microwave Journal*, vol. 41, no. 9, Sep 1998, pp. 24-26.

[81] York, p. 293.

[82] York, pp. 293-296.

[83] York, p. 296.

[84] York, p. 409.

[85] York, p. 415.

[86] Brown, p. 26.

[87] Schoenberg, J.S.H., *Quasi-Optical Constrained Lens Amplifiers*, Ph.D. Dissertation, University of Colorado, Boulder, 1995, p. 151.

[88] Curlander, p. 105.

[89] Schoenberg, p. 154.

[90] Fourikis, N., *Phased Array-Based Systems and Applications*, John Wiley & Sons, 1997 p. 142.

[91] Curlander, pp. 21, 73.

[92] Skolnik, M. I., *Introduction to Radar Systems*, McGraw-Hill, 1980, p. 517.

[93] *Seeing Earth In a New Way*, JPL Publication 400-823, 1999, p. 2.

[94] Skolnik, M. I., *A Perspective of Synthetic Aperture Radar for Remote Sensing*, Naval Research Laboratory Memorandum Rept. 3783, 1978.

[96] Curlander, pp. 34-39

[97] Steinhardt, A., DARPATech2000 Speech on Discoverer II.

[98] Dorsey, M., *Funding Cut Threatens Space Project*, Air Force News, 25 Aug 1999.

[99] Collin, p. 207.

[100] York, p. 1.

[101] Brown, p. 26.

[102] York, p. 1.

[103] Mink, J., "Quasi-optical power combining of solid-state sources", *IEEE Transactions on Microwave Theory and Techniques*, vol. 34, Feb 1986, pp. 273-279.

[104] York, p. 12.

[105] York, p. 19.

[106] York, p. 18.

[107] Blake, p. 409.

[108] Butler, J. L., "Digital, Matrix, and Intermediate Frequency Scanning", in *Microwave Scanning Antennas*, *Vol III*, R. C. Hansen, ed., ch. 3, Academic Press, 1966.

[109] Rotman, W. and Turner, R. F., "Wide-Angle Microwave Lens for Line-Source Applications", *IEEE Transactions on Antennas and Propagation*, vol AP-11, no. 11, Nov 1963, pp. 623-632.

[110] Gent, H., "The Bootlace Aerial", *Royal Radar Establishment Journal*, Oct 1957, pp. 47-57.

[111] McGrath, D. T., "Planar three dimensional constrainted lenses", *IEEE Transactions on Antennas and Propagation*, vol AP-34, no. 1, Jan 1986, pp. 46-50.

[112] York, p. 229.

[113] York.

[114] Hollung, S., *Quasi-Optical Transmit/Receive Lens Amplifier Arrays*, Ph.D. dissertation, University of Colorado, Boulder, 1998.

[115] Popović, D., *Discrete Lens Arrays for Diversity Communication Systems*, Ph.D. comprehensive examination, University of Colorado, Boulder, 2001.

[116] http://www.ims2000.org/ss_xbndtr_ovrvw.pdf

[117] http://itri.loyola.edu/satcom2/03_05.htm

APPENDIX A

SAR MISSION REQUIREMENT FLOWDOWN

The following sections provide system-level traceability from SAR mission requirements to SAR antenna requirements. The emphasis is on sizing the radar antenna rather than the details of the radar electronics or digital data processing. As a result there are many important aspects of SAR system design (e.g., optimal waveform design, platform motion compensation, iso-doppler and iso-range contours, earth rotation effects, image formation) that are not covered. It is clear, however, that the choice of SAR antenna parameters has pervasive implications on the performance of the SAR system. The SAR antenna is not only the largest physical component in the radar system, but it also is the component upon which the overall SAR performance most depends.

A.1 Cross-Track Resolution

One of the most basic relationships in radar is range resolution. It is the measure of how closely two “targets” can be located in range and yet still be detected as separate “targets.” One can imagine that as the “target” range separation is decreased there will be a point beyond which their individual return echoes will overlap and therefore be indistinguishable. This point (δ_s) is half of the time length of the return echo (τ), the factor of one-half being necessary to account for the two-way distances involved in the range separation of the two “targets:”

$$\delta_s = \frac{c\tau}{2} \tag{A.1}$$

where c is the speed of electromagnetic propagation in air.

In unmodulated radar transmissions, the length of the return echo (τ) is typically just the length of the transmitted radar pulse (τ_t). Radar transmissions are oftentimes modulated or coded, however, to get the average power benefit of a longer pulse while retaining the range resolution performance of a shorter pulse. This technique, known as pulse compression, involves changing the carrier frequency within the transmit pulse length in a prescribed manner which is matched upon receiving the return echoes. The result after this range processing is a return echo "compressed" in time relative to the transmit pulse length. This compressed pulse length (τ_c) is inversely proportional to the bandwidth over which the carrier frequency is changed (B_r), the constant of proportionality being the frequency weighting factor k_f. Frequency weighting is done to control the compressed pulse shape and/or time sidelobe level. k_f ranges from 0.886 to 1.94 for a representative set of frequency weighting functions [18]. With pulse compression the slant range resolution (δ_s) expression becomes:

$$\delta_s = \frac{ck_f}{2B_r} \tag{A.2}$$

Equations (A.1) and (A.2) deal with resolution capability in the slant range direction relative to the radar. This is a performance measure used extensively in surveillance radars where the targets are "discretes" (e.g., ground vehicles, aircraft) and unwanted returns from the Earth are called clutter. In imaging radars where the Earth (or other planet) is the target of interest, the concept of resolution still applies, however, it is meaningful only in the "plane" of the image. In this case it is a measure of the granularity of the resulting image in the range direction. Since SARs are usually side-looking radars relative to the motion of the platform (see Section A.2), this range direction is commonly called cross-track.

Consider the idealized flat-earth geometry of an airborne or spaceborne radar looking down at the Earth in Figure A-1:

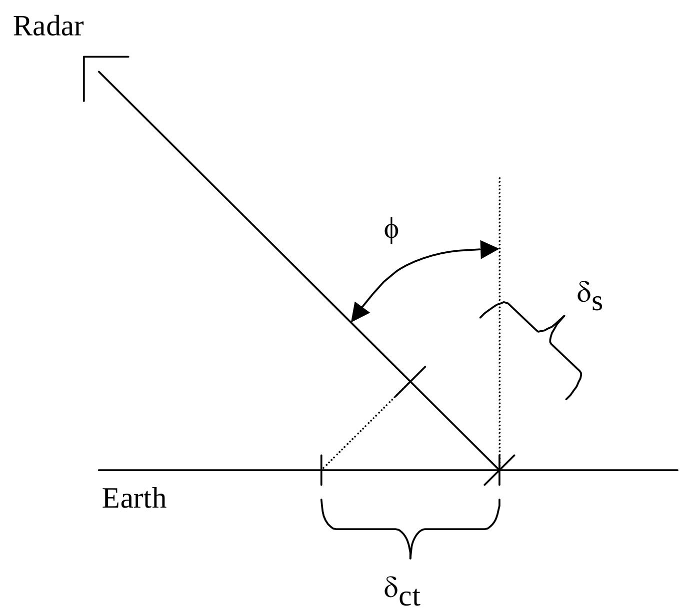

Figure A-1 Idealized flat-earth imaging geometry. Slant range resolution is projected down onto imaging "plane."

The slant range resolution is projected onto the Earth (the "plane" of the image), and the resulting cross-track resolution (δ_{ct}) depends on the incidence angle (ϕ):

$$\delta_{ct} = \frac{ck_f}{2B_r \sin(\phi)} \tag{A.3}$$

This idealized formulation, while not completely accurate, is useful in illustrating that image resolution in the cross-track dimension is inversely proportional to the bandwidth and the sine of the incidence angle.

Equation (A.3) is not completely accurate, of course, because the Earth is not flat. While the error may be acceptable in some airborne cases, it becomes significant when considering satellite altitudes. The curved-earth geometry is shown in Figure A-2.

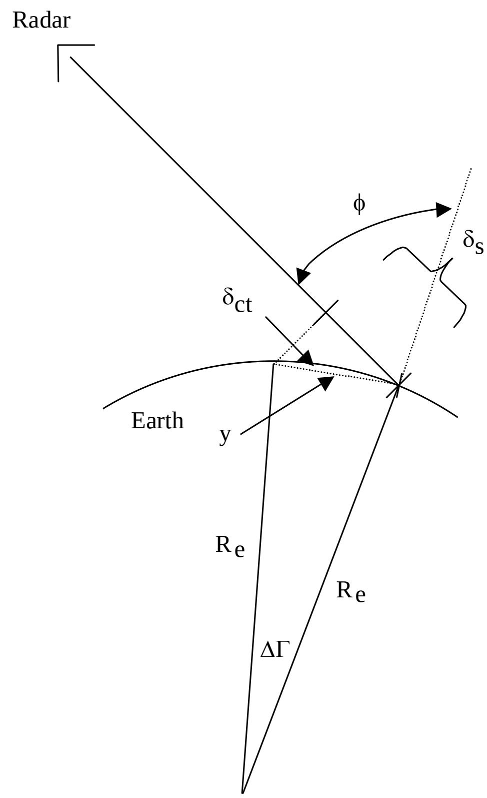

Figure A-2 Practical curved-earth imaging geometry. Slant range resolution is in reality projected onto the curved surface of the Earth.

If one generates an expression for "y" from each triangle of which it is a side, one can solve for the difference (ΔΓ) in the center-of-earth angle Γ and therefore the projection of the slant range resolution onto the Earth's curved surface:

$$\delta_{ct} = R_e \left[\phi - \cos^{-1}\left(\frac{ck_f}{2B_r R_e} + \cos(\phi) \right) \right] \tag{A.4}$$

where R_e is the Earth's radius. Although Equation (A.4) is quite different from Equation (A.3), the relationships between resolution, bandwidth, and incidence angle still apply. It is important to note that neither representation of cross-track resolution depends on the radar altitude or slant range to the target.

A.2 Along-Track Resolution

Imaging radars using the SAR technique rely on the relative motion of the platform for resolution in the "cross-range" direction and therefore are usually side-looking radars. In the perfectly side-looking case, the antenna beam is normal to the velocity vector (or track) of the platform. The dimension parallel to the velocity vector is commonly called the along-track dimension.

Before the SAR technique was invented, along-track image resolution was limited by the length of the antenna (L) in that dimension. This is because the length of the antenna nominally defines the 3-dB azimuth beamwidth (β_a), which together with the slant range (R_s) determines how closely two image features can be spaced along the track and still be separately detectable (see Figure A-3).

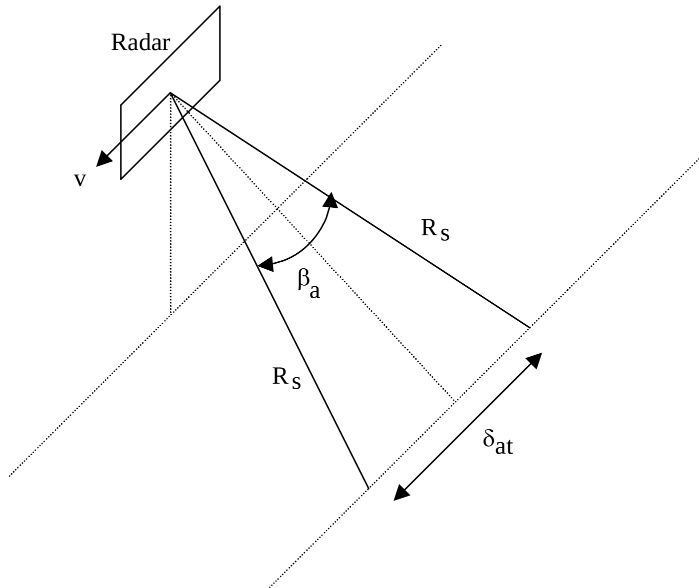

Figure A-3 Real-aperture along-track resolution. Without SAR along-track resolution was the extent of the azimuth beamwidth on the ground.

The footprint of the azimuth beamwidth on the ground defines the along-track resolution (δ_{at}) available:

$$\delta_{at} = 2R_s \sin\left(\frac{\beta_a}{2}\right) \approx R_s\beta_a \approx \frac{R_s\lambda}{L} \tag{A.5}$$

One sees immediately that the problem with this "real-aperture" imaging is that the along-track resolution is proportional to the slant range. While this may be marginally acceptable in some airborne cases, for spaceborne radars the length of the antenna required to produce a beamwidth narrow enough to compensate for the large slant range is prohibitive.

The SAR technique uses coherent azimuth signal processing to synthesize the long antenna needed for fine along-track resolution over time utilizing the motion of the platform. As depicted in Figure A-4 the basic idea is to coherently combine the target return echoes obtained as the radar's field of view sweeps by the target.

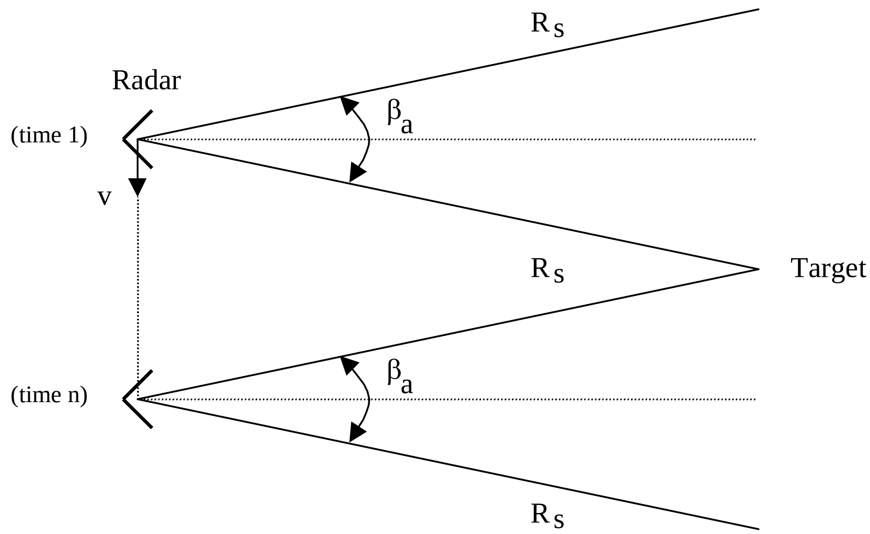

Figure A-4 Top view of SAR geometry. A long aperture is synthesized over time by coherently combining target returns as the radar's field of view sweeps by the target.

One can jump to the conclusion from Figure A-4 that, given the approximate synthetic aperture length of $R_s\beta_a$, the corresponding along-track resolution is L (obtained by substituting $R_s\beta_a$ for L in Equation (A.5)). This result, while not completely correct, is close enough to illustrate that with SAR processing the resolution is no longer dependent on range or frequency and is proportional to the antenna length, meaning that better resolution is possible with smaller antennas. The correct result is even better by the factor of two needed to account for the two-way phase correction required by SAR [1], and the previous conclusions still apply.

To verify this qualitative description, a look at the situation from the doppler-frequency perspective arrives at the same conclusion. Figure A-5 shows two targets separated in the along-track dimension parallel to the velocity vector of the radar platform.

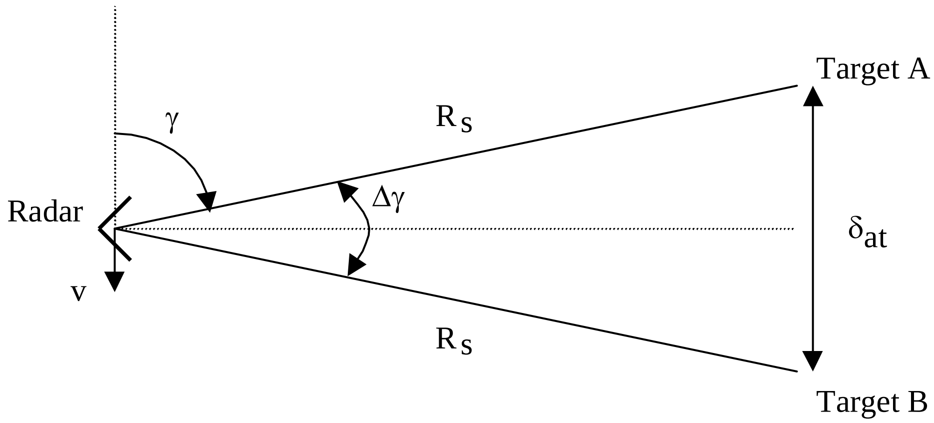

Figure A-5 Along-track target separation. SAR utilizes the different doppler shifts produced by closely-spaced targets in the along-track angle γ.

The SAR technique depends on the following observation that dates back to the early 1950s and is credited to Carl Wiley [2]. The two targets in Figure A-5 will produce different doppler frequency shifts in a given pulse's return echo by virtue of their separation in along-track angle (γ). Since the doppler frequency shift (f_d) is proportional to the radial velocity of the target [3], the difference in the doppler frequency shifts caused by each target is calculated as follows:

$$f_d(A) = \frac{2v}{\lambda}\cos(\gamma)$$

$$f_d(B) = \frac{2v}{\lambda}\cos(\gamma + \Delta\gamma)$$

$$\Delta f_d = \frac{2v}{\lambda}\left(\cos(\gamma) - \cos(\gamma + \Delta\gamma)\right) \tag{A.6}$$

The physical along-track separation of the targets (δ_{at}) is also a function of the two angles and can be substituted into Equation (A.6):

$$\delta_{at} = R_s\left(\cos(\gamma) - \cos(\gamma + \Delta\gamma)\right)$$

$$\Delta f_d = \frac{2v}{\lambda}\frac{\delta_{at}}{R_s} \qquad \text{(A.7)}$$

In order to be able to resolve two frequencies separated by Δf_d, one must have an observation time greater than the reciprocal of Δf_d [4]. This observation time is defined from Figure A-4 to be no greater than the synthetic aperture length (L_s) divided by the platform speed (v). These relationships result in an inequality that, with the appropriate substitutions (Equation (A.7) for Δf_d and Equation (A.5) for L_s), produces the desired result. Note that the synthetic aperture length is limited by the 3-dB azimuth beamwidth of the antenna:

$$\frac{1}{\Delta f_d} \leq T_o \leq \frac{L_s}{v} \longrightarrow \frac{1}{\Delta f_d} \leq \frac{L_s}{v}$$

$$\Delta f_d = \frac{2v}{\lambda}\frac{\delta_{at}}{R_s}$$

$$L_s \approx \frac{R_s\lambda}{L}$$

$$\therefore \delta_{at} \geq \frac{L}{2} \qquad \text{(A.8)}$$

This is the result that makes even modest-resolution imaging possible from a spaceborne platform. For example, Seasat, with a 10.7 m L-Band antenna, produced 6 m along-track resolution from an orbital altitude of 800 km using SAR processing [5]. Without

SAR processing, the Seasat radar would produce along-track resolution more than three orders of magnitude worse. The result in Equation (A.8) assumes that the radar coherently sums target return echoes as the entire 3-dB azimuth beamwidth sweeps by the target. It is the best along-track SAR resolution possible with an antenna beam that is not steered in the along-track dimension as the radar moves by. This fixed-beam mapping mode is called "stripmap" [6], and coherent processing of all of the pulses in the along-track beamwidth is termed "single-look" or "fully-focused" processing [7].

The well-known result in Equation (A.8), while being illustrative of the importance of SAR azimuth processing, contains some approximations as indicated in the supporting equations. In the interest of completeness, the exact relationship uses the expression for δ_{at} in Equation (A.5) as the synthetic aperture length and the particular expression for the beamwidth of the type of antenna being considered. For example, researching the antenna pattern calculation for the rectangular aperture most commonly used for spaceborne SAR, one finds the familiar sinc function in each dimension. In the azimuth dimension the antenna gain pattern ($g(\gamma)$) is calculated as follows [8]:

$$g(\gamma) = \left(\frac{\sin(u)}{u} \right)^2 \;\; ; \;\; u = \frac{\pi L}{\lambda} \sin(\gamma) \qquad \text{(A.9)}$$

where L is the uniformly-illuminated aperture length and λ is the wavelength. The azimuth beamwidth is calculated from Equation (A.9) by setting $g(\gamma)$ equal to ½, solving for γ, and then setting the result to half of the beamwidth:

$$g(\gamma) = \left(\frac{\sin(u)}{u} \right)^2 = \frac{1}{2} \qquad \longrightarrow \qquad u = 1.3915 = \frac{\pi L}{\lambda} \sin(\gamma)$$

$$\gamma = \sin^{-1}\left(\frac{1.3915\lambda}{\pi L} \right) = \frac{\beta_a}{2}$$

$$\beta_a = 2\sin^{-1}\left(\frac{1.3915\lambda}{\pi L} \right) \tag{A.10}$$

For small azimuth beamwidths, Equation (A.10) reduces to the familiar expression of 0.886 (λ/L) [9] for a uniformly-illuminated, rectangular aperture. While many different aperture illumination functions could be considered, probably the most common other than uniform are non-uniform amplitude and/or phase illuminations designed to reduce the azimuth sidelobes. These can be considered in general terms by interpreting L in Equation (A.10) to be the "effective azimuth aperture" L_e:

$$\beta_a = 2\sin^{-1}\left(\frac{1.3915\lambda}{\pi L_e} \right) \tag{A.11}$$

where L_e is less than L by an azimuth illumination factor k_a:

$$L_e = k_a L \tag{A.12}$$

Getting back to the exact representation for δ_{at}, the exact expression for the synthetic aperture length becomes the following using Equation (A.5):

$$L_s = 2R_s \sin\left(\frac{\beta_a}{2} \right) = 2R_s \sin\left(\sin^{-1}\left[\frac{1.3915\lambda}{\pi L_e} \right] \right) = 2R_s \frac{1.3915\lambda}{\pi L_e} \tag{A.13}$$

Using this in the formulation of δ_{at} followed in Equation (A.8), one calculates the exact relationship for a rectangular aperture to be:

$$\frac{\lambda R_s}{2v\delta_{at}} \leq \frac{2R_s 1.3915\lambda}{\pi L_e v}$$

$$\delta_{at} \geq \frac{\pi}{2(1.3915)}\frac{L_e}{2} \approx 1.13\frac{L_e}{2} \qquad \text{(A.14)}$$

One may coherently sum target return echoes over a smaller synthetic aperture length than the maximum in Equation (A.13) at the cost of along-track resolution. It is a linear relationship. If one coherently sums over half of the maximum synthetic aperture length, the resolution gets worse by a factor of two. This is typically done to improve the quality of the image when the best available resolution is not necessary. Due to the random nature of the individual scatterers in any given image, single-look processing often results in a grainy or speckled appearance representative of the particular realizations of the random scatterers. For example, the noncoherent addition of two images of the same area, each using one half of the maximum synthetic aperture length, can help to reduce this image speckle by averaging two realizations of each scatterer [10]. Equation (A.14) is modified to include this factor by inserting the along-track resolution degradation factor (k_r) into the definition of the synthetic aperture length. k_r is the ratio of the actual along-track resolution to the best possible along-track resolution given by Equation (A.14):

$$k_r = \frac{\delta_{at}}{\left(\frac{\pi L_e}{4(1.3915)}\right)}$$

$$L_s = \frac{2R_s}{k_r}\frac{1.3915\lambda}{\pi L_e} \approx \frac{0.886 R_s \lambda}{k_r L_e}$$

$$\delta_{at} = \frac{k_r \pi L_e}{4(1.3915)} \approx 1.13 k_r \frac{L_e}{2} \tag{A.15}$$

One notes that along-track resolution with SAR processing is inversely proportional to the time that the target is in the radar's field of view. That is, the longer the observation time the better the resolution. In the "stripmap" imaging mode where the beam is fixed in along-track angle, this time is limited by the azimuth beamwidth and therefore the effective aperture length. These are the relationships that produce Equation (A.14). This limitation does not always exist, however, if the radar has the capability of steering its beam in the along-track direction to increase the time a target is in its field of view. This beam steering, either electronic or mechanical, involves periodic shifting of the position of the beam's instantaneous field of view to obtain multiple "passes" of that field of view over the target location. Figure A-6 shows that each additional pass is obtained by steering the beam back by an azimuth beamwidth.

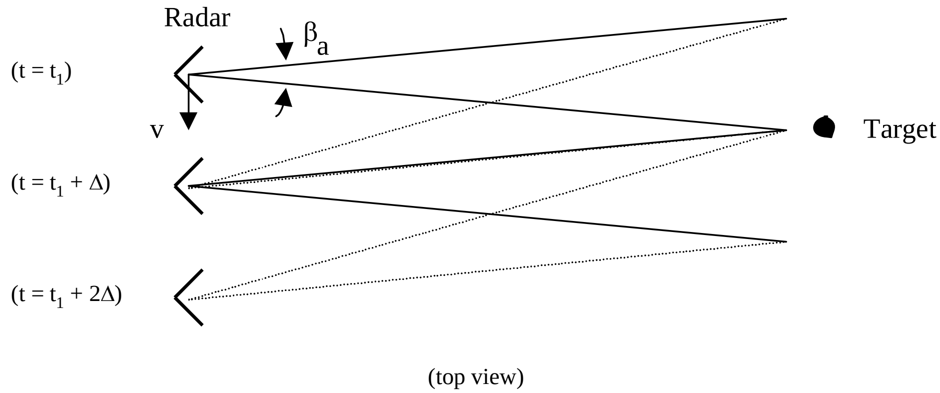

Figure A-6 Azimuth beamsteering in "spotlight" imaging mode. Target observation time can be increased and along-track resolution improved by steering the beam back (see dashed beam) so as to keep the target in the radar's field of view.

As indicated in Figure A-6, this type of imaging mode is known as "spotlight" imaging. Spotlight imaging makes the relationship between the azimuth and along-track dimensions a non-parallel one, but these complications can be accommodated in the coherent SAR processing. While spotlight imaging appears to offer unlimited resolution improvement, with that improvement comes a loss of along-track imaging coverage and the additional complexity of beam steering. One can easily see that each additional "pass" on a given target area obtained by beam steering is a "pass" taken away from another target area. For example, one can use beam steering to enhance along-track resolution by a factor of two so long as one accepts that only half of the along-track dimension can be mapped at that enhanced resolution. For this reason, spotlight imaging is intended more for tactical targets of opportunity than for general-purpose mapping. It is, therefore, more of a special-purpose capability that drives azimuth beam steering requirements rather than antenna length. Given an antenna effective length determined by the stripmap resolution required, the antenna's total azimuth beam steering capability must be enough to cover $\Delta\gamma$ in the following calculation:

$$\Delta\gamma = k_{sp}\beta_a \qquad (A.16)$$

where k_{sp} is the spotlight along-track resolution improvement factor.

A.3 Swath Width

As indicated in Figure A-7, swath width is the cross-track width of the strip or swath covered by the radar's field of view as it moves by.

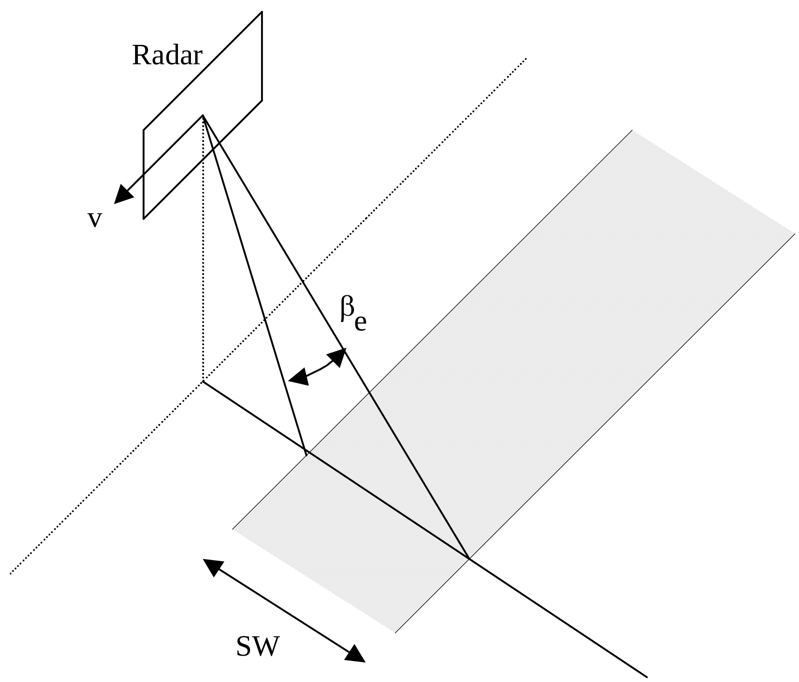

Figure A-7 SAR Swath Width. Swath width is the cross-track dimension of the area covered by the radar.

Swath width can be easily visualized when considering a single beam, in which case the swath is usually limited by the area covered by the beam's elevation 3-dB beamwidth (β_e).

Figure A-8 shows the idealized flat-earth geometry for which the 3-dB swath (SW_3) is approximated as follows:

$$SW_3 \approx \frac{R_s \beta_e}{\cos(\phi)} \approx \frac{R_s \lambda}{H \cos(\phi)} \tag{A.17}$$

The approximation correctly indicates that the swath width is dependent on slant range, wavelength, incidence angle, and the height of the antenna (H).

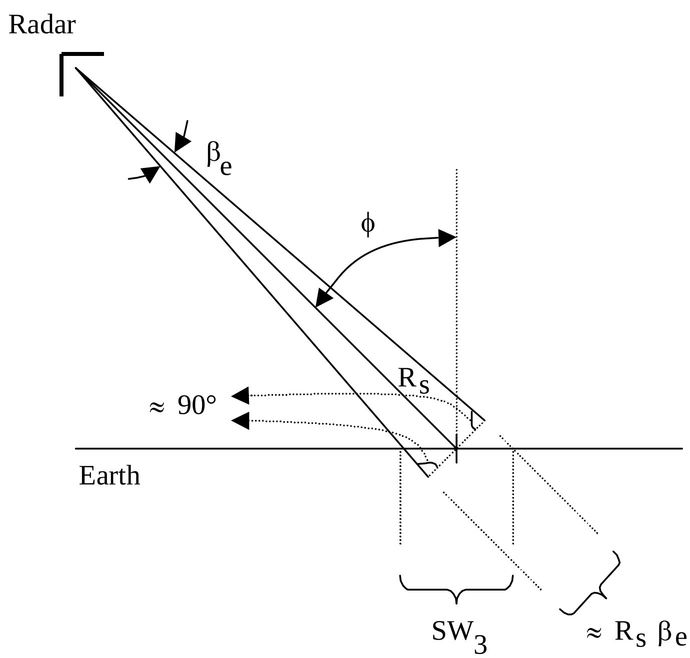

Figure A-8 Flat-Earth Approximation to Swath Width. Swath width is the projection of the elevation coverage of the beam onto the image plane.

As with cross-range resolution the curved-earth image plane must be used to obtain an exact relationship. Figure A-9 shows the calculation of the 3-dB swath width to be the difference between the ground range calculated at the near and far edges of the swath.

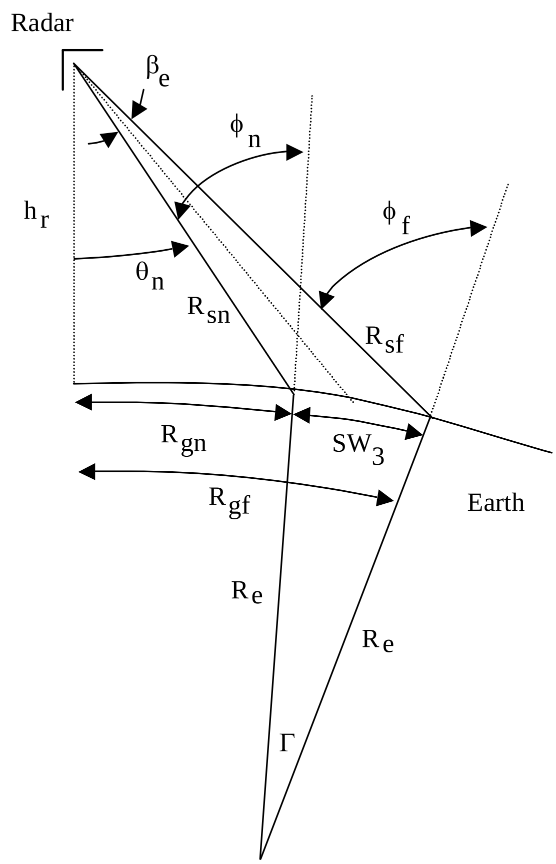

Figure A-9 Curved-Earth Geometry for Swath Width. Swath width is calculated as the difference in ground ranges to the near and far edges of the swath.

Using the law of sines one can calculate the ground range to the near edge of the 3-dB swath (R_{gn}) from the radar altitude (h_r) and the near-edge incidence angle (ϕ_n):

$$\theta_n = \sin^{-1}\left(\frac{R_e}{R_e + h_r}\sin(\phi_n)\right)$$

$$\Gamma_n = 180 - \theta_n - (180 - \phi_n) = \phi_n - \theta_n$$

$$R_{gn} = \Gamma_n R_e = R_e\left[\sin^{-1}\left(\frac{R_e + h_r}{R_e}\sin(\theta_n)\right) - \theta_n\right] \qquad \text{(A.18)}$$

One can similarly calculate the ground range to the far edge of the swath (R_{gf}) and then the 3-dB swath width as the difference between the two:

$$R_{gf} = R_e\left[\sin^{-1}\left(\frac{R_e + h_r}{R_e}\sin(\theta_n + \beta_e)\right) - (\theta_n + \beta_e)\right] \tag{A.19}$$

$$SW_3 = R_e\left[\sin^{-1}\left(\frac{R_e + h_r}{R_e}\sin(\theta_n + \beta_e)\right) - \sin^{-1}\left(\frac{R_e + h_r}{R_e}\sin(\theta_n)\right) - \beta_e\right] \tag{A.20}$$

where θ_n is the look angle at the near edge of the swath and β_e is the elevation 3-dB beamwidth defined similarly to the azimuth 3-dB beamwidth in Equation (A.11) with H_e being the effective elevation aperture:

$$H_e = k_e H$$

$$\beta_e = 2\sin^{-1}\left(\frac{1.3915\lambda}{\pi H_e}\right) \tag{A.21}$$

Although Equation (A.20) appears to bear little resemblance to Equation (A.17), it possesses the same relationships. As the effective elevation aperture grows, the 3-dB swath width decreases and vice-versa.

As is the case with coherent along-track processing over the azimuth beamwidth, one can certainly process less of the elevation 3-dB beamwidth if a narrower swath is desired. With the processed look angle range ($\Delta\theta_p$) replacing the 3-dB elevation beamwidth and the processed swath (SW_p) replacing the 3-dB swath in Figure A-9 and Equation (A.20), one can solve for $\Delta\theta_p$ as a function of SW_p. This assumes that $\Delta\theta_p$ begins at θ_n. This expression for

$\Delta\theta_p$ can also be used to calculate the necessary look angle interval from the near edge of the swath for a particular swath width:

$$SW_p = R_e\left[\sin^{-1}\left(\frac{R_e + h_r}{R_e}\sin(\theta_n + \Delta\theta_p)\right) - \sin^{-1}\left(\frac{R_e + h_r}{R_e}\sin(\theta_n)\right) - \Delta\theta_p\right]$$

$$\Delta\theta_p = \tan^{-1}\left[\frac{R_e\sin\left(\frac{SW_p}{R_e} + \sin^{-1}\left[\frac{R_e + h_r}{R_e}\sin(\theta_n)\right]\right) - (R_e + h_r)\sin(\theta_n)}{-R_e\cos\left(\frac{SW_p}{R_e} + \sin^{-1}\left[\frac{R_e + h_r}{R_e}\sin(\theta_n)\right]\right) + (R_e + h_r)\cos(\theta_n)}\right] \tag{A.22}$$

A.4 Range Ambiguity

At the heart of radar is “ranging” or deducing the range to a target by means of a measurement of the time delay between the transmission of a pulse of energy and the receipt of that portion of the pulse reflected from the target. Knowing the speed of propagation (usually the speed of light c), one can estimate the target range (R_{est}) by halving the product of the speed (c) and the measured time delay (Δt):

$$R_{est} = \frac{c\Delta t}{2} \tag{A.23}$$

This is easily visualized when considering the transmission of a single pulse. When one transmits the next pulse, however, “ranging” by time delay measurement becomes ambiguous. The ambiguity results from the possibility of receiving return echoes from more than one pulse at any one time. Figure A-10 illustrates this problem with a two-target scenario.

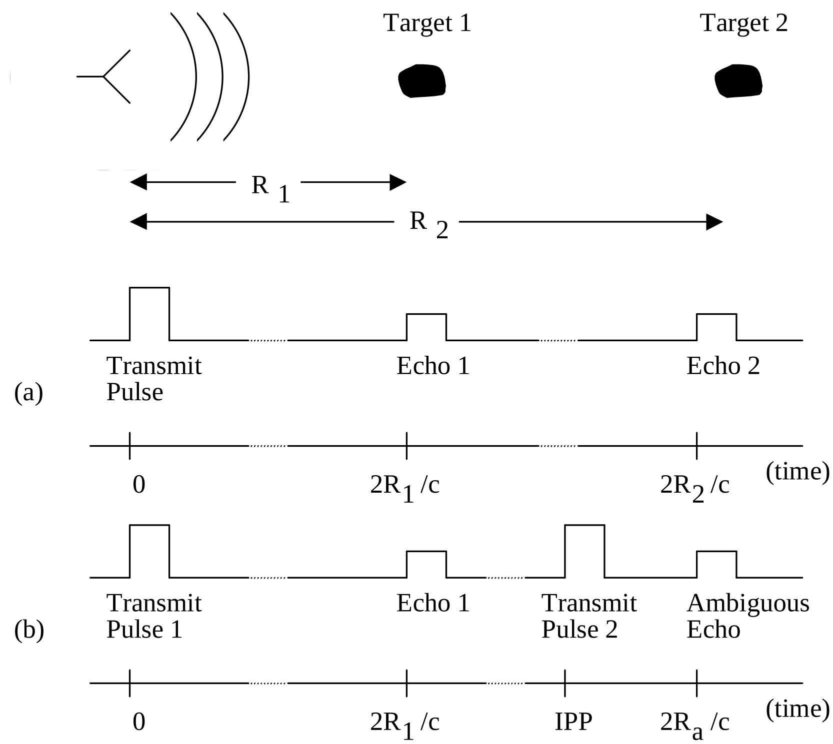

Figure A-10 Range Ambiguity. The ambiguity in range estimation results from the inability to distinguish one pulse's target return echo from another's.

In Figure A-10(a) a single pulse produces target return echoes that are delayed in time proportional to the respective slant ranges. The transmission of a second pulse at an interpulse period (*IPP*) less than the two-way propagation time to the second target (see Figure A-10(b)) creates ambiguity in the interpretation of the return from the second target. One cannot tell whether it came from the first pulse, in which case the time delay would be $2R_2/c$, or the second pulse, in which case the time delay would be $2R_a/c$. The IPP creates a maximum unambiguous range (R_{umax}), beyond which target ranges estimated by time delay are ambiguous:

$$R_{u\max} = \frac{cIPP}{2} \tag{A.24}$$

R_a in the Figure A-10(b) example would be R_2 modulo R_{umax}, which is always less than R_{umax}. In this manner all target ranges beyond R_{umax} “fold in” to the unambiguous range interval from 0 to R_{umax} when estimating range by time delay.

While range ambiguities must be resolved in surveillance or air traffic control radars attempting to detect and track targets over large range intervals, they have a different implication for imaging radars where the slant range intervals (Equation (A.22)) containing the targets of interest are typically much smaller. Imaging radars have the rather unique combination of long absolute slant ranges and narrow slant range intervals of interest. For example, Seasat, operating at an altitude of 800 km at a 20 deg look angle with a 2.2 m elevation aperture at L-Band, achieved its 100 km swath with a 38 km slant range interval of interest 859 km away from the satellite. Since the slant range interval of interest is usually narrow and predictable, absolute range measurement is usually less important than relative range measurement. Imaging radars typically take advantage of this situation by allowing the absolute slant range measurement to be ambiguous as long as the slant range interval of interest is less than the maximum unambiguous range (R_{umax}). The result is a shorter IPP or, equivalently, a longer PRF (PRF = 1/*IPP*) that allows more pulses (more average power) to be delivered while ensuring that all of the target returns are in the correct range order in relative terms. This also implies that there can be multiple pulses “in the air” at one time.

Range ambiguities, therefore, force a maximum limit on the PRF. Figure A-11 shows that the minimum time delay possible for a target return echo is the transmitted pulse length. This is the situation where the radar receiver is opened up immediately following the end of the transmitted pulse. The maximum time delay is shown to be the IPP less the transmitted pulse length. This ensures that the entire pulse will be received before the next pulse is transmitted.

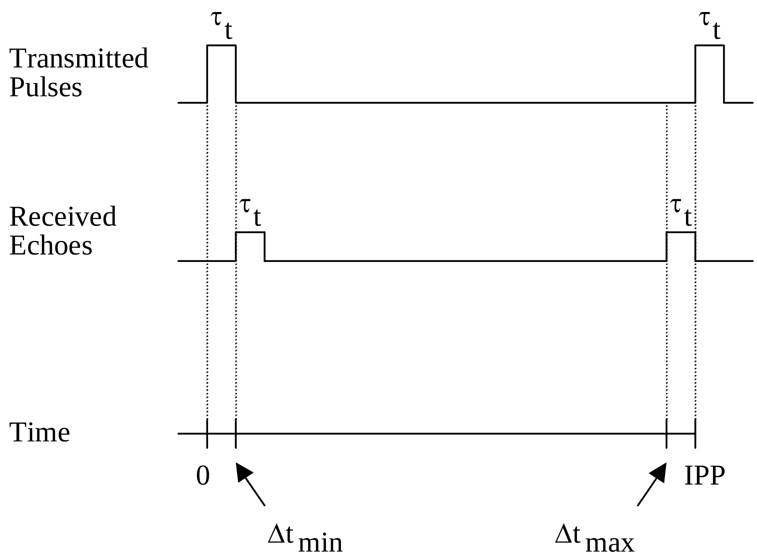

Figure A-11 Minimum and Maximum Target Return Echo Time Delays. These extremes define the minimum IPP needed to ensure that the entire slant range interval of interest is in the correct range order.

The upper limit on the PRF is calculated from the difference between the minimum and maximum ambiguous ranges as follows:

$$\Delta t_{\min} = \tau_t \quad ; \quad R_{\min} = \frac{c\tau_t}{2}$$

$$\Delta t_{\max} = IPP - \tau_t \quad ; \quad R_{\max} = \frac{c(IPP - \tau_t)}{2}$$

$$\Delta R_s = R_{\max} - R_{\min} = \frac{cIPP}{2} - c\tau_t = \frac{c}{2PRF} - c\tau_t$$

$$\therefore PRF \le \frac{c}{2(\Delta R_s + c\tau_t)} \tag{A.25}$$

The proper interpretation of Equation (A.25) is that the PRF must not be greater than the right-hand side of the equation, which is driven by the slant range interval of interest (ΔR_s

– see Equation (A.22)) and ultimately the look angle and swath width. Because real pulse shapes have sidelobes in time and real beam patterns have sidelobes in elevation, one can never completely eliminate ambiguous energy from other range intervals. This ambiguous energy reduces the sensitivity of the radar by effectively adding noise on top of the internal thermal noise. The smaller the PRF relative to the maximum PRF, however, the smaller the reduction of the target signal-to-noise ratio (*SNR*).

A.5 Azimuth Ambiguity

As is the case in the range domain, the use of multiple pulses creates ambiguities in the doppler or azimuth domain. Where range ambiguities required in an upper limit on the PRF used, the control of azimuth ambiguities forces a lower limit on the PRF. Doppler is related to azimuth in a side-looking radar by virtue of the doppler frequency shift being proportional to the relative speed of the target either towards or away from the radar. For a beam pointed normally to the velocity vector of the radar, the doppler frequency shift of a ground return at the peak of the beam will be zero since there is no component of the relative speed in the range direction. As one processes more of the azimuth beamwidth to get better resolution, however, the non-normal azimuth angles produce components of the relative velocity in the range direction that cause non-zero doppler frequency shifts in both the positive and negative directions (see Equation (A.6)).

The power spectrum of a series of transmitted pulses at a particular carrier frequency and a particular PRF is a set of discrete lines at the carrier frequency and at sideband frequencies separated on both sides from the carrier by integer multiples of the PRF. The envelope of this power spectrum is determined by the power spectrum of the pulse shape [11]. In ideal terms the power spectrum of a series of received echoes from a discrete target has the same set of lines and the same envelope, but the entire spectrum is shifted in frequency by the doppler shift of the discrete target. Figure A-12 shows the unshifted spectrum along with a number of shifted spectra representative of different doppler frequencies or in this case different azimuths. One can see from Figure A-12 that the PRF must be large enough so that the maximally-shifted doppler spectrum does not extend beyond an equivalent frequency shift of PRF/2.

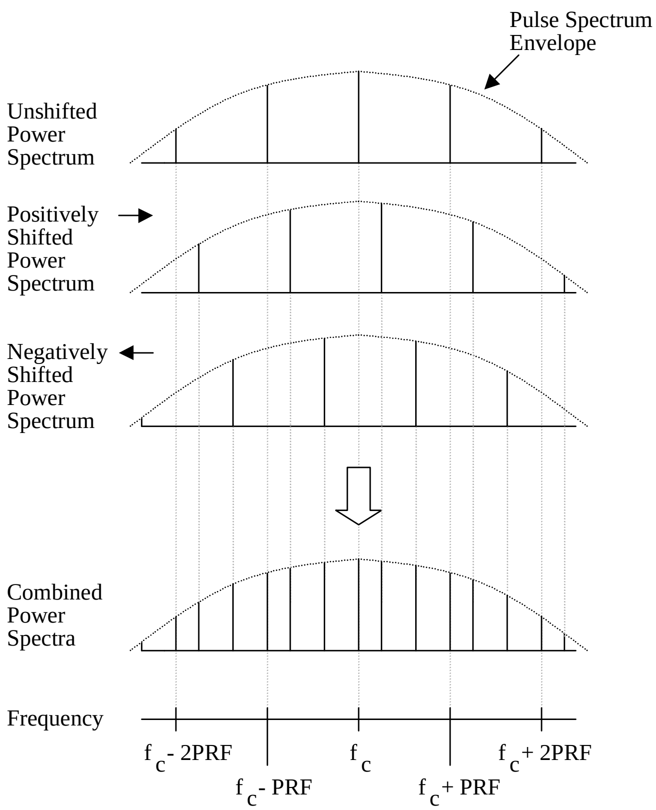

Figure A-12 Doppler Ambiguities. The PRF must be large enough so that the maximally-shifted positive and negative doppler spectra do not overlap.

This is the Nyquist criterion that ensures the absence of aliasing so that sampled, band-limited, continuous-time signals can be exactly reconstructed [12]. If, for the ideal case shown in Figure A-12, the PRF was less than the Nyquist frequency, negatively-shifted spectra would be confused with positively-shifted spectra resulting in ambiguity.

The Nyquist frequency (f_N) in the general sense is equal to the doppler frequency bandwidth (B_d) of the collection of target return echoes expected in the particular beam. This doppler frequency bandwidth is typically calculated over the 3-dB azimuth beamwidth to determine the minimum PRF. One can use Equation (A.6) to arrive at the minimum PRF:

$$B_d = \frac{2v}{\lambda}\left(\cos(\gamma) - \cos(\gamma + \Delta\gamma)\right) \ ; \ \gamma = \gamma_b - \frac{\beta_a}{2} \ , \ \Delta\gamma = \beta_a$$

$$B_d = \frac{2v}{\lambda}\left(2\sin(\gamma_b)\sin\left(\frac{\beta_a}{2}\right)\right) \ ; \ \beta_a = 2\sin^{-1}\left(\frac{1.3915\lambda}{\pi L_e}\right)$$

$$f_N = B_d = \frac{4v}{\lambda}\sin(\gamma_b)\left(\frac{1.3915\lambda}{\pi L_e}\right) \approx \frac{1.77v}{L_e}\sin(\gamma_b)$$

$$\therefore PRF \geq f_N \approx \frac{1.77v}{L_e}\sin(\gamma_b) \tag{A.26}$$

where γ_b is the along-track angle of the beam boresight. Note that this term disappears for the side-looking case where γ_b is 90 degrees.

In reality the target return echo doppler spectra are not strictly bandlimited since the only bandlimiting mechanism is the antenna beam pattern in azimuth that has sidelobes which degrade slowly. The result is that even with a PRF equal to the Nyquist frequency there will be portions of positively-shifted spectra confused with portions of negatively-shifted spectra. In short there will always be ambiguous energy that will increase the equivalent noise level. The higher the PRF rises above the minimum calculated in Equation (A.26) the lower this doppler or azimuth ambiguity impact on SNR.

A.6 Radar Range Equation

As basic to radar operation as the estimation of range by the measurement of round-trip time delay, the radar range equation provides a way of calculating the strength or amplitude of the target return echo. The power level of the target return echo relative to the power level of the noise in the receiver is the signal-to-noise ratio that is indicative of the detectability of a discrete target or the image quality of a distributed target. The development of the radar range equation is traced through the range (pulse compression) and azimuth (SAR) signal processing stages typical of imaging radars.

Pre-Processing. The power received by the radar (P_r) from a single return echo from a discrete target at a slant range R_s is [13]:

$$P_r = \frac{P_t G_t}{4\pi R_s^{\,2}} \sigma \frac{1}{4\pi R_s^{\,2}} A_r \tag{A.27}$$

where P_t is the peak transmit power at the transmit input to the antenna elements, G_t is the transmit antenna gain at the transmit input to the antenna elements, A_r is the effective receive antenna aperture, and σ is the radar cross-section (RCS) of the discrete target. A_r is related to the receive antenna gain (G_r) at the receive output of the antenna elements according to:

$$A_r = \frac{G_r \lambda^2}{4\pi} \tag{A.28}$$

P_r is therefore the receive signal power at the receive output of the antenna elements.

Noise power in the radar receiver that is independent of the presence of the target return echo is calculated from the equivalent noise temperature (T_s) at the receive input of the antenna elements [14]:

$$T_s = T_{ext} + \sum_n T_a(n)\left[NF(n) - 1\right]\frac{1}{G_p(n)}$$

$$N = kT_s B_{rx} \tag{A.29}$$

where k is Boltzmann's constant (1.38 x 10^{-23} W/HzK) and B_{rx} is the bandwidth of the receiver. T_s includes the noise contributions from the external environment (T_{ext}) and all components (component index = n) in the radar receive path, each contribution being translated to the receive reference point (the receive input of the antenna elements) via $G_p(n)$ which is the total gain from the reference point to the component input. The generic noise contribution of each component at the input to that component is the product of the component's ambient temperature (T_a) and its noise figure (NF) minus one.

The pre-processing signal-to-noise ratio (SNR_{pre}) at the receive output of the antenna elements for the discrete target is obtained by combining these three previous equations:

$$SNR_{pre} = \frac{P_r}{Nl} = \frac{P_t G_t}{4\pi R_s^{\ 2}} \sigma \frac{1}{4\pi R_s^{\ 2}} \frac{G_r \lambda^2}{4\pi} \frac{1}{kT_s B_{rx}} \frac{1}{l}$$

$$SNR_{pre} = \frac{P_t G_t G_r \sigma \lambda^2}{(4\pi)^3 R_s^{\ 4} k T_s B_{rx} l} \tag{A.30}$$

where l takes into account all appropriate losses. While care must be taken to define P_t and G_t at the same point and G_r and T_s at the same point, the locations of these two RF reference points are arbitrary. The transmit (x_t) and receive (x_r) reference points used here are the transmit output of the elements and the receive inputs to the elements, respectively (see Figure A-13). These two particular reference points are chosen to be generic and not unique to any particular antenna architecture. In practice these points are often chosen to coincide with the points at which the various RF quantities are easily measured for the particular antenna.

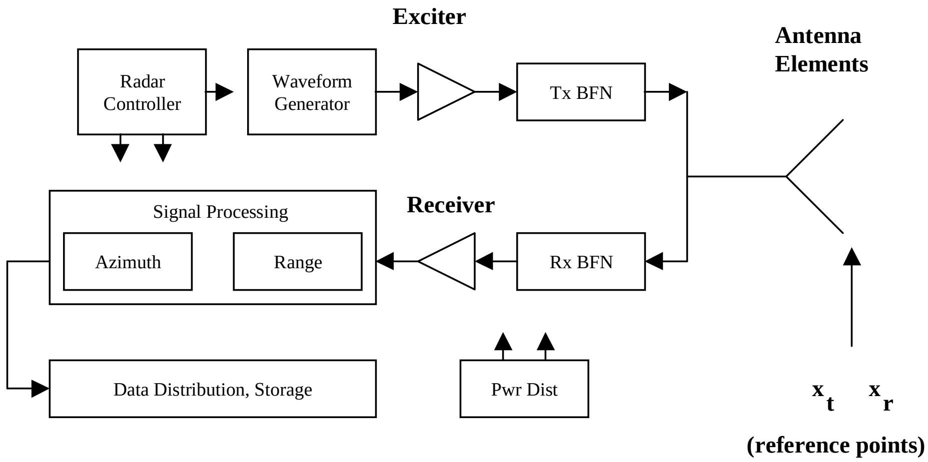

Figure A-13 Generic Radar Block Diagram. While the locations of the transmit and receive reference points (x_t and x_r) are arbitrary, the range equation parameters must be defined accordingly.

The RCS of a discrete target has the dimensions of area but is not necessarily the physical area of the target projected in the direction of the radar. It is the equivalent area of the discrete target assuming isotropic far-field reflection that would produce the received power intensity (W/m^2) actually measured (I_{rec}) at the radar [15]:

$$\sigma = \frac{I_{rec}}{I(R_s)} 4\pi R_s^{\ 2} \tag{A.31}$$

where $I(R_s)$ is the transmit power intensity incident on the target at slant range R_s.

For imaging radar applications the targets (earth's surface, sea surface, etc.) are extended or distributed, and the interpretation of target RCS must be expanded. In this case the extended target physical area (A) is broken up into elemental areas (dA), each of which is assigned a discrete RCS value. The ratio of these quantities is the unitless backscatter coefficient (σ_0) at that particular point [15]:

$$\sigma_0 = \frac{\sigma}{dA} \tag{A.32}$$

Due to the fact that there are usually multiple individual scatterers in any elemental area *dA*, considered to be at least as large as the two-dimensional resolution cell of the radar, the backscatter coefficient is a random variable. It is a mapping of the mean (σ^0) of this random variable (σ_0) that is usually the desired SAR image [16]:

$$\sigma^0 = E\{\sigma_0\} \tag{A.33}$$

The individual realizations of the σ_0 random variable are the source of image speckle described in Section A.2.

Given that this mean backscatter coefficient is a normalized measure of radar reflection from a distributed target [17], it must be multiplied by the applicable surface area (A_σ) to produce the extended target RCS. This applicable area, considering that range and azimuth processing will produce finer resolution, is the post-processing two-dimensional resolution cell of the radar. This cell is the area bounded by the post-processing cross-track resolution cell (δ_{ct}) and the post-processing along-track resolution cell (δ_{at}). The pre-processing SNR for the extended target at the receive output of the antenna elements is then:

$$SNR_{pre} = \frac{P_t G_t G_r \lambda^2}{(4\pi)^3 R_s^{\,4} k T_s B_{rx} l} \sigma^0 \delta_{ct} \delta_{at} \tag{A.34}$$

Range Processing. The signal processing typical of imaging radars in the range dimension is for pulse compression as described in Section A.1. This is denoted generically in Figure A-13 because it can be implemented by analog means, by digital means, or by a hybrid approach. The particular method, to be chosen based on operational flexibility and the time-bandwidth products required, is otherwise important only for its effect upon pre-processing signal power and noise power. This effect, while different depending on the particular implementation, is the same for signal and noise making the combined effect on the signal-to-noise ratio independent of the implementation.

The slant range resolution improvement provided by pulse compression is the ratio of the transmitted pulse (τ_t) to the compressed pulse (τ_c) as described in Section A.1. This resolution improvement, approximated as the signal's time-bandwidth product ($\tau_t B_r$), comes with a signal-to-noise ratio improvement courtesy of the range signal processing involved [19]:

$$\frac{\tau_t}{\tau_c} = \frac{\tau_t B_r}{k_f} \approx \tau_t B_r$$

$$SNR_r = SNR_{pre}\frac{\tau_t}{\tau_c} = SNR_{pre}\frac{\tau_t B_r}{k_f} \approx SNR_{pre}\tau_t B_r \tag{A.35}$$

where SNR_r is the signal-to-noise ratio after range processing.

Azimuth Processing. The azimuth processing in Figure A-13 is the coherent combining of target returns from multiple transmit pulses necessary to synthesize the longer aperture needed for the fine along-track resolution enabled by SAR. The signal-to-noise ratio improvement provided by this coherent azimuth processing is equal to the number of pulses coherently integrated. This number (n_a) is the product of the PRF used and the synthetic aperture time. The PRF used must exceed the minimum value shown in Equation (A.26) but is independent of the along-track resolution sought. The synthetic aperture time is a function of the along-track resolution by virtue of the synthetic aperture length shown in Equation (A.15):

$$PRF = k_p PRF_{\min} = \frac{4vk_p}{\lambda}\sin(\gamma_b)\frac{1.3915\lambda}{\pi L_e}$$

$$L_s = \frac{2R_s}{k_r}\sin\left(\frac{\beta_a}{2}\right) = 2R_s\frac{1.3915\lambda}{\pi L_e}\frac{\left(\frac{\pi L_e}{4(1.3915)}\right)}{\delta_{at}} = \frac{R_s\lambda}{2\delta_{at}}$$

$$SNR_{ra} = SNR_r n_a = SNR_r PRF\frac{L_s}{v} = SNR_r k_p PRF_{\min}\frac{R_s\lambda}{2v\delta_{at}} \qquad \text{(A.36)}$$

where k_p is the minimum PRF multiplier and SNR_{ra} is the integrated SNR after both range and azimuth processing. When the PRF is equal to the minimum PRF (k_p = 1) and the boresight along-track angle is 90 degrees, the SNR gain provided by azimuth processing is identical to the along-track resolution improvement provided (resolution without SAR processing (Δ_{at}) divided by resolution with SAR processing (δ_{at})):

$$\frac{SNR_{ra}}{SNR_r} = k_p PRF_{\min}\frac{R_s\lambda}{2v\delta_{at}} = k_p\frac{4v\sin(\gamma_b)(1.3915)}{\pi L_e}\frac{R_s\lambda}{2v\delta_{at}} = k_p\sin(\gamma_b)\frac{2(1.3915)R_s\lambda}{\pi L_e\delta_{at}}$$

$$\Delta_{at} = 2R_s\sin\left(\frac{\beta_a}{2}\right) = \frac{2R_s(1.3915)\lambda}{\pi L_e} \qquad \text{(from Equation (A.5))}$$

$$\frac{\Delta_{at}}{\delta_{at}} = \frac{2R_s(1.3915)\lambda}{\pi L_e\delta_{at}} = \frac{SNR_{ra}}{SNR_r} \qquad \text{(A.37)}$$

Increasing the PRF above the minimum value (k_p > 1) provides additional SNR improvement but does not affect the along-track resolution since the synthetic aperture length is unchanged.

Post-Processing. The range and azimuth signal processing described in the previous paragraphs provides signal-to-noise ratio gain to the pre-processing SNR (SNR_{pre}) of Equation (A.34). Equations (A.35) and (A.36) describe the range and azimuth signal processing gains provided:

$$SNR_{pre} = \frac{P_t G_t G_r \lambda^2}{(4\pi)^3 R_s^{\,4} k T_s B_{rx} l} \sigma^0 \delta_{ct} \delta_{at} \qquad \text{(from Equation (A.34))}$$

$$SNR_r = SNR_{pre} \frac{\tau_t B_r}{k_f} \qquad \text{(from Equation (A.35))}$$

$$SNR_{ra} = SNR_r k_p PRF_{\min} \frac{R_s \lambda}{2v\delta_{at}} = SNR_r PRF \frac{R_s \lambda}{2v\delta_{at}} \qquad \text{(from Equation (A.36))}$$

$$SNR_{ra} = SNR_{pre} \frac{\tau_t B_r}{k_f} PRF \frac{R_s \lambda}{2v\delta_{at}} = \frac{P_t \tau_t PRF G_t G_r \lambda^3 \sigma^0 \delta_{ct} B_r}{(4\pi)^3 R_s^{\,3} k T_s k_f\, 2v B_{rx} l} \qquad \text{(A.38)}$$

One can substitute Equation (A.3) for δ_{ct} to generate an approximate although more familiar form of the integrated signal-to-noise ratio:

$$\delta_{ct} \approx \frac{c k_f}{2B_r \sin(\phi)} \qquad \text{(from Equation (A.3))}$$

$$SNR_{ra} \approx \frac{P_t \tau_t PRF G_t G_r \lambda^3 \sigma^0 c}{(4\pi)^3 R_s^{\,3} k T_s B_{rx} l 4v \sin(\phi)} \qquad \text{(A.39)}$$

Adequacy. SNR in surveillance radars is a measure of discrete target detectability. For example, a discrete target exhibiting RCS fluctuation according to the Swerling I model has an 80% probability of detection with a 10^{-6} probability of false alarm if it has a SNR of 17.8 dB [20]. For imaging radars detecting extended or distributed targets, however, the SNR goal is 0 dB above which thermal noise is not the dominant noise effect in the image [21]. This enables processing designed to reduce other noise effects (e.g., speckle) to be effective. The unity SNR requirement is often translated to a requirement on the backscatter coefficient. This noise-equivalent backscatter coefficient (σ_{ne}^{0}) [22] is the backscatter coefficient for which the signal power is equivalent to the noise power:

$$\sigma_{ne}^{\ 0} = \frac{(4\pi)^3 R_s^{\ 3} k T_s k_f \, 2vB_{rx} l}{P_t \tau_t PRF G_t G_r \lambda^3 \delta_{ct} B_r} \tag{A.40}$$

When comparing noise-equivalent backscatter coefficients, the lower the better.

Ambiguity Levels. As noted in Sections A.4 and A.5 even properly chosen PRFs will result in some level of ambiguous energy that increases the equivalent noise level with which the target signal must compete. These noise terms (azimuth ambiguity to signal ratio (*AASR*) and range ambiguity to signal ratio (*RASR*) [23]) are multiplicative in that they are proportional to the level of the signal:

$$ASR = AASR + RASR$$

$$SNR_{total} = \frac{1}{\dfrac{1}{SNR_{ra}} + ASR} \tag{A.41}$$

If the total ambiguity to signal ratio (*ASR*) term is on the order of -20 dB or lower, it can be ignored. If the impact of ASR given the choice of PRF is not tolerable, one must consider sidelobe reduction measures in the appropriate dimensions (time, azimuth, and/or elevation).

A.7 Prime Power

A practical constraint on radar system design not unique to imaging radars is the average electrical (prime) power needed to make the system operate as designed. Some of the active components that use electrical power depend on the parameters described in Section A.6 while others are constant and unrelated.

Often the largest user(s) of prime power is (are) the amplifier(s) generating the transmit signal. While every amplifier in the transmit path must be accounted for, the HPAs are the largest contributors. For each individual HPA the average prime power consumed while the radar is operating (P_{h-p}) is proportional to the product of the peak RF power out of the amplifier (P_{h-r}), the transmit pulsewidth (τ_t), and the *PRF*:

$$P_{h-p} = \frac{\tau_t PRF}{\eta_{DC}} \left(\frac{P_{h-r} - \frac{P_{h-r}}{g}}{\eta_{PAE}} \right) = \frac{\tau_t PRF}{\eta_{DC}} \frac{P_{h-r}}{\eta_{PAE}} \left(1 - \frac{1}{g} \right) \qquad \text{(A.42)}$$

where η_{DC} is the DC/DC conversion efficiency, η_{PAE} is the power-added efficiency of the amplifier, and g is the amplifier gain. The sum of the P_{h-r} values over all of the HPAs less any losses between the HPA output and the transmit reference point is the peak RF power term (P_t) in the radar range equation. The total prime power required for transmit amplifiers (P_{tx-p}) is the summation of Equation (A.42) over all HPAs as well as any driver amplifiers used:

$$P_{tx-p} = \sum_{nt} P_{h-p}(nt) \qquad \text{(A.43)}$$

where *nt* includes all of the transmit amplifiers.

Amplifiers in the receive path are "on" longer (between pulses) than the HPAs but consume less power per amplifier due to the low signal powers on receive. Assuming that these LNAs are "on" for the entire time between pulses, one calculates the average prime power per amplifier ($P_{l\text{-}p}$) as a function of the DC power required when the amplifier is on ($P_{l\text{-}d}$).

$$P_{l-p} = \frac{(1-\tau_t PRF)}{\eta_{DC}} P_{l-d} \tag{A.44}$$

The total average receive prime power ($P_{rx\text{-}p}$) is the sum of Equation (A.44) over all of the receive amplifiers used (nr):

$$P_{rx-p} = \sum_{nr} P_{l-p}(nr) \tag{A.45}$$

This total is often much less than the transmit total. When the antenna is large in terms of wavelengths, however, the receive amplifier average prime power can exceed that consumed by the transmit amplifiers:

There are other electronics in the radar that require prime power independent of transmit and receive operation. While these can be summed into one, the individual components are notable. They are radar control electronics (*RC*), antenna control electronics (*AC*) including phase shifters used for beam steering, signal processing electronics (*SP*), and data distribution electronics (*DD*). The total average prime power required by the radar when operating is the sum of the transmit, receive, and electronics components:

$$P_{rc-p} = \frac{1}{\eta_{DC}} P_{rc-d}$$

$$P_{ac-p} = \frac{1}{\eta_{DC}} P_{ac-d}$$

$$P_{sp-p} = \frac{1}{\eta_{DC}} P_{sp-d}$$

$$P_{dd-p} = \frac{1}{\eta_{DC}} P_{dd-d}$$

$$P_p = P_{tx-p} + P_{rx-p} + P_{rc-p} + P_{ac-p} + P_{sp-p} + P_{dd-d} \qquad \text{(A.46)}$$

A.8 Data Rate

Imaging radars must eventually get their data to Earth for use. Where the missions are limited in time and the platform returns to Earth, the data are typically recorded on board and processed after the mission. Examples are SIR-C and SRTM. Limited "live" downlink of data is done in order to verify the quality of the data being recorded. For satellite-based radars all of the data must be downlinked over a space-to-ground communication channel that is limited in capacity. Even with unlimited access, the capacity of the downlink channel often restricts the operation of the radar in resolution and coverage. In reality the finite number of satellite ground stations able to receive radar data further limits the amount of data that can be downlinked in any given orbit.

Satellite-based systems implement a data storage buffer to temporarily hold radar data until it can be downlinked to Earth. The size of this buffer is driven by the rate of the data being produced relative to the data rate capacity of the downlink channel, the amount of time the radar operates per orbit, and the amount of time available for data downlink per orbit. Alternatively, maximum downlink data rate, storage buffer size, and ground station access time limit the amount of useful data that can be produced by the radar per orbit. This restricts either radar coverage (the amount of time the radar can operate) or resolution or both.

The data rate of the satellite-to-ground communication channel (d_c) times the time that this communication channel is available per orbit (t_c) defines the data capacity of the channel per orbit (D_c):

$$D_c = d_c t_c \tag{A.47}$$

On average the data produced by the radar per orbit (D_r) must not exceed the data capacity of the channel (D_c), the alternative implying infinite data storage on board.

The radar produces both telemetry data (data describing the status of the radar) and target return data. Both require overhead bits to be downlinked over the communication channel. Communication overhead is described by an overhead factor (k_o) in units of bits per bit. Telemetry data (b_t) can be considered a constant number of bits per orbit, whereas the volume of target return data depends on the analog-to-digital converter (ADC) sampling rate (f_s), the number of bits per ADC sample (b_s), and the time per orbit that target return data is being sampled (t_s). The ADC sampling rate must be larger than the RF bandwidth of the transmitted signal (B_r), which in turn depends on the cross-track resolution desired (see Equation (A.4)):

$$f_s = k_s B_r \tag{A.48}$$

where k_s is the bandwidth oversampling factor ($k_s \geq 1$). The better the resolution, the wider the RF bandwidth and the faster the ADC sampling rate. The data sampling time per orbit (t_s) is a function of radar coverage:

$$t_s = \sum_i \left(\frac{2\Delta R_{s\,i}}{c} + \tau_{t\,i} \right) \qquad \text{(A.49)}$$

where *i* includes all of the pulses processed, ΔR_s is the slant range interval processed between pulses, and τ_t is the transmit pulsewidth. The larger the coverage, either the larger the slant range interval or the larger the number of pulses. In short, better performance requires that more digital data be produced:

$$D_r = k_o \left(b_t + f_s b_s t_s \right) \qquad \text{(A.50)}$$

The data storage capacity on board the satellite must be at least D_r, even with a communication channel capacity D_c each orbit, to allow for the worst-case situation where all of the radar activity in any particular orbit is scheduled to happen before the satellite has access to the ground station.

A.9 Airborne vs Spaceborne Platforms

The preceding sections have treated the parameter/performance relationships generically with limited discussion of the unique features of airborne and spaceborne radars. In addition to the data rate constraints noted in Section A.8 for the spaceborne sensor, there are other differences of interest that stem from the characteristic differences in platform altitudes.

The most obvious difference in the much longer absolute slant ranges for the spaceborne case. With slant range being cubed in its denominator, the radar range equation (Equation (A.38)) indicates that the spaceborne radar will likely require more transmit power and/or higher antenna gain to compensate for the range loss. While increasing transmit power is possible, it quickly becomes an expensive proposition in space. The more common alternative is to increase antenna gain by increasing the aperture size(s). In addition to the associated cost penalty, implementing a larger antenna also degrades along-track resolution (via a longer antenna in azimuth – Equation (A.14)) and/or reduces the swath width (via a taller antenna in elevation – Equation (A.17)).

These two performance measures are also adversely impacted by virtue of the much higher platform speeds necessary in the spaceborne case. The QuickLook SAR Model worksheet calculates the necessary orbital speed for spaceborne systems given the orbit altitude based on orbital mechanics. Airborne platforms are not similarly constrained. The result is that spaceborne platform speeds are more than an order of magnitude higher than airborne platform speeds. The performance impact of the higher speed is apparent when one determines that along-track resolution and swath width are fundamentally related [28]. Using the expressions already developed for along-track resolution and minimum/maximum PRF, one concludes that the ratio of the along-track resolution (δ_{at}) and the slant range interval (ΔR_s) that defines the swath is proportional to the platform speed:

$$\delta_{at} \geq \frac{\pi}{2(1.3915)}\frac{L_e}{2} = \frac{\pi L_e}{4(1.3915)} \qquad \text{(from Equation (A.14))}$$

$$PRF \geq f_N \approx \frac{1.77v}{L_e}\sin(\gamma_b) \approx \frac{1.77v}{L_e} \qquad \text{(from Equation (A.26))}$$

$$PRF \leq \frac{c}{2(\Delta R_s + c\tau_t)} \approx \frac{c}{2\Delta R_s} \qquad \text{(from Equation (A.25))}$$

$$\frac{1.77v}{L_e} \leq PRF \leq \frac{c}{2\Delta R_s} \longrightarrow \frac{1.77v}{L_e} \leq \frac{c}{2\Delta R_s} \longrightarrow \Delta R_s \leq \frac{cL_e}{2(1.77)v}$$

$$\therefore \frac{\delta_{at}}{\Delta R_s} \geq \frac{1.77\pi}{2(1.3915)c}v \qquad \text{(A.51)}$$

The interpretation of Equation (A.51) is that a larger platform speed implies either degraded resolution or a reduced swath or both.

On the other hand increased platform speed positively impacts the area coverage rate. Section A.10 notes that the area coverage rate (*ACR*) is the ratio of the product of the swath width (*SW*) and the azimuth footprint (FP_{az}) to the observation time (T_o). Realizing that the observation time is the azimuth footprint divided by the platform speed, one concludes that the area coverage rate for stripmap operation is the product of the swath width and the platform speed:

$$ACR = \frac{SW\,FP_{az}}{T_o} \quad ; \quad T_o = \frac{FP_{az}}{v}$$

$$ACR = SW\,v \qquad \text{(A.52)}$$

Therefore, for the same swath, regardless of the resolution, the spaceborne radar covers the imaging area faster than the airborne radar by the ratio of the speeds.

The area coverage rate along with the expanded spatial field of view (for a given angular field of view) are two of the more important reasons that spaceborne sensors are considered despite their obvious cost disadvantages.

A.10 Antenna Parameter Selection

Given all of the relationships documented in Sections A.1 through A.8, where does one begin in the design of a SAR antenna? As a way of generating a systematic approach that ensures that all of the radar performance requirements are met and all of the resulting impacts are understood, an Excel model was developed that provides guidance. This model, shown in Appendix B, includes a "quick-look" high-level flowdown of SAR performance requirements as well as detailed performance calculations at the individual beam level.

A high-level evaluation is the purpose of the QuickLook SAR Model (QuickLook worksheet tab). Appendix B shows that this evaluation is broken down into Mission Requirements and Constraint Calculations. The mission requirement inputs, noted in italics, include altitude, frequency, resolution, and noise equivalent sigma zero. Calculations based on these inputs are shown in regular font. The constraint calculations are organized into three regimes of incidence angles, each regime doing the same calculations but with different inputs. The two inputs for each incidence angle regime are the incidence angle at the beginning of the swath and the width of the swath. Everything else is calculated including the look-angle interval (minimum elevation beamwidth) necessary to cover the swath (Equation (A.22)) and the corresponding maximum effective antenna height (Equation (A.21)). The maximum effective antenna length is calculated, assuming stripmap SAR operation, from the desired along-track resolution (Equation (A.14)). The desired cross-track resolution together with the particular incidence angle determine the minimum transmit signal bandwidth (Equation (A.4)). Finally, a relative measure of radar sensitivity (RS_{rel}) is calculated from Equations (A.28) and (A.40), with some simplifying assumptions, that can be used to determine the *relative* difficulty of achieving the desired peak-of-beam performance at the various incidence angles:

$$\sigma_{ne}{}^{0} = \frac{(4\pi)^3 R_s{}^3 k T_s k_f\, 2\nu B_{rx} l}{P_t \tau_t PRF G_t G_r \lambda^3 \delta_{ct} B_r} \qquad \text{(from Equation (A.40))}$$

$$A_r = \frac{G_r \lambda^2}{4\pi} \qquad A_t = \frac{G_t \lambda^2}{4\pi} \qquad \text{(from Equation (A.28))}$$

$$k_f = 1 \qquad B_{rx} = B_r \qquad l = 1$$

$$RS_{rel} = \frac{P_t \tau_t PRF A_t A_r}{T_s} = \frac{8\pi\lambda R_s{}^3 k \nu}{\delta_{ct}\sigma_{ne}{}^{0}} \qquad \text{(A.53)}$$

Note that RS_{rel} equates terms composed of mission requirements (rightmost term) and radar parameters (middle term). The QuickLook SAR Model stops here with the only guidance for the selection of the individual radar parameters being the relative sensitivity and the maximum effective antenna heights and lengths.

As one delves deeper into the detailed relationships, there is surprisingly little freedom in the selection of the radar parameters suggested by RS_{rel}. The Beam SAR Model (Beam 1 worksheet tab – Appendix B) begins with the Mission Requirements reproduced from the QuickLook SAR Model worksheet. The initial inputs are the Antenna Parameters that are independent of the particular individual beam. These are the antenna boresight angles and scan loss, the height and length, the aperture efficiencies, the element losses, the receive parameters for system noise temperature, the digital processing loss, the number of bits used in digital sampling, and the power requirements of the RF and digital components.

Beam Parameters begins with the selection of incidence angle at the near Edge of Coverage (EOC) or the near edge of the swath. This selection is constrained only by the fact that incidence angles can range from 0 to 90 degrees. Constrained input cells or performance cells are outlined in yellow. When the particular value violates the accompanying constraint, its cell is filled with yellow. Based on the near EOC incidence angle, the near EOC look angle and slant range are calculated using the law of sines. Based on the near EOC incidence angle and the cross-track resolution requirement, the minimum signal (transmit) bandwidth for the beam is calculated (Equation (A.4)).

The azimuth beam-broadening factor is selected next subject to the constraint that this factor cannot be less than unity. This is the factor by which the azimuth beamwidth is broadened relative to its focused or minimum value. The effective antenna length and resulting azimuth beamwidth are then calculated based on the beam-broadening factor, the physical antenna length, the aperture efficiency, and the wavelength. The effective antenna length is constrained to be less than the maximum value calculated in the QuickLook model in order to achieve the required (stripmap) along-track resolution. Equivalently, the 3-dB along-track resolution for the particular effective antenna length is calculated (Equation (A.14)). The effective antenna length is also used to determine (Equation (A.26)) the bandwidth of doppler frequencies illuminated by the azimuth beamwidth, which is the minimum value for the PRF.

Of the radar parameters that comprise the relative sensitivity measure (Equation (A.53)), the transmit pulsewidth is the next to be specified (after the system noise temperature) in order to facilitate the subsequent selections of swath width and PRF. In addition to the constraint that the time (slant-range) interval of the swath returns must be less than the IPP (maximum unambiguous range – Section A.4), the swath return time interval must also be uncorrupted by the transmit pulse and the receipt of the nadir return. While the IPP and the transmit pulse event are independent of the geometry of the imaging scenario, the relative locations of the nadir return and the beginning of the swath are functions of the radar altitude and look angle. Figure A-14 shows a representative situation. Given the transmit pulse length, the nadir return length (suggested to be the length of two transmit pulses [24]), and the geometry, the maximum available imaging slant-range interval is calculated in a table as a function of PRF. The largest maximum slant-range interval over the appropriate range of PRFs is extracted from the table and used to calculate the corresponding maximum swath width available. With the upper limit being the smaller of the maximum swath available versus PRF and the maximum swath limited by the horizon, the swath width is next selected and subsequently used to calculate the corresponding look-angle interval and the look angle, incidence angle, and slant range at the far EOC. From the near and far EOC slant ranges and the pulsewidth, the maximum PRF is calculated (Equation (A.25)). One can ensure that the range of PRFs in the maximum-swath table covers the minimum-to-maximum-PRF range by adjusting the PRF delta for the table.

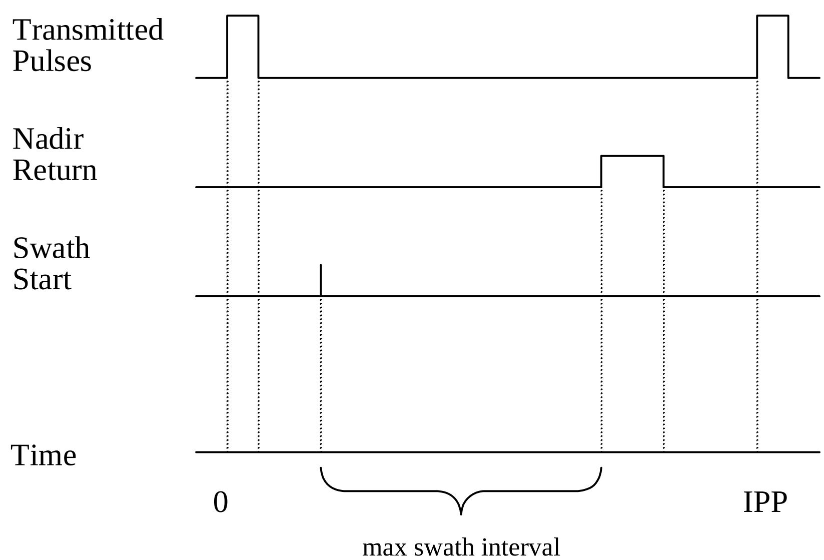

Figure A-14 Maximum Available Swath Time Interval. Given the imaging geometry, the swath time interval must not be corrupted by the transmit pulse or the nadir return.

The near and far EOC look angles guide the selection of the peak-of-beam (POB) look angle or RF elevation boresight angle. With this selection the POB incidence angle and slant range are calculated along with the elevation scan angle and scan loss. The minimum and maximum PRFs are the bounds for PRF selection. The selection of PRF must also support a swath at least as large as the selected swath and produce acceptable range and azimuth ambiguity ratios. The PRF supporting the maximum swath is shown for reference as is a plot of maximum slant-range delta (proportional to ground-range swath) versus PRF. Once the PRF is chosen, the corresponding maximum slant-range delta and swath are calculated along with the transmit duty cycle and the ambiguous range interval.

Of importance to the range ambiguity ratio as well as vulnerability to electronic counter-measures (ECM) is the antenna elevation sidelobe structure. The model contains two design options for antenna elevation amplitude weighting. The uniform amplitude distribution weights all elevation elements evenly and produces the well-known sinc-function antenna pattern. The Taylor amplitude distribution is a representative means of further suppressing the antenna sidelobes at the expense of a wider mainlobe and reduced mainlobe gain. The Taylor parameters are generally restricted to be between 4 and 20 (nbar) and 20 and 50 dB (sidelobe level). A table [25] in the Ref Tables worksheet is used to calculate via interpolation the corresponding reduction in mainlobe gain or aperture taper loss. The elevation antenna pattern is calculated [26, 27] in a beam-specific table using the amplitude distribution, the height of the physical aperture, the aperture efficiency, and the elevation beam-broadening factor. The 3-dB width of the mainlobe of the antenna pattern (elevation beamwidth) should be larger than the look angle interval required to cover the selected swath. The mainlobe pattern is also used to determine the beamshape losses, relative to the peak of the beam, that are incurred at the near and far edges of the swath.

As noted in Section A.2 one can “average” more than one image of or “look” at a particular area to improve the image quality at the expense of along-track resolution. The maximum number of stripmap along-track looks is therefore the ratio of the required along-track resolution to the best (3-dB) stripmap resolution available. The stripmap along-track resolution is selected between the product of the 3-dB stripmap resolution and the number of stripmap looks and the required resolution. With this selection the beamwidth utilization is calculated along with the synthetic aperture length, image footprint width, footprint observation time, image azimuth width, and image doppler width. A beam-specific table that calculates the (uniformly-distributed) azimuth antenna pattern is also used to calculate the average azimuth beamshape loss considering that portion of the azimuth beamwidth used. If along-track resolution better than that available from stripmap operation is needed, spotlight processing is available. The final along-track resolution, relative to the stripmap resolution, defines the minimum number of spotlight beams required. The area coverage rate for the selected along-track resolution *while imaging* is calculated as the product of the swath and the azimuth footprint divided by the observation time and the number of spotlight beams. This does not account for any inefficiency in scheduling imaging data takes.

The frequency weighting factor (Section A.1) and the bandwidth of the transmit signal are chosen next to support cross-track resolution performance. As with along-track resolution, multiple looks can be used to improve image quality at the expense of cross-track resolution. Therefore, the per-look transmit signal bandwidth is constrained to be as large as the minimum transmit bandwidth. The resulting cross-track resolution performance is then calculated for the incidence angles across the swath. The receiver bandwidth is also chosen subject to the constraint that it be as large as the total transmit bandwidth.

Although the peak RF transmit power has no direct constraint, it is the final means of influencing the overall sensitivity performance of the radar in the form of noise-equivalent sigma zero. Average RF transmit power is subsequently calculated as the product of the peak RF transmit power and the transmit duty cycle. The antenna gains for transmit and receive (here constrained to be equal) along with the receive system noise temperature are calculated based on inputs already provided. As noted in Section A.6, these quantities must be referenced to the same point in order to be properly used in the radar range equation. The reference point used here for transmit and receive is the receive input (transmit output) to the element.

The final inputs to the calculation of noise-equivalent sigma zero are the noise contributions from ambiguous returns in range and azimuth. Section A.6 notes that these noise contributions are multiplicative. The peak *RASR* is the maximum value of *RASR* over the swath considering contributions from up to five ambiguous ranges on either side of the swath range in question. Ten uniformly-space range samples are used over the swath. *RASR* is simply the ratio of the sum of the ambiguous range returns to the return of interest. Since *RASR* is a ratio, only the range-dependent terms survive [30]:

$$RASR(r) = \frac{\sum_n \frac{\sigma^0(r,n)\delta_{ct}(r,n)}{L_{ebs}{}^2(r,n)R_s{}^3(r,n)}}{\frac{\sigma^0(r,0)\delta_{ct}(r,0)}{L_{ebs}{}^2(r,0)R_s{}^3(r,0)}} \tag{A.54}$$

where $L_{ebs}{}^2$ is the two-way elevation beamshape loss, r is the range index within the swath, and n is the ambiguous range index ($n = 0$ being the processed swath). The *AASR* is calculated similarly except that the numerator and denominator are both integrated over the processed doppler-frequency (azimuth) interval [31]:

$$AASR = \frac{\sum_{m \neq 0} \int_{-\frac{B_p}{2}}^{\frac{B_p}{2}} G^2\left(f_d + mPRF\right) df_d}{\int_{-\frac{B_p}{2}}^{\frac{B_p}{2}} G^2\left(f_d\right) df_d} \tag{A.55}$$

where f_d is the doppler frequency, m is the ambiguous doppler (azimuth) index (m = 0 being the processed doppler (azimuth) interval), B_p is the processed doppler interval, and G^2 represents the two-way antenna pattern in azimuth.

These two ambiguity-to-signal ratios should be less than –20 dB as a qualitative check of the PRF selection. The noise-equivalent sigma zero calculation uses the AASR along with the values of RASR over the swath to quantitatively determine the impact of the ambiguous signals. Using Equation (A.41) one concludes that these ratios increase the noise-equivalent sigma zero by the following factor:

$$\sigma_{ne}{}^{0}(r, with\ ambiguities) = \frac{\sigma_{ne}{}^{0}(r, without\ ambiguities)}{(1 - RASR(r) - AASR)} \tag{A.56}$$

The noise-equivalent sigma zero, with this “ambiguity loss”, is calculated at the beginning, middle, and end of the swath according to:

$$l = L_p L_{abs}{}^{2} L_{amb} L_{ebs}{}^{2}$$

$$\sigma_{ne}{}^{0} = \frac{(4\pi)^3 R_s{}^{3} k T_s k_f\, 2vB_{rx} l}{\lambda^3 P_t \tau_t PRF \delta_{ct} B_r G_t G_r} \tag{A.57}$$

where L_p is the signal processing loss, $L_{abs}{}^{2}$ is the two-way azimuth beamshape loss over the synthetic aperture length, L_{amb} is the ambiguity loss, and $L_{ebs}{}^{2}$ is the two-way elevation beamshape loss at the particular point in the swath. The noise-equivalent sigma zero across the swath is constrained to be less than the maximum mission requirement. In this equation G_t and G_r calculated according to:

$$G_t = G_r = \frac{4\pi A_e}{\lambda^2}\frac{1}{L_{no}L_{tap}L_{asc}L_{esc}} \tag{A.58}$$

where L_{no} is the non-ohmic element loss, L_{tap} is the sidelobe taper loss, L_{asc} is the (one-way) azimuth scan loss, and L_{esc} is the (one-way) elevation scan loss. Finally, the absolute measure of radar sensitivity (RS_{abs}) is calculated from the relative measure (RS_{rel} – Equation (A.53)) without the simplifying assumptions:

$$RS_{abs} = \frac{P_t \tau_t PRF A_e{}^2}{T_s} = RS_{rel}\, \frac{k_f B_{rx} l L_{no}{}^2 L_{tap}{}^2 L_{asc}{}^2 L_{esc}{}^2}{B_r} \tag{A.59}$$

Prime power (the DC power drawn by the radar) is approximated relative to the detailed formulation noted in Section A.7. The peak prime power drawn by the HPA(s) to generate the transmit pulse is calculated from the peak RF transmit power (P_t) translated back to the HPA from the transmit reference point:

$$PP_{pHPA} = P_t L_o L_{HPA-el} \eta_{RF} \eta_{DC} \tag{A.60}$$

where L_o is the element ohmic loss, $L_{HPA\text{-}el}$ is the loss from the HPA to the element, η_{RF} is the HPA DC-to-RF efficiency, and η_{DC} is the DC-to-DC conversion efficiency of the radar system power supply. The peak prime power drawn by the LNA(s) to receive the return pulse is calculated as the product of the number of LNAs, the DC power per LNA, and the power supply DC-to-DC conversion efficiency. Similarly, the peak prime power drawn by the remainder of the radar electronics is the product of the DC power required and the power supply DC-to-DC conversion efficiency.

The average prime power in each case over the IPP is the peak prime power times the appropriate duty cycle. The transmit duty cycle (pulsewidth x PRF) is used for the HPA(s), and the "complement" of the transmit duty cycle (1 – transmit duty cycle) is used for the LNA(s). The average prime power of the radar electronics equals the peak prime power as they are always on during operation. The average prime power over a data take is further reduced by the beam utilization factor (the percentage the particular beam is used in a multi-beam data take) in each case. Finally, the average prime power over the orbit is calculated by applying the ratio of the data take time per orbit to the orbit period.

The minimum peak data rate produced by the digital sampling of the radar returns is the product of the transmit bandwidth and the number of bits per complex sample. This is the minimum peak value since the actual sampling rate may exceed the transmit signal bandwidth (Section A.8). Over the IPP the average data rate is reduced from the peak data rate by the ratio of the swath time to the IPP. Average data rates over the data take and the orbit are calculated as are the average prime powers. The amounts of digital data produced per IPP, data take, and orbit are calculated as the products of the particular data rates and time periods.

APPENDIX B

SAR PERFORMANCE MODEL

This appendix provides a detailed look at the Excel model developed to exercise the SAR relationships summarized in Chapter 3 and developed in Appendix A. As noted in Section A.10, the QuickLook worksheet is a high-level evaluation of the SAR mission requirements. Figure B-1 shows the mission requirement inputs (altitude, frequency, resolution, noise equivalent sigma zero, swath) in italicized type and the subsequent calculations of parameter constraints in normal type. These constraint calculations are organized into three groups, each with a different incidence angle. The parameters constrained due to the mission requirements include the maximum effective antenna height (from the incidence angle and the swath), the maximum effective antenna length (from the resolution), the minimum transmit signal bandwidth (from the resolution and the incidence angle), and a relative measure of the radar sensitivity.

Mission Requirement Inputs

spaceborne vs airborne =	*spaceborne*				
altitude =	*800*	km			
speed =	*300*	m/s	frequency =	*9.6*	GHz
range to horizon =	3292	km	wavelength =	0.0313	m
horizon look angle =	62.7	deg	cross-track resolution =	*7*	m
speed =	7454	m/s	along-track resolution =	*7*	m
orbit period =	100.8	min	noise-equiv sigma zero =	*-20*	dB

Constraint Calculations

	Minimum Look Angle				**Intermediate Look Angle**				**Maximum Look Angle**		
incidence angle =	*20*	deg		incidence angle =	*30*	deg		incidence angle =	*40*	deg	
look angle =		17.7	deg	look angle =		26.4	deg	look angle =		34.8	deg
swath width =	*100*	km		swath width =	*100*	km		swath width =	*100*	km	
look angle interval for swath =		6.08	deg	look angle interval for swath =		5.14	deg	look angle interval for swath =		4.06	deg
	near	**POB**	**far**		**near**	**POB**	**far**		**near**	**POB**	**far**
look angle (deg)	17.7	20.7	23.8	look angle (deg)	26.4	28.9	31.5	look angle (deg)	34.8	36.9	38.9
incidence angle (deg)	20.0	23.5	27.0	incidence angle (deg)	30.0	33.0	36.0	incidence angle (deg)	40.0	42.5	45.0
slant range (km)	845	863	885	slant range (km)	907	932	962	slant range (km)	1006	1038	1074
min bandwidth (MHz)	62.7	53.8	47.2	min bandwidth (MHz)	42.9	39.3	36.4	min bandwidth (MHz)	33.3	31.7	30.3
ensitivity (dB Wm^4/K)		-1.3		sensitivity (dB Wm^4/K)		-0.3		sensitivity (dB Wm^4/K)		1.1	
max eff antenna height =		0.26	m	max eff antenna height =		0.31	m	max eff antenna height =		0.39	m
max eff antenna length =		12.40	m	max eff antenna length =		12.40	m	max eff antenna length =		12.40	m

Figure B-1 Excel SAR Model – QuickLook worksheet.

The heart of the Excel model is the detailed beam-level modeling of SAR performance. Figures B-2, B-3, B-4, and B-5 capture all of these calculations. Separate worksheets are provided for each of five distinct beams. Figure B-2 begins with the mission requirements duplicated from the QuickLook worksheet. The initial inputs at the beam level are the Antenna Parameters, which are common to all beams. These include the aperture efficiencies and physical dimensions. The Beam Parameters section is unique to each beam. This section begins with the selection of the incidence angle at the beginning or near edge of the swath. Outlines around individual cells indicate that those values are constrained according to the values noted either below or beside the cell in question. When any constrained value violates its constraint, its cell is highlighted. The remainder of the Beam X worksheet implements the specific equations developed in Appendix A with the inputs noted by italic type. Section A.10 contains a more-detailed description of the sequence employed.

Mission Requirement Inputs

spaceborne vs airborne =	spaceborne	
altitude =	800	km
range to horizon =	3292	km
horizon look angle =	62.7	deg
speed =	7454	m/s
orbit period =	100.8	min
frequency =	9.6	GHz
wavelength =	0.0313	m
cross-track resolution =	7	m
along-track resolution =	7	m
noise equiv sigma zero =	-20.0	dB sqm/sqm

Antenna Parameters

az RF boresight angle =	$\boxed{90.0}$	deg	(	0	<=	<=	180	)
az mech boresight angle =	$\boxed{90.0}$	deg	(	0	<=	<=	180	)
az scan angle =	0.0	deg		(fore)			(aft)	
az 1-way scan loss =	0.0	dB						
az antenna length =	*13.0*	m						
az efficiency =	*95*	%						
elev mech boresight angle =	$\boxed{55.0}$	deg	(	0	<=	<=	90	)
elev antenna height =	*0.50*	m		(vert)			(horiz)	
elev efficiency =	*95*	%						
element ohmic loss =	*1*	dB						
misc element non-ohmic loss =	*0*	dB						
external noise =	*290*	K						
antenna physical temperature =	*0*	C						
element-to-LNA ohmic losses =	*0.5*	dB						
LNA noise figure =	*2.0*	dB						
LNA gain =	*30.0*	dB						
LNA-to-receiver ohmic losses =	*15.0*	dB						
receiver noise figure =	*4.0*	dB						
processing loss =	*1.5*	dB						
bits per complex sample =	*8*	bits						
data-take time per orbit =	*10*	min						
HPA-to-element loss =	*0.0*	dB						
HPA DC-to-RF efficiency =	*50*	%						
DC-to-DC conversion efficiency =	*75*	%						
total number of LNAs =	*500*							
DC power per LNA =	*200*	mW						
total DC pwr, radar electronics =	*100*	W						

Figure B-2 Excel SAR Model – Antenna Parameters.

Beam 1 Parameters				***Beam 1 Performance***					
near EOC incidence angle =	*30.0*	deg		near EOC look angle =	26.4	deg			
(0	<= <=	90	)	near EOC slant range =	907	km			
(nadir)		(horizon)		min transmit bandwidth =	42.9	MHz			
azimuth beam broadening factor =	*1.0*			effective antenna length =	12.35	m	(max =	12.40	)
	(min =	1	)	azimuth beamwidth =	0.13	deg			
				min PRF =	1069	Hz	(optimal doppler bandwidth)		
				3-dB strip along-track resolution =	6.97	m			
transmit pulsewidth =	*30.0*	microsec		max possible swath width =	2635.3	km			
nadir return length =	*2*	pulsewidths		max slant range delta vs PRF =	74.5	km			
				max swath width vs PRF =	133.2	km			
swath width =	*70.0*	km		look angle interval for swath =	3.67	deg			
	(max =	133.2	)	far EOC look angle =	30.0	deg			
				far EOC incidence angle =	34.3	deg			
				far EOC slant range =	944	km			
PRF delta in swath table =	*4.5*	Hz		max PRF =	3242	Hz	(swath table max =	3314.5	)
POB look angle =	*28.28*	deg		POB incidence angle =	32.2	deg			
(26.4	<= <=	30.0	)	POB slant range =	926	km			
				POB elevation scan angle =	-26.7	deg			
				POB elevation scan loss =	0.5	dB			
PRF =	*1723*	Hz		max slant range delta for chosen PRF =	48.8	km	(min =	37.3	)
(1069	<= <=	3242	)	max swath for chosen PRF =	90.1	km	(min =	70.0	)
(max swath PRF =	1528	)		HPA duty cycle =	5.2	%			
				ambiguous range interval =	87.1	km			

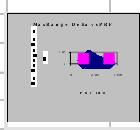

Figure B-3 Excel SAR Model – Beam X worksheet, part 1 of 3.

	elev taper =	*uniform*		(	uniform	or	Taylor	)				
	nbar (Taylor) =	*18*		(	4	<= nbar <=	20	)				
	sidelobe level (Taylor) =	*50*	dB	(	20	<= SLL <=	50	)				
	elev beam broadening factor =	*1.00*					effective antenna height =	0.42	m			
		(min =	1	)			elevation beamwidth =	3.74	deg	(min =	3.67	)
							near EOC 2-way elev beamshape loss =	6.3	dB			
							far EOC 2-way elev beamshape loss =	5.3	dB			
							elev aperture taper loss =	0.0	dB			
	# of strip along-track looks =	*1*										
(	1.0	<= <=	1.0	)								
	strip along-track resolution =	*7.0*	m				strip imaging duty cycle =	99.6	%			
		(min =	7.0	)								
									Range Coverage			
								near		**far**		
								EOC	**POB**	**EOC**		
							SA length, az footprint (km)	2.02	2.07	2.11		
							observation time (s)	0.272	0.277	0.283		
									Azimuth Coverage			
	final along-track resolution =	*7.0*	m					**leading**		**trailing**		
		(max =	7.0	)			azimuth (deg)	89.94		90.06		
							processed doppler (Hz)	532		-532		
	# of spotlight beams =	*1*										
		(min =	1.0	)			strip azimuth beamshape loss =	1.65	dB			
							peak area coverage rate =	522	sqkm/s			
	chirp weighting factor =	*1*										
	total transmit bandwidth =	*45*	MHz									
	number of cross-track looks =	*1*					per-look transmit bandwidth =	45	MHz	(min =	42.9	)
	total receive bandwidth =	*45*	MHz									
		(min =	45.0	)			ear EOC cross-track resolution =	6.67	m	(max =	7.0	)
							POB cross-track resolution =	6.25	m	(max =	7.0	)
							far EOC cross-track resolution =	5.92	m	(max =	7.0	)

Figure B-4 Excel SAR Model – Beam X worksheet, part 2 of 3.

peak RF transmit power =	*6060*	W
range delta in RASR table =	*1.3*	km
elev delta in pattern table =	*0.075*	deg
az delta in pattern table =	*0.003*	deg
beam utilization per data take =	*50*	%

avg RF transmit power =	313	W	(at transmit reference)		
transmit antenna area gain =	47.8	dB	(at transmit reference)		
receive antenna area gain =	47.8	dB	(at receive reference)		
Ts =	674	K			
max slant range in RASR calculation =	1380	km	(max =	1449	)
max possible elev offset =	34.4	deg	(max =	36.4	)
peak RASR =	-21.6	dB	(max =	-20.0	)
integrated RASR =	-28.3	dB	(max =	-20.0	)
max az offset in AASR calculation =	1.10	deg	(max =	1.461	)
AASR =	-25.2	dB	(max =	-20.0	)

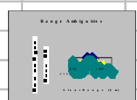

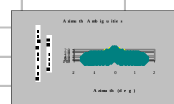

	Range Coverage					
	near		far			
	EOC	POB	EOC			
ambiguity loss (dB)	0.04	0.02	0.01			
noise equivalent sigma zero (dB)	-21.0	-26.8	-21.0	(max =	-20.0	)
sensitivity (dB)		11.1				

	Prime Power (W)			
			data	
		IPP	take	orbit
	peak	avg	avg	avg
HPAs	20344	1052	526	52
LNAs	133	126	63	6
radar electronics	133	133	67	7
total	1311	656	65	

	Data Rate, Volume			
			data	
		IPP	take	orbit
	peak	avg	avg	avg
data rate (Mbps)	360	173	86	9
data volume (Mbits)		0.100	51815	51815

Figure B-5 Excel SAR Model – Beam X worksheet, part 3 of 3.

After the individual beam parameters are determined so that the required performance is achieved, they are collected along with the resulting performance characteristics on a Summary worksheet (see Figure B-6) so that the parameters can be compared beam to beam.

	Beam *1*	Beam *2*	Beam *3*	Beam *4*	Beam *5*
near incidence (deg)	30.0	33.8	37.5	25.9	21.5
far incidence (deg)	34.3	38.0	41.7	30.5	26.4
near look (deg)	26.4	29.6	32.7	22.8	19.0
POB look (deg)	28.28	31.48	34.58	24.90	21.20
far look (deg)	30.0	33.2	36.3	26.8	23.2
swath (km)	70.0	74.0	80.0	70.0	70.0
el utilization (%)	98	98	99	102	105
el eff aperture (m)	0.42	0.44	0.45	0.41	0.39
el beam broadening	1.0	1.0	1.0	1.0	1.0
el taper	uniform	uniform	uniform	uniform	uniform
Taylor nbar	na	na	na	na	na
Taylor SLL	na	na	na	na	na
el beamwidth (deg)	3.74	3.64	3.56	3.86	4.02
near el beamshape loss (dB)	6.3	5.5	6.4	6.4	6.6
far el beamshape loss (dB)	5.3	4.5	5.3	5.2	5.5
near CT res (m)	6.67	6.74	6.84	6.87	6.82
POB CT res (m)	6.25	6.38	6.52	6.33	6.14
far CT res (m)	5.92	6.09	6.26	5.91	5.63
# CT looks	1	1	1	1	1
AT res (m)	7.00	7.00	7.00	7.00	7.00
# AT looks	1	1	1	1	1
# spot beams	1	1	1	1	1
az utilization (%)	100	100	100	100	100
az eff aperture (m)	12.35	12.35	12.35	12.35	12.35
az beam broadening	1	1	1	1	1
az beamwidth (deg)	0.13	0.13	0.13	0.13	0.13
az beamshape loss (dB)	1.6	1.7	1.6	1.6	1.7
az footprint (km)	2.1	2.1	2.2	2.0	1.9
tx bandwidth (MHz)	45	40	36	50	60
peak power (W)	6060	6660	5690	8160	9634
pulsewidth (μsec)	30.0	30.0	30.0	30.0	30.0
PRF (Hz)	1723	1325	1850	1313	1325
avg power (W)	313	265	316	321	383
peak RASR (dB)	-21.6	-23.9	-20.8	-33.9	-34.8
AASR (dB)	-25.2	-20.6	-25.6	-19.7	-20.6
noise temp (K)	674	674	674	674	674
near NESZ (dB)	-21.0	-21.1	-21.0	-21.1	-21.2
POB NESZ (dB)	-26.8	-26.1	-26.9	-26.9	-27.1
far NESZ (dB)	-21.0	-21.0	-21.0	-21.1	-21.0
POB sensitivity (dB Wm^4/K)	11.1	10.6	11.5	10.9	11.3
IPP-avg prime power (W)	1311	1150	1319	1340	1547
IPP-avg data rate (Mbps)	173	135	197	132	140
peak ACR (sqkm/s)	522	552	596	522	522

Figure B-6 Excel SAR Model – Beam Summary worksheet.

APPENDIX C

QUASI-OPTICAL ANTENNA EVALUATION FOR HIGH-RESOLUTION SPACEBORNE SAR

This appendix documents the comparative evaluation of QO antenna solutions for the high-resolution version of the spaceborne SAR mission described in Chapter 5. The results of this evaluation are referenced at the end of Chapter 7. As was done for the other SAR missions considered, QO antenna solutions are compared to the traditional AESA antenna solution in terms of the power, mass, and cost resources required to achieve the required RF performance. The AESA and QO antenna design work is high level in nature and is intended only to describe the antenna approaches in sufficient detail to estimate the fundamental characteristics of mass, power, and cost. The antenna requirements for this mission are listed in Table 5-4.

C.1 AESA Antenna solution

To achieve the ±6.7° electronic beam steering required in elevation without grating lobes, the AESA must have phase control at a spacing of 0.89λ or less. Considering a 1.85m elevation dimension, this spacing results in 66 phase control points in elevation. Increasing this to a higher-integer number of 72 results in a spacing of 0.82λ, which is acceptable for beam steering. The 400 MHz instantaneous bandwidth will cause the beam to squint in elevation by about 0.3° if non-true-time-delay phase shifters are used for steering. This is probably not acceptable considering the elevation beamwidth is about 0.9°. True-time-delay phase shifters are therefore needed in elevation.

Using the 0.82λ element spacing in azimuth as well, one determines the element count to be 5184, 72 in elevation and 72 in azimuth. Solving for total radiated power from the absolute sensitivity requirement, one concludes that the necessary peak power per element is roughly 12 W. Given this value an HPA at the limit of the current state-of-the-art is required at each element for the traditional fully-distributed AESA solution. One does not need a phase shifter at each element, however, since electronic beam steering is required only in elevation. Given the 1.85m x 1.85m aperture size, it makes sense to implement the aperture via four subarrays each measuring 0.92m x 0.92m. This leads to an architecture where 36 elements in azimuth for each subarray are combined per row followed by an intermediate amplifier and a phase shifter per row. The intermediate amplifier is needed to properly drive the element-level HPAs. Considering the loss of the 36-way combiner network, an LNA is also needed at each element to control the noise temperature. The 36 rows per subarray are then combined followed by the combination of the four subarrays. Figure C-1 also shows an HPA driver amplifier and an LNA post-amplifier at the input to the antenna, primarily to provide the necessary transmit drive level to the intermediate HPAs.

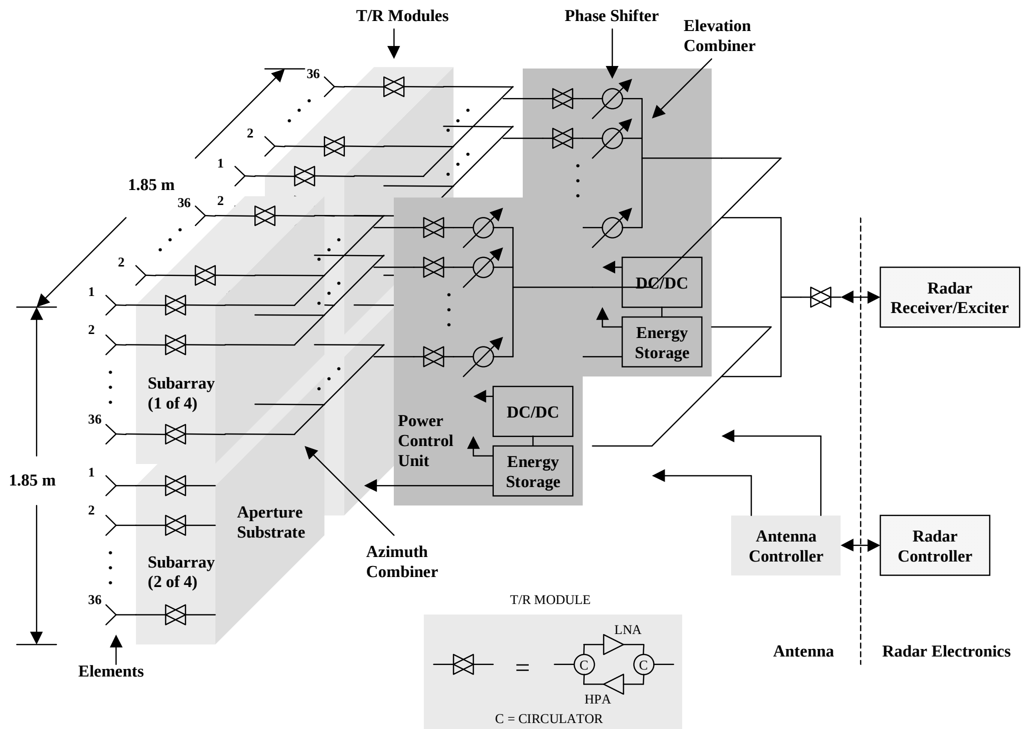

Figure C-1 AESA antenna block diagram for spaceborne high-resolution reference SAR mission.

Given an external input noise temperature of 290K, Figure C-2 calculates the system noise temperature, an estimate of which was used to determine the per-element radiated power. Figure C-2 also shows the transmit signal levels throughout the antenna, justifying the need for intermediate HPAs, and estimates the prime power required by the antenna amplifiers to produce the required RF performance. It is again the case that the element-level HPAs drive the average prime power required.

Sensitivity (dB Wm4/K)	17.7
Effective Elevation Aperture (m)	1.61
Effective Azimuth Aperture (m)	1.76
Pulsewidth (ms)	8
PRF (Hz)	9905
HPA Duty Cycle (%)	7.9
LNA Duty Cycle (%)	50
number of elements	5184
ambient temperature (C)	0
DC/DC conversion efficiency (%)	75

System Noise Temperature (K)	589
Array Transmit Power (W)	54548
Element Transmit Power (W)	10.5

Component	Receive Ohmic Loss (dB)	Receive Amp Gain (dB)	Receive Amp NF (dB)	Receive Combine (ways)	CW DC Power (mW)	Transmit Ohmic Loss (dB)	Transmit Amp Gain (dB)	Transmit Divide (ways)	Transmit Eff (%)	Sys Noise (K)	Transmit Loss (dB)	Input Power (dBm)	Output Power (dBm)	Quantity	Receive Prime Power (W)	Transmit Prime Power (W)
external										290.0						
element	0.3	na	na	na	na	0.3	na	na	na	19.5	0.3	40.5	40.2	5184		
feedthrough	0.2	na	na	na	na	0.2	na	na	na	13.8	0.2	40.7	40.5	5184		
amplifier interface	1.0	na	na	na	na	0.8	na	na	na	79.3	0.8	41.5	40.7	5184		
amplifier	na	20	1.5	na	50	na	30	na	35	169.0	-30.0	11.5	41.5	5184	172.8	22190.2
amplifier interface	0.8	na	na	na	na	0.8	na	na	na	0.8	0.8	12.3	11.5	5184		
transmission line	0.7	na	na	na	na	0.7	na	na	na	0.8	0.7	13.0	12.3	5184		
az combine/divide	2.6	na	na	36	na	2.6	na	36	na	4.5	18.2	31.2	13.0	144		
transmission line	0.5	na	na	na	na	0.5	na	na	na	1.2	0.5	31.7	31.2	144		
amplifier interface	0.8	na	na	na	na	0.8	na	na	na	2.2	0.8	32.5	31.7	144		
amplifier	na	20	1.5	na	50	na	30	na	35	5.9	-30.0	2.5	32.5	144	4.8	76.9
amplifier interface	0.8	na	na	na	na	0.8	na	na	na	0.0	0.8	3.3	2.5	144		
transmission line	0.3	na	na	na	na	0.3	na	na	na	0.0	0.3	3.6	3.3	144		
phase shifter	5.0	na	na	na	na	5.0	na	na	na	0.4	5.0	8.6	3.6	144		
el combine/divide	2.6	na	na	36	na	2.6	na	36	na	0.4	18.2	26.7	8.6	4		
transmission line	0.7	na	na	na	na	0.7	na	na	na	0.2	0.7	27.4	26.7	4		
el combine/divide	0.6	na	na	4	na	0.6	na	4	na	0.2	6.6	34.1	27.4	1		
transmission line	0.3	na	na	na	na	0.3	na	na	na	0.1	0.3	34.4	34.1	1		
amplifier interface	0.8	na	na	na	na	0.8	na	na	na	0.3	0.8	35.2	34.4	1		
amplifier	na	20	1.5	na	50	na	30	na	35	0.8	-30.0	5.2	35.2	1	0.0	1.0
amplifier interface	0.8	na	na	na	na	0.8	na	na	na	0.0	0.8	6.0	5.2	1		
transmission line	1.0	na	na	na	na	1.0	na	na	na	0.0	1.0	7.0	6.0	1		
receiver interface	0.5	na	na	na	na	0.5	na	na	na	0.0				1		
receiver	na	na	4	na	na	na	na	na	na	0.0				1		
														subtotals	177.6	22268.2
														total		22445.8

Figure C-2 AESA antenna RF performance for spaceborne high-resolution reference SAR mission.

Figures C-3 and C-4 in turn estimate the antenna mass and cost. The element-level HPAs and LNAs are assumed to be integrated into the antenna substrate without the individual packaging that often drives mass and cost. The DC/DC converters and energy storage capacitors are housed in the elevation divider/phase shifter units. The size of the aperture requires a simple deployment structure. In addition to the inverse relationship between resolution-cell size and prime power, one again sees that the beamforming network behind the element-level amplifiers is significant to both mass and cost.

aperture length (m)		1.85			***Substrate Layup***	
aperture height (m)		1.85				**g/sqm**
number of panels		4			paint - 2 mil	107
radiating element density (g/sqm)		3138			elements - 50%, 1/2 oz Cu	79
structural panel density (g/sqm)		6858			substrate - 50 mil Duroid	2794
					ground plane - 1/2 oz Cu	158
	Unit		**Total**			3138
	Mass	**Qty**	**Mass**			
	(g)		**(kg)**			
radiating element substrate	2685	4	11			
structural panel	5868	4	23			
Beamforming Network					***PCU Mass***	
element T/R modules	10	5184	52			
element T/R RF cables	15	5184	78		number of power supplies	60
36-way	200	144	29		power supply unit mass (g)	140
36-way RF cables	10	144	1		capacitor mass factor	1.5
intermediate T/R modules	50	144	7			**g**
intermediate T/R RF cables	10	144	1		substrate + housing	1800
36-way, PS, PCU	14400	4	58		power supplies + caps	12600
36-way RF cables	25	4	0			14400
4-way	50	1	0			
array T/R modules	50	1	0			
array RF cables	110	1	0			
PCU DC cables	40	4	0			
controller	6000	1	6			
controller DC cables	1290	4	5			
deployment structure	50000	1	50			
deployment actuators	5000	1	5			
		subtotal	327			
		20% contingency	65			
		total	392			

Figure C-3 AESA antenna mass for spaceborne high-resolution reference SAR mission.

	Unit Cost (k$)	Qty	Total Parts Cost (k$)		
radiating element substrate	3.4	4	14	***PCU Cost***	
structural panel	3.4	4	14		
				unit T/R ($)	0
Beamforming Network				unit phase shifter ($)	200
element T/R modules	0.5	5184	2592	unit power supply ($)	500
element T/R RF cables	0.05	5184	259	number of phase shifters	36
36-way	1	144	144	number of power supplies	60
36-way RF cables	0.05	144	7	capacitor cost factor	1.01
intermediate T/R modules	1.5	144	216		
intermediate T/R RF cables	0.05	144	7	housing + substrate	2000
36-way, PS, PCU	39.5	4	158	T/R + phase shifter parts	7200
36-way RF cables	0.1	4	0	power supplies + caps	30300
4-way	0.3	1	0		39500
4-way RF cables	0.05	1	0		
array T/R modules	1.5	1	2		
array RF cables	0.3	1	0		
PCU DC cables	0.5	4	2		
controller	50	1	50		
controller DC cables	1	4	4		
deployment structure	1000	1	1000		
deployment actuators	100	1	100		
		subtotal	4569		
	20% contingency		914		
		total	5483		

Figure C-4 AESA antenna cost for spaceborne high-resolution reference SAR mission.

C.2 Fully-Distributed QO Antenna Solution

This is an active microwave lens with HPAs and LNAs at each lens element. Refer to Chapter 4 for an operational description. To achieve the ±6.7° electronic beam steering in elevation without grating lobes, the QO antenna has the same element-spacing requirements as the AESA. Section C.1 justifies a 72 x 72 array of elements over the 1.85 x 1.85 m aperture area. The 400 MHz instantaneous bandwidth will not cause the QO beam to squint in elevation since no phase shifters are used for beam steering. Given the elevation beamwidth and the viewing geometry noted in Table 5-4, one concludes that the required incidence-angle range can be covered by a collection of five separate beams at different elevation angles. Elevation beam steering will be done by switching between five individual feeds on the focal arc of the microwave lens. Considering the 1:1 aspect ratio of the lens, a single feed horn can adequately illuminate the lens for each steered beam.

Solving for total radiated power from the absolute sensitivity requirement, one concludes that the necessary peak power per element remains at roughly 12 W. Given this value an HPA at the limit of the current state-of-the-art is required at each element. The fully-distributed QO antenna architecture also calls for an LNA at each element for noise temperature control. Figure C-5 shows the QO antenna functional block diagram.

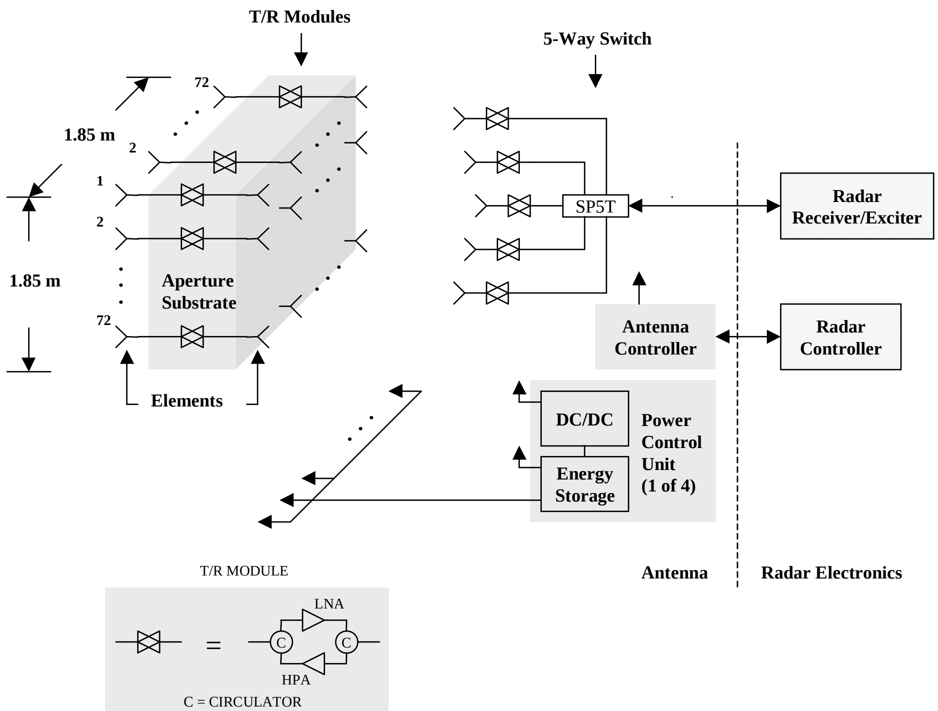

Figure C-5 Fully-distributed QO antenna block diagram for spaceborne high-resolution reference SAR mission.

Given the external input noise temperature of 290K, Figure C-6 calculates the actual system noise temperature. Figure C-6 also shows the transmit signal levels throughout the antenna and estimates the prime power required by the antenna amplifiers to produce the required RF performance. Due to the high power required and the large numbers of amplifiers, it is again the case that the element-level HPAs drive the average prime power required.

Sensitivity (dB Wm4/K)	17.7
Effective Elevation Aperture (m)	1.61
Effective Azimuth Aperture (m)	1.76
Pulsewidth (ms)	8
PRF (Hz)	9905
HPA Duty Cycle (%)	7.9
LNA Duty Cycle (%)	50
number of elements	5184
ambient temperature (C)	0
DC/DC conversion efficiency (%)	75

avg spillover level (dB)	-10
spillover loss (dB)	3.8
illumination loss (dB)	1

System Noise Temperature (K)	596
Array Transmit Power (W)	55163
Element Transmit Power (W)	11

Component	Receive Ohmic Loss (dB)	Receive Amp Gain (dB)	Receive Amp NF (dB)	Receive Combine (ways)	CW DC Power (mW)	Transmit Ohmic Loss (dB)	Transmit Amp Gain (dB)	Transmit Eff (%)	Sys Noise (K)	Transmit Loss (dB)	Input Power (dBm)	Output Power (dBm)	Quantity	Receive Prime Power (W)	Transmit Prime Power (W)
external primary									290						
outer element	0.3	na	na	na	na	0.3	na	na	19.5	0.3	40.6	40.3	5184		
feedthrough	0.2	na	na	na	na	0.2	na	na	13.8	0.2	40.8	40.6	5184		
amplifier interface	1.0	na	na	na	na	0.8	na	na	79.3	0.8	41.6	40.8	5184		
amplifier	na	20	1.5	na	50	na	30	35	169.0	-30.0	11.6	41.6	5184	173	22440
amplifier interface	0.8	na	na	na	na	0.8	na	na	0.8	0.8	12.4	11.6	5184		
transmission line	0.2	na	na	na	na	0.2	na	na	0.2	0.2	12.6	12.4	5184		
inner element	0.3	na	na	na	na	0.3	na	na	0.3	0.3	12.9	12.6	5184		
space feed	na	-4.8	0	5184	na	na	-41.9	na	0.0	41.9	54.8	12.9	1		
external secondary									1.7						
feed	1.2	na	na	na	na	1.2	na	na	5.0	1.2	56.0	54.8	1		
amplifier interface	0.8	na	na	na	na	0.8	na	na	4.2	0.8	56.8	56.0	1		
amplifier	na	20	1.5	na	50	na	30	50	10.9	-30.0	26.8	56.8	1	0	101
amplifier interface	0.8	na	na	na	na	0.8	na	na	0.1	0.8	27.6	26.8	1		
transmission line	0.5	na	na	na	na	0.5	na	na	0.0	0.5	28.1	27.6	1		
beam switch	1.0	na	na	na	na	1.0	na	na	0.1	1.0	29.1	28.1	1		
transmission line	1.0	na	na	na	na	1.0	na	na	0.1	1.0	30.1	29.1	1		
receiver interface	0.5	na	na	na	na	0.5	na	na	0.1				1		
receiver	na	na	4	na	na	na	na	na	1.0				1		
													subtotals	173	22542
													total		22715

Figure C-6 Fully-distributed QO antenna RF performance for spaceborne high-resolution reference SAR mission.

Figures C-7 and C-8 estimate the QO antenna mass and cost. The element-level HPAs and LNAs are assumed to be integrated into the antenna substrate without the individual packaging that often drives mass and cost. The DC/DC converters and energy storage capacitors are housed remotely from where they distribute DC power via a distribution network integrated into the aperture substrate. Simple deployment structures and mechanisms are needed for both the radiating aperture and the feed cluster.

aperture length (m)	*1.85*
aperture height (m)	*1.85*
number of panels	*4*
radiating element density (g/sqm)	6011
structural panel density (g/sqm)	*6858*

	Unit Mass (g)	**Qty**	**Total Mass (kg)**
radiating element substrate	5143	4	21
structural panel	5868	4	23
Beamforming Network			
element T/R modules	*13*	*5184*	67
PCU	15440	*4*	62
feed	*500*	*5*	3
array driver module	*50*	*5*	0
feed RF cable	*10*	*5*	0
beam switch	*100*	*1*	0
panel RF cables	*110*	*1*	0
PCU DC cables	*40*	*4*	0
controller	*6000*	*1*	6
controller DC cables	*1290*	*4*	5
deployment structure	*40000*	*1*	40
feed structure	*5000*	*1*	5
deployment actuators	*6000*	*1*	6
		subtotal	239
		20% contingency	48
		total	286

Substrate Layup	**g/sqm**
paint - 2 mil	*107*
elements - 50%, 1/2 oz Cu	*79*
substrate - 50 mil Duroid	*2794*
ground plane - 1/2 oz Cu	*158*
substrate - 50 mil Duroid	*2794*
elements - 50%, 1/2 oz Cu	*79*
	6011

PCU Mass	
number of power supplies	*64*
power supply unit mass (g)	*140*
capacitor mass factor	*1.5*
	g
substrate + housing	*2000*
power supplies + caps	13440
	15440

Figure C-7 Fully-distributed QO antenna mass for spaceborne high-resolution reference SAR mission.

	Unit Cost (k$)	Qty	Total Parts Cost (k$)
radiating element substrate	*7.0*	*4*	28
structural panel	*3.7*	*4*	15
Beamforming Network			
element T/R modules	*0.7*	*5184*	3629
PCU	33.8	*4*	135
feed	*1*	*5*	5
array driver module	*1.5*	*5*	8
feed RF cable	*0.05*	*5*	0
beam switch	*0.3*	*1*	0
panel RF cables	*0.3*	*1*	0
PCU DC cables	*0.5*	*4*	2
controller	*50*	*1*	50
controller DC cables	*1*	*4*	4
deployment structure	*750*	*1*	750
feed structure	*2*	*1*	2
deployment actuators	*100*	*1*	100
		subtotal	4728
		20% contingency	946
		total	5674

PCU Cost	
unit T/R ($)	*0*
unit phase shifter ($)	*200*
unit power supply ($)	*500*
number of phase shifters	*0*
number of power supplies	*64*
capacitor cost factor	*1.01*
housing + substrate	*1500*
T/R + phase shifter parts	0
power supplies + caps	32320
	33820

Figure C-8 Fully-distributed QO antenna cost for spaceborne high-resolution reference SAR mission.

C.3 Partially-Distributed QO Antenna Solution

The partially-distributed QO antenna architecture shown in Figure C-9 requires a prohibitively large amount of DC power. Figure C-10 indicates that the 23 kW required by the fully-distributed QO antenna is increased by 8 dB to about 147 kW due to the centralization of the HPA function.

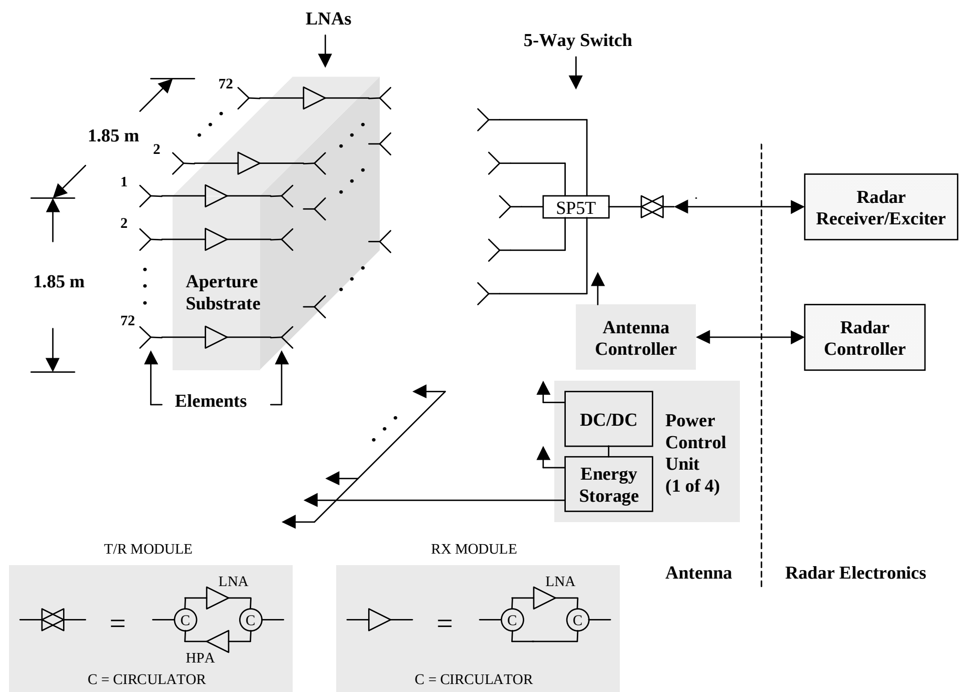

Figure C-9 Partially-distributed QO antenna block diagram for spaceborne high-resolution reference SAR mission.

Sensitivity (dB Wm4/K)	17.7				
Effective Elevation Aperture (m)	1.61				
Effective Azimuth Aperture (m)	1.76				
Pulsewidth (ms)	8				
PRF (Hz)	9905	avg spillover level (dB)	-10	System Noise Temperature (K)	611
HPA Duty Cycle (%)	7.9	spillover loss (dB)	3.8		
LNA Duty Cycle (%)	50	illumination loss (dB)	1		
				Array Transmit Power (W)	56521
number of elements	5184			Element Transmit Power (W)	10.9
ambient temperature (C)	0				
DC/DC conversion efficiency (%)	75				

Component	Receive Ohmic Loss (dB)	Receive Amp Gain (dB)	Receive Amp NF (dB)	Receive Combine (ways)	CW DC Power (mW)	Transmit Ohmic Loss (dB)	Transmit Amp Gain (dB)	Transmit Eff (%)	Sys Noise (K)	Transmit Loss (dB)	Input Power (dBm)	Comp Output Power (dBm)	Quantity	Receive Prime Power (W)	Transmit Prime Power (W)
external primary									290						
outer element	0.3	na	na	na	na	0.3	na	na	19.5	0.3	40.7	40.4	5184		
feedthrough	0.2	na	na	na	na	0.2	na	na	13.8	0.2	40.9	40.7	5184		
amplifier interface	1.0	na	na	na	na	0.8	na	na	79.3	0.8	41.7	40.9	5184		
amplifier	na	20	1.5	na	50	na	0	0	169.0	0.0	41.7	41.7	5184	173	
amplifier interface	0.8	na	na	na	na	0.8	na	na	0.8	0.8	42.5	41.7	5184		
transmission line	0.2	na	na	na	na	0.2	na	na	0.2	0.2	42.7	42.5	5184		
inner element	0.3	na	na	na	na	0.3	na	na	0.3	0.3	43.0	42.7	5184		
space feed	na	-4.8	0	5184	na	na	-41.9	na	0.0	41.9	84.9	43.0	1		
external secondary									1.7						
feed	1.2	na	na	na	na	1.2	na	na	5.0	1.2	86.1	84.9	1		
transmission line	0.5	na	na	na	na	0.5	na	na	2.5	0.5	86.6	86.1	1		
beam switch	1.0	na	na	na	na	1.0	na	na	6.0	1.0	87.6	86.6	1		
amplifier interface	0.8	na	na	na	na	0.8	na	na	5.9	0.8	88.4	87.6	1		
amplifier	na	20	1.5	na	50	na	30	50	15.4	-30.0	58.4	88.4	1	0	146787
amplifier interface	0.8	na	na	na	na	0.8	na	na	0.1	0.8	59.2	58.4	1		
transmission line	1.0	na	na	na	na	1.0	na	na	0.1	1.0	60.2	59.2	1		
receiver interface	0.5	na	na	na	na	0.5	na	na	0.1				1		
receiver	na	na	4	na	na	na	na	na	1.0						
													subtotals	173	146787
													total		146960

Figure C-10 Partially-distributed QO antenna RF performance for spaceborne high-resolution reference SAR mission.

Table C-1 summarizes the resource estimates for this high-resolution spaceborne SAR mission.

SPACEBORNE HIGH-RESOLUTION Figures of Merit	**AESA Solution**	**Fully-Distributed QO Solution**	**Partially-Distributed QO Solution**	**Centralized QO Solution**
Prime Power (W)	22445	22715	146960	-
Mass (kg)	392	286	-	-
Recurring Cost (k$)	5483	5674	-	-

Table C-1 Figures of merit for spaceborne high-resolution reference SAR mission. Recurring cost includes materials, fabrication, and assembly.

The fully-distributed QO antenna provides a 25% mass advantage for comparable power and cost. This is probably not convincing, however, due to the dominating nature of the 23 kW power requirement in both cases. The partially-distributed and centralized QO antennas require too much power to be practical.

APPENDIX D

ACRONYMS

AASR = Azimuth Ambiguity to Signal Ratio

ACR = Area Coverage Rate

ADC = Analog-to-Digital Converter

ADEOS = Advanced Earth Observing Satellite

ADTS = Advanced Detection Technology Sensor

AESA = Active Electronically Scanned Antenna

AGS = Airborne Ground Surveillance

ALOS = Advanced Land Observing Satellite

AMTI = Airborne Moving Target Indicator

ASAR = Advanced Synthetic Aperture Radar

ASR = Ambiguity to Signal Ratio

ASTOR = Airborne Stand-Off Radar

AWACS = Airborne Warning and Control System

BFN = Beamforming Network

CCRS = Canadian Center for Remote Sensing

CRL = Communications Research Laboratory

CSA = Canadian Space Agency

DARPA = Defense Advanced Research Projects Agency

DC = Direct Current

DCRS = Danish Center for Remote Sensing

DLR = German Aerospace Research Establishment

ECM = Electronic Countermeasures

EIRP = Equivalent Isotropically-Radiated Power

EMISAR = Electromagnetics Institute SAR

EOC = Edge of Coverage

ERIM = Environmental Research Institute of Michigan

ERS = Earth Resources Satellite

ESA = Electronically-Scanned Antenna

E-SAR = Experimental SAR

F/D = Focal Length to Diameter Ratio

GMTI = Ground Moving Target Indicator

G/T = Antenna Gain to Noise Temperature Ratio

HPA = High-Power Amplifier

IFSARE = Interferometric SAR for Elevation

IPP = Interpulse Period

ISR = Intelligence, Surveillance, and Reconnaissance

JERS = Japanese Earth Resources Satellite

Joint STARS = Joint Surveillance and Target Attack Radar System

JPL = Jet Propulsion Laboratory

LEO = Low-Earth Orbiting

LNA = Low-Noise Amplifier

MESFET = Metal Semiconductor Field-Effect Transistor

MMIC = Monolithic Microwave Integrated Circuit

MTI = Moving Target Indicator

NASA = National Aeronautics and Space Administration

NASDA = National Space Development Agency of Japan

Natar = NATO Transatlantic Advanced Radar

NATO = North Atlantic Treaty Organization

NIMA = National Imaging and Mapping Agency

NRO = National Reconnaissance Office

PALSAR = Phased Array L-Band SAR

PHARUS = Phased Array Universal SAR

PHEMT = Pseudomorphic High Electron Mobility Transistor

POB = Peak of Beam

PRF = Pulse Repetition Frequency

QO = Quasi-Optical

RAR = Real Aperture Radar

RASR = Range Ambiguity to Signal Ratio

RCS = Radar Cross-Section

RF = Radio Frequency

RTIP = Radar Technology Insertion Program

SAR = Synthetic Aperture Radar

SAROS = SAR for Open Skies

SBR = Space-Based Radar

SIR-A = Shuttle Imaging Radar A

SIR-B = Shuttle Imaging Radar B

SIR-C/X-SAR = Shuttle Imaging Radar C/X-Band SAR

SNR = Signal-to-Noise Ratio

Sostar = Stand-Off Surveillance and Target Acquisition Radar

SRTM = Shuttle Radar Topography Mission

TESAR = Tactical Endurance SAR

T/R = Transmit/Receive

TWTA = Traveling Wave Tube Amplifier

UAV = Unmanned Aerial Vehicle

UHF = Ultra-High Frequency